PAVOL JOZEF ŠAFÁRIK
UNIVERSITY
IN KOŠICE

NFA 2026

The 10th International Conference on

NOVEL MATERIALS

Fundamentals and Applications 2026

24 -27th May 2026

Tatranská Lomnica, High Tatras

https://nfa.science.upjs.sk

Pavol Jozef Šafárik University in Košice
Faculty of Science

BOOK OF ABSTRACTS

The 10th International Conference on Novel Materials Fundamentals and Applications

May 24-27, 2026

Organized by:

Department of Physical Chemistry
Faculty of Science
Pavol Jozef Šafárik University in Košice
&
Slovak Chemical Society
Bratislava

Košice 2026

10th International Conference on Novel Materials: Fundamentals and Applications 2026
High Tatras, 24.05.-27.05.2026

Book of Abstracts

EDITED BY

Mgr. Soňa Király, UPJŠ Košice, Slovakia, *sona.kiraly@upjs.sk*

REVIEWED BY

Evghenii Harea, PhD., Centre of Polymer Systems, Tomas Bata University in Zlín, CZ
harea@utb.cz

RNDr. Ondrej Petruš, PhD., Institute of Materials Research, Slovak Academy of Science, Košice, SK
opetrus@saske.sk

SCIENTIFIC COMMITTEE

Assoc. Prof. Andrea Straková Fedorková	UPJŠ Košice
Prof. Renáta Oriňaková	UPJŠ Košice
Dr. Ivana Šišoláková	UPJŠ Košice
Dr. Radka Gorejová	UPJŠ Košice
Dr. Jana Shepa	UPJŠ Košice

ORGANIZING COMMITTEE

Assoc. Prof. Andrea Straková Fedorková	UPJŠ Košice
Prof. Renáta Oriňaková	UPJŠ Košice
Dr. Ivana Šišoláková	UPJŠ Košice
Dr. Radka Gorejová	UPJŠ Košice
Dr. Jana Shepa	UPJŠ Košice
Mgr. Andrej Oriňak	UPJŠ Košice
Ing. Michaela Halinkovičová	SCHS Bratislava

ORGANIZED BY

Pavol Jozef Šafárik University in Košice
Slovak Chemical Society
Slovak Battery Alliance

Available at: unibook.upjs.sk
Publication date: 21.05. 2026

ISBN 978-80-574-0521-4 (e-publication)
DOI: https://doi.org/10.33542/TIC-0521-4

LIST OF CONTENTS

LIST OF AUTHORS

PREFACE

This volume presents the Book of Abstracts of the 10th International Conference on Novel Materials Fundamentals and Applications (NFA 2026), to be held on 24–27 May 2026 at the Grandhotel Praha in Tatranská Lomnica, situated in the High Tatras, Slovakia. The conference is organized by Pavol Jozef Šafárik University in Košice in cooperation with the Slovak Academy of Sciences and the Slovak Battery Alliance.

The year 2026 marks a distinguished milestone - the tenth anniversary of the NFA conference series. Over the past decade, this conference has steadily grown into a respected international forum, bringing together leading scientists, early-career researchers, and industry experts in the rapidly evolving field of advanced materials. This jubilee edition stands as both a reflection of the conference's enduring legacy and a celebration of its continued growth, scientific excellence, and international impact.

NFA 2026 continues its tradition of fostering interdisciplinary dialogue and collaboration, providing a platform for the presentation of novel research, the exchange of ideas, and the exploration of emerging directions in materials science. The contributions collected in this Book of Abstracts, encompassing both oral and poster presentations, reflect the diversity, depth, and dynamism of the topics addressed during the conference.

We extend our sincere and heartfelt appreciation to all contributing authors for their high-quality submissions and to the reviewers for their careful and dedicated work. Our special thanks also go to the organizing committee for their commitment and tireless efforts in preparing this anniversary event. Furthermore, we gratefully acknowledge the support of funding agencies and research initiatives that have made the presented work possible.

It is our firm belief that this special tenth anniversary edition of NFA will not only provide an inspiring setting for scientific exchange, but will also strengthen existing collaborations and spark new partnerships across the international research community, contributing to the advancement of materials science in the years to come.

Ivana Šišoláková

Invited speakers

ArtificiaI-Intelligence Driven Platforms for the Discovery and Optimization of Catalytic Reactors for Continuous-flow Sustainable Transformations

C. Tinajero[a], M. Zanatta[a,b], J. E. Sánchez-Velandia[a], E. García-Verdugo[b], V. Sans[a]*
[a] Institute of Advanced Materials (INAM), Univesitat Jaume I, Avda Sos Baynat s/n, 12071, Castellón, Spain
[b] Departamento de Química Inorgánica y Orgánica, Jaume I, E-12071 Castellón, Spain
*sans@uji.es

Keywords: artificial intelligence, self-driving laboratories, additive manufacturing, process intensification, sustainability

Additive manufacturing (AM) is redefining reactor engineering by unlocking complex geometries that surpass the mass- and heat-transfer limits of conventional packed beds.[1] Structured 3D-printed reactors offer tunable flow regimes and precise interfacial control, leading to marked gains in catalytic performance for CO_2 capture and conversion. In particular, polymeric and ionic-liquid-functionalized AM reactors, in which catalytic sites are embedded within high-resolution epoxy-functionalized matrices, have demonstrated enhanced activity, selectivity, and operational stability in the cycloaddition of CO_2 to epoxides.[2–4] Yet exploiting the vast design space opened by AM demands new tools capable of navigating geometry, chemistry, and process variables simultaneously.
To address this challenge, we introduce Reac-Discovery, a digital and autonomous platform that integrates reactor topology design, additive manufacturing, and self-driving experimentation in a single closed loop.[5] Its three modules, namely Reac-Gen, Reac-Fab, and Reac-Eval combine parametric geometry generation, high-resolution fabrication, and in-line NMR-guided optimization under AI orchestration. Applied to multiphase hydrogenation and CO_2 valorization, Reac-Discovery delivered record space-time yields and uncovered previously hidden structure–performance relationships for the cycloaddition of CO_2 to epoxides. By coupling AM, automation, and artificial intelligence, this approach establishes a new paradigm in which reactor geometry and catalysis co-evolve, paving the way toward intelligent, sustainable continuous-flow technologies.

References

[1] C. Tinajero, G. Palmara, M. Zanatta, V. Sans, „New frontiers in sustainable process engineering with additive manufacturing for continuous-flow applications," *Chem. Eng. J.*, vol. 505, pp. 159442, Feb. 2025, doi: 10.1016/j.cej.2025.159442.
[2] D. Valverde, R. Porcar, M. Zanatta, S. Alcalde, B. Altava, V. Sans, E. García-Verdugo, „Towards highly efficient continuous-flow catalytic carbon dioxide cycloadditions with additively manufactured reactors," *Green Chem.*, vol. 24, pp. 3300-3308, Mar. 2022, doi: 10.1039/D1GC04593H.
[3] D. Iglesias, C. Tinajero, S. Marchetti, I. Roppolo, M. Zanatta, V. Sans, „Multi-step oxidative carboxylation of olefins with carbon dioxide by combining electrochemical and 3D-printed flow reactors," *Green Chem.*, vol. 25, pp. 9934–9940, Nov. 2023, doi: 10.1039/D3GC03360K.
[4] S. Marchetti, C. Tinajero, G. Palmara, E. García-Verdugo, I. Roppolo, M. Zanatta, V. Sans, „High-resolution 3D printable inks based on functional polymeric ionic liquids for applications in carbon dioxide valorization," *Additive Manufacturing*, vol. 89, pp. 104304, Jun. 2024, doi: 10.1016/j.addma.2024.104304.
[5] C. Tinajero, M. Zanatta, J. E. Sánchez-Velandia, E. García-Verdugo, V. Sans, „Reac-Discovery: an artificial intelligence–driven platform for continuous-flow catalytic reactor discovery and optimization," *Nat Commun*, vol. 16, pp. 9062, Oct. 2025, doi: 10.1038/s41467-025-64127-1.

Rational Design and Biomedical Applications of Biomimetic Micro/nanomotors

L. Wang[a]*
[a] School of Chemistry and Chemical Engineering, Harbin Institute of Technology, Harbin 150001, China
*leiwang_chem@hit.edu.cn

Artificial-cell-based micromotors are new intelligent biomimetic materials based on multidisciplinary knowledge of chemistry, physics, synthetic biology, materials science, fluid mechanics and life science. Based on the "bottom-up" concept, through the rational design and integration of a variety of building elements, such as inorganic nanomaterials, functional polymers, biomaterials, etc., the multifunctional and multi-responsive micromotors can be realized, and the function and behavior of natural cells can be further simulated and studied; in the meanwhile, the artificial-cell-based micromotors can also be used as an intelligent building block to realize hierarchical assembly, so as to build advanced functional materials such as micro-scale or macro-scale artificial actuator and artificial tissue, etc. Therefore, in-depth study of the structure, properties and functions of artificial cell models can not only lay the foundation for simulating natural cellular functions, but also provide new ideas and new platforms for the design of new bionic materials.

From the perspective of fundamental cellular functions, motility behavior is not only a key attribute of living cells but also a critical criterion for evaluating the synergy between internal and external cellular functions. However, at the micro/nanoscale, the effective design and construction of artificial-cell-based micromotors with controllable motility, through the integration of multidisciplinary knowledge, remains a scientific challenge across various fields. To address this important issue, this report presents the latest research progress from our team on the construction of artificial-cell-based micromotors and their life-like behaviors for biomedical applications[1-10]. We outline the design principles and control strategies for artificial cell motility, and reveal the dynamic laws governing the motion of these micromotors in the context of life science and synthetic biology. Furthermore, we discuss how such motility behaviors influence multiple life functions and serve as a therapeutic strategy, thereby offering a new research paradigm for understanding the motile behavior of artificial cells, as well as the rapid proliferation mechanisms and treatment approaches for malignant cells such as tumors.

Acknowledgements

L. Wang would like to appreciate the funding support from NSFC (52473109, 52530002), the High-level Talent programme of Heilongjiang Province, and the China-Bulgaria Mobility Project.

References

[1] L. Wang, D. Zhang and X. Wu, "Rationally designed modular train-style nanorobots for multi-modal colorectal cancer therapy," *Matter,* vol. 9, no. 2, p. 102662, Feb. 2026, doi: 10.1016/j.matt.2026.102662.
[2] L. Wang, M. Tang, J. Ni, Z. Yue, T. Sun, C. Chen and X. Ma, "Polyoxometalate-Nanozyme-Integrated Nanomotors (POMotors) for Self-Propulsion-Promoted Synergistic Photothermal-Catalytic Tumor Therapy," *Angew. Chem. Int. Ed.,* vol. 63, no. 6, p. e202315031, Feb. 2024, doi: 10.1002/anie.202315031.
[3] L. Wang, H. Chen, W. Li, Y. Lin, X. Liu and X. Huang, "Fusion-Induced Structural and Functional Evolution in Binary Emulsion Communities," *Angew. Chem. Int. Ed.,* vol. 59, no. 39, pp. 16953-16960, Sep. 2020, doi: 10.1002/anie.202004617.
[4] L. Wang, M. Marciello, M. Estévez-Gay, P. E. D. S. Rodriguez, Y. L. Morato, J. Iglesias-Fernández, X. Huang, S. Osuna, M. Filice and S. Sánchez, "Enzyme Conformation Influences the Performance of Lipase-powered Nanomotors," *Angew. Chem. Int. Ed.,* vol. 59, no. 47, pp. 21080-21087, Nov. 2020, doi: 10.1002/anie.202008339.
[5] L. Wang, A. C. Hortelão, X. Huang and S. Sánchez, "Lipase-Powered Mesoporous Silica Nanomotors for Triglyceride Degradation," *Angew. Chem. Int. Ed.,* vol. 58, no. 24, pp. 7992-7996, Jun. 2019, doi: 10.1002/anie.201900697.
[6] L. Wang, Y. Lin, Y. Zhou, H. Xie, J. Song, M. Li, Y. Huang, X. Huang and S. Mann, "Autonomic Behaviors in Lipase-Active Oil Droplets," *Angew. Chem. Int. Ed.,* vol. 58, no. 4, pp. 1067-1071, Jan. 2019, doi: 10.1002/anie.201812111.
[7] L. Wang, Y. Gao, J. Guo, Y. Lai, J. Lin, J. Liu, J. Ji. P. Yin, W. Wang, H. Zhao, G. Chen and X. Fang, "Polyoxometalate–Organic Hybrid "Calixarenes" as Supramolecular Hosts," *Angew. Chem. Int. Ed.,* vol. 63, no. 4, p. e202315691, Jan. 2024, doi: 10.1002/anie.202315691.
[8] L. Wang, D. Zhang, L. Lin, C. Deng, M. S. Osman, P. E. D. S. Rodriguez, F. Han and M. Li, "Advanced Imaging Strategies Based on Intelligent Micro/Nanomotors," *Cyborg. Bionic. Syst.,* vol. 6, p. 0384, Sep. 2025, doi: 10.34133/cbsystems.0384.
[9] L. Wang, H. Yang and X. Huang, "MOF-based micro/nanomotors (MOFtors): Recent progress and challenges," *Coord. Chem. Rev.,* vol. 495, p. 215372, Nov. 2023, doi: 10.1016/j.ccr.2023.215372.

[10] L. Wang, J. Zhang, H. Zhang, N. Anastassova, G. Wang, P. Lin, Y. Song, H. Jin and Y. Sun, "Myocardial ischemia-reperfusion therapies based on lipase@CeO_2 nanomotors that target and permeate the myocardium and activate the PPARα pathway," *J. Control. Release,* vol. 388, p. 114357, Dec. 2025, doi: 10.1016/j.jconrel.2025.114357.

Lectures

Probing structure-property relationships in nanocomposites using X-ray techniques

J. Bednarcik[a]*
[a] Institute of Physics, Faculty of Science, Pavol Jozef Šafárik University in Košice
Park Angelinum 9, 040 01 Košice
*jozef.bednarcik@upjs.sk

Establishing a robust link between microscopic architecture and macroscopic performance is a central challenge in materials science. X-ray scattering and spectroscopy serve as indispensable tools in this pursuit, offering non-destructive, high-penetration probes capable of resolving structural features from the atomic to the mesoscale. The advent of synchrotron radiation facilities has revolutionized this domain, providing the high brilliance and energy tunability required for sophisticated in-situ and operando experiments. Unlike laboratory-scale instruments, synchrotrons allow for the real-time observation of material evolution under external stimuli including thermal cycling, high pressure, and mechanical deformation.

A defining strength of the modern synchrotron is its inherent multimodality. By integrating diverse techniques, such as Small-Angle and Wide-Angle X-ray Scattering (SAXS/WAXS), X-ray Absorption Spectroscopy (XAS), and nano-computed tomography - researchers can capture a holistic view of material response. This multimodal approach enables the observation of structural dynamics across broad spatial and temporal scales, providing the critical insights necessary to engineer the next generation of high-performance nanocomposites.

In the present study, the influence of wet mechanical alloying (MA) on the glass-forming ability of Co-based alloys was systematically investigated. To track structural evolution, a multi-analytical approach was employed, integrating high-energy X-ray diffraction (HEXRD), X-ray absorption spectroscopy (XAS), and high-resolution transmission electron microscopy (HRTEM), alongside vibrating sample magnetometry (VSM) and thermomagnetic measurements to assess magnetic properties. Specifically, pair distribution function (PDF) analysis and extended X-ray absorption fine structure (EXAFS) spectroscopy were utilized to resolve the local atomic architecture at successive stages of the milling process.

In the closing segment of the talk, emphasis will be placed on complementary laboratory-based X-ray methods such as XRD, SAXS/WAXS, and XAS. These techniques are currently being established and refined within the framework of the ongoing MASS PRAM project (Multimodal Approach to Study Structure-Property Relationships in Advanced Materials). The aim of this project is to link synchrotron and in-house experimental approaches by combining multiple methodologies, creating a more systematic and accessible way to explore structure-property relationships in advanced and functional materials. By merging synchrotron and laboratory capabilities, this approach demonstrates the powerful synergy of multimodal X-ray techniques in resolving complex structural questions in contemporary materials science.

Acknowledgements

This study was funded by the EU Next,Generation-EU through the Recovery and Resilience Plan for Slovakia under the project No. 09I03-03-V03-00034.

Biocompatibility of Nanocellulose-Based Formulations: Differential Responses in Fibroblast (CV-1) and Epithelial (A549) Cell Lines

E. Bencurova[a]*, E. Ekrami[b], E. M. Othman[b], T. Dandekar[a,c]
[a] Julius Maximilian University of Wuerzburg, Department of Bioinformatics, Wuerzburg, Germany
[b] Cancer Therapy Research Center (CTRC), Department of Biochemistry-I, Biocenter, University of Wuerzburg, Wuerzburg, Germany
[c] European Molecular Biology Laboratory, Heidelberg, Germany
*elena.bencurova@uni-wuerzburg.de

Introduction

Nanocellulose has emerged as a promising biomaterial for skin rejuvenation and wound healing applications due to its high water retention capacity, mechanical strength, and biocompatibility [1,2]. However, the cellular and molecular responses to nanocellulose-based formulations, particularly when combined with emollients such as plant oils, remain incompletely characterized. This study evaluates the biocompatibility of nanocellulose alone and in combination with different concentrations of raps oil (12.5%, 25%, 37.5% V/V) in two distinct cell lines: CV-1 (fibroblast-like, derived from monkey kidney) and A549 (human alveolar epithelial carcinoma). Fibroblasts are key players in dermal aging and extracellular matrix remodeling, while A549 cells serve as a model for epidermal barrier function [3,4].

Methods

Cells were treated with nanocellulose alone ("NC only") or nanocellulose supplemented with 12.5%, 25%, or 37.5% V/V oil for 24 hours, for the MTT assay, 50% concentration was tested in addition. Cell viability was assessed using the MTT assay [Sigma-Aldrich]. Gene expression changes in selected markers – EGR1 (early growth response, cellular stress), CCL2 (inflammation), MMP10 (matrix remodeling), SMAD3 (TGF-β signaling), and TGFB1 (growth factor) were quantified by qRT-PCR [StepOne, Thermo Fisher using PerfeCTa SYBR® Green FastMixes™ with ROX reference dye, Quanta Bio]. Fold changes were calculated using the 2^(−ΔΔCT) method with β-actin as reference control.

Results

MTT viability assays revealed that nanocellulose alone reduced viability to 55% in CV-1 cells and approximately 70–80% in A549 cells, suggesting cell-type-specific sensitivity. Oil addition partially rescued viability in CV-1 cells (75–85% of control) but had minimal effect in A549 cells. These results indicate that nanocellulose exhibits moderate cytotoxicity that can be mitigated by emollient co-formulation, particularly in fibroblast-like cells.

Gene expression analysis revealed striking differences between the two cell lines. In A549 cells, nanocellulose alone strongly upregulated MMP10 (69.6-fold), EGR1 (4.5-fold), TGFB1 (2.25-fold), and SMAD3 (2.16-fold), indicating activation of matrix remodeling and TGF-β signaling pathways. Oil addition at 12.5% and 25% further increased EGR1 expression (6.3- and 6.2-fold, respectively) while reducing MMP10 to 43.9- and 16.2-fold. Notably, CCL2 was downregulated at higher oil concentrations (0.59- and 0.82-fold at 25% and 37.5%), suggesting an anti-inflammatory effect of the oil component.

In CV-1 cells, a contrasting pattern emerged. Nanocellulose alone upregulated MMP10 (7.2-fold) and CCL2 (2.6-fold) but downregulated SMAD3 (0.86-fold, i.e., −1.16 in log2). The addition of 12.5% oil dramatically increased CCL2 expression (16-fold) and further enhanced MMP10 (11.1-fold), while 25% oil reduced these effects.

The differential responses between CV-1 and A549 cells highlight the importance of cell-type specificity in evaluating nanocellulose biocompatibility. CV-1 cells, representing dermal fibroblasts (normal cells, without pathogenic features), showed moderate viability reduction and strong induction of inflammatory (CCL2) and matrix-remodeling (MMP10) genes, particularly at 12.5% oil. This suggests that nanocellulose with low oil content may activate fibroblast-mediated tissue repair pathways. In contrast, A549 epithelial cells (cancer cells) exhibited a more robust stress response (EGR1, MMP10, TGFB1) but lower sensitivity to oil rescue.

The biphasic dose-response of several genes peaking at 12.5% oil and declining at higher concentrations may indicate an optimal oil concentration for bioactivity, beyond which cytotoxic or saturating effects occur.

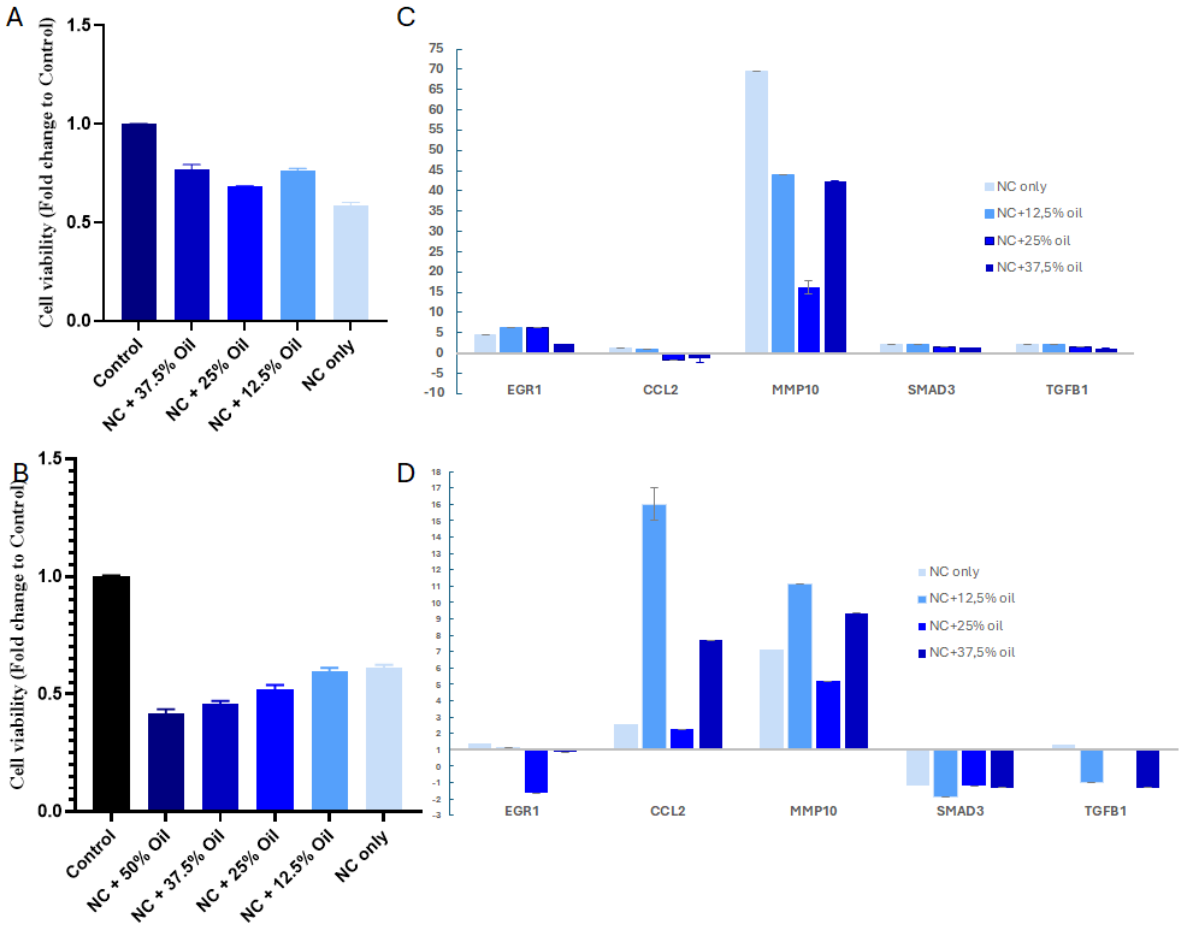

Figure 1 Cell viability and gene expression responses of CV-1 and A549 cells to nanocellulose (NC) with different oil concentrations.

CV-1 cells (A, C) and A549 cells (B, D). Cells were treated with nanocellulose alone (NC only) or nanocellulose supplemented with 12.5%, 25%, or 37.5% rapeseed oil. Control cells received no treatment and NC. Cell viability was assessed by MTT assay and is shown as fold change relative to control (A, B). Gene expression of EGR1, CCL2, MMP10, SMAD3, and TGFβ1 was quantified by qRT-PCR and is presented as fold change (log_2 scale) relative to control (C, D, Y axis represent fold change of gene expression compare to non-treated cells). Error bars represent standard deviation from three independent replicates.

Conclusion

Nanocellulose exhibits cell-type-dependent biocompatibility, with moderate cytotoxicity mitigated by oil co-formulation. The strong induction of MMP10 and CCL2 in CV-1 fibroblasts at 12.5% oil suggests potential pro-regenerative effects, while the downregulation of inflammatory markers in A549 cells at higher oil concentrations points to anti-inflammatory properties. These findings support the development of nanocellulose-oil formulations for skin rejuvenation, with optimal oil concentration around 12.5%. Further studies should investigate long-term effects, in vivo skin models, and the molecular mechanisms underlying the observed dose-dependent responses.

Acknowledgment

We thank Research Consortium Grants Project Nr. RDIA-004656, KSA for supporting this project.

References

[1] L. Bacakova, J. Pajorova, M. Bacakova, A. Skogberg, P. Kallio, K. Kolarova, and V. Svorcik, “Versatile application of nanocellulose: From industry to skin tissue engineering and wound healing,“ *Nanomaterials*, vol. 9, no. 2, pp. 164, Jan. 2019, doi: 10.3390/nano9020164.

[2] R. Nicu, F. Ciolacu and D. E. Ciolacu, “Advanced functional materials based on nanocellulose for pharmaceutical/medical applications,” *Pharmaceutics*, vol. 13, no. 8, pp. 1125, Jun. 2021, doi: 10.3390/pharmaceutics13081125.

[3] B. C. Barros, B. R. Almeida, D. T. Barros, M. S. Toledo and E. Suzuki, „Respiratory epithelial cells: more than just a physical barrier to fungal infections," *Journal of Fungi*, vol. 8, no. 6, pp. 548, May 2022, doi: 10.3390/jof8060548.
[4] G. J. Fisher, B. Wang, Y. Cui, M. Shi, Y. Zhao, T. Quan and J. J. Voorhees, „Skin aging from the perspective of dermal fibroblasts: The interplay between the adaptation to the extracellular matrix microenvironment and cell autonomous processes," *J Cell Commun and Signal.,* vol. 17, no. 3, pp. 523-529, Sep. 2023, doi: 10.1007/s12079-023-00743-0.

Magnetically Guided Fe_3O_4@SiO_2 Nanoparticles for Localised Antithrombotic Treatment: SEM Evaluation of Clot–Nanoparticle Interactions

E. Benova[a]*, N. Kiraly[a], M. Sulekova[b], L. Nagy[c], P. Hrubovcak[c], A. Zelenakova[c], V. Zelenak[a]

[a] Department of Inorganic Chemistry, Institute of Chemistry, Pavol Jozef Šafárik University in Košice, Moyzesova 11, 041 54 Kosice, Slovak Republic

[b] University of Veterinary Medicine and Pharmacy in Košice, Komenského 73, 041 81 Košice, Slovak Republic

[c] Institute of Physics, Faculty of Science, Pavol Jozef Šafárik University in Košice, Park Angelinum 9, 04001 Košice, Slovakia

*eva.benova@upjs.sk

Introduction

Thrombotic disorders remain a serious clinical problem, and their treatment is still largely based on systemic administration of antithrombotic drugs. Although these drugs are clinically effective, systemic delivery is associated with limited site selectivity, repeated dosing requirements, and an increased risk of adverse effects, particularly bleeding complications. Nanoparticle-based drug delivery systems offer a promising strategy to overcome these limitations by enabling controlled and potentially localised drug administration directly at the thrombotic site [1], [2], [3].

In our previous experiments with spherical mesoporous silica nanoparticles, SMS-60, we demonstrated that silica-based carriers can prolong the release of apixaban. This sustained release may potentially extend the biological effect of apixaban in the body and reduce dosing frequency, for example, from the current twice-daily administration to once every three days. Although these results are preliminary and require further biological verification, they indicate that silica-based nanocarriers could contribute to more controlled and prolonged antithrombotic therapy.

In parallel, our group has developed magnetic Fe_3O_4@SiO_2 nanoparticles that have already been successfully applied to SARS-CoV-2 RNA isolation and detection [4]. In the present work, these magnetic nanoparticles are further investigated as potential carriers for local antithrombotic treatment of blood clots. The Fe_3O_4 core provides magnetic responsiveness, while the SiO_2 shell offers chemical stability, biocompatibility, and the possibility of drug loading or further surface modification. Apixaban, a direct factor Xa inhibitor, was selected as a model antithrombotic drug.

Aim of the Study

The main objective of this study was to determine whether Fe3O4@SiO2 nanoparticles can be magnetically accumulated near a model blood clot and whether contact with apixaban-loaded nanoparticles induces observable changes in clot morphology. Since direct proof of clot dissolution remains financially challenging at this stage, scanning electron microscopy was used as the primary method to indirectly assess structural changes in the fibrin network and to identify nanoparticles on the clot surface.

Materials and Methods

To simulate targeted delivery under dynamic physiological conditions, experiments were performed in a model circulation system containing a blood clot in physiological medium. A pump drove circulation, while an external magnet positioned near the clot retained magnetic nanoparticles within the clot. In the absence of the magnet, the nanoparticles circulated freely in the system. This setup allowed us to evaluate whether magnetic guidance can promote the accumulation of Fe_3O_4@SiO_2 nanoparticles near thrombotic material (Figure 1).

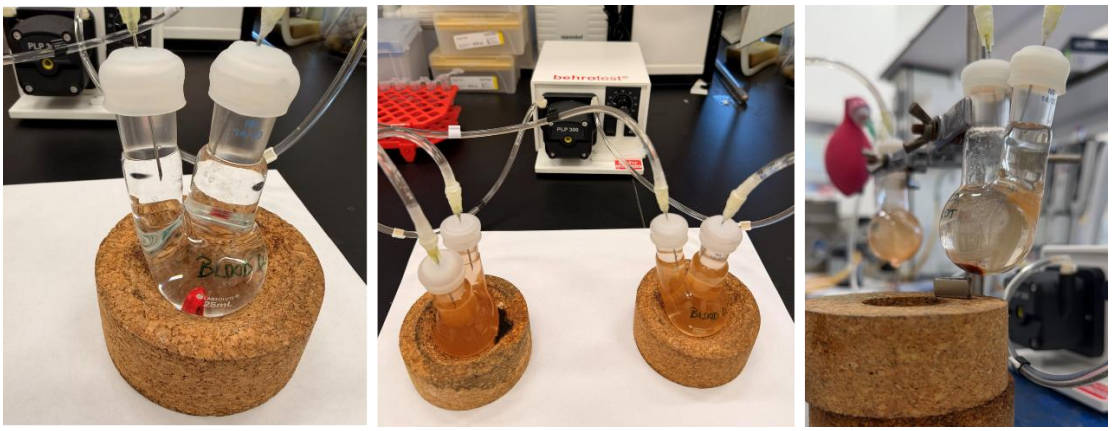

Figure 1 Simulated blood circulation model for magnetic targeting of Fe_3O_4@SiO_2 nanoparticles toward a blood clot. The setup shows a model clot in physiological medium, circulation of magnetic nanoparticles through the system, and their accumulation near the clot under the influence of an external magnet.

SEM samples were prepared from model blood clots incubated under several conditions: untreated clot in physiological medium, clot exposed to different concentrations of apixaban solution, clot treated with blank Fe3O4@SiO2 nanoparticles, and clot treated with apixaban-loaded Fe3O4@SiO2 nanoparticles. After incubation, the clot samples were fixed, dehydrated, dried, and prepared for SEM imaging.

Results and Discussion

SEM analysis revealed clear differences in the fibrin network under different treatment conditions. The untreated control clot showed a relatively compact fibrin structure with dense fibre arrangement. Clots incubated with apixaban solutions exhibited concentration-dependent morphological changes, including partial disruption of the fibrin mesh, thinning of fibrin fibres, and increased pore size within the network. These changes were more pronounced after longer incubation times and at higher apixaban concentrations, suggesting that apixaban exposure affects clot morphology under in vitro conditions.

In samples treated with blank Fe_3O_4@SiO_2 nanoparticles, the fibrin network remained more like the control clot, although nanoparticle aggregates were identified on the clot surface. This confirmed that the magnetic nanoparticles could interact with and adhere to thrombotic material. In clots treated with apixaban-loaded Fe_3O_4@SiO_2 nanoparticles, SEM images showed both the presence of nanoparticles on the clot surface and visible changes in fibrin architecture. Compared with blank nanoparticle-treated samples, the fibrin network appeared less compact and showed signs of structural disruption. These observations suggest that apixaban-loaded magnetic nanoparticles may influence clot morphology through localised contact with the drug-loaded carrier.

Additional preliminary experiments were performed to investigate whether variation of the magnetic field could promote nanoparticle penetration into the clot interior (Figure 2). Magnetic hyperthermia was considered an indirect method for detecting nanoparticles within the clot. However, Fe_3O_4-based nanoparticles did not generate sufficient heat under the applied conditions, unlike materials with higher heating efficiency, such as cobalt ferrite-based nanoparticles. Therefore, this approach did not provide conclusive evidence. Selected clot samples were subsequently embedded in resin, sectioned, and are currently being prepared for transmission electron microscopy analysis to evaluate nanoparticle distribution inside the clot.

Conclusion and Outlook

Overall, this study highlights the potential of Fe3O4@SiO2 magnetic nanoparticles as carriers for localised antithrombotic treatment. SEM imaging provided indirect evidence that contact with apixaban-loaded magnetic nanoparticles is associated with changes in fibrin morphology and confirmed the presence of nanoparticles on the clot surface. Future work will focus on optimising drug loading into magnetic nanocarriers, quantifying apixaban release under dynamic physiological conditions, and verifying nanoparticle penetration into clot cross-sections by TEM. Importantly, the next step will be to evaluate clot dissolution using D-dimer quantification, enabling a more reliable, quantitative assessment of the antithrombotic effect induced by locally delivered apixaban.

Figure 2 Experimental setup designed to investigate deeper penetration of Fe_3O_4@SiO_2 nanoparticles into a blood clot under the influence of an alternating magnetic field. The setup included a coil system for modulation of the magnetic field strength. A model blood clot was placed in physiological medium inside the experimental vessel, in the presence of a magnet. Magnetic nanoparticles accumulated in the clot region, while the alternating magnetic field was intended to promote oscillation of the magnetic cores and facilitate deeper nanoparticle penetration into the clot structure.

Acknowledgements

This work was supported by the EU NextGenerationEU through the Recovery and Resilience Plan for Slovakia, project No. 09I03-03-V04-00722 (MELODY) and by the Slovak Research and Development Agency under Contract APVV-23-0097 (SIBILA).

References

[1] M. Alquwaizani, L. Buckley, C. Adams, and J. Fanikos, 'Anticoagulants: A Review of the Pharmacology, Dosing, and Complications', *Curr Emerg Hosp Med Rep*, vol. 1, no. 2, pp. 83–97, 2013, doi: 10.1007/s40138-013-0014-6.

[2] S. Hassanpour, H.-J. Kim, A. Saadati, P. Tebon, C. Xue, F. W. van denDolder, J. Thakor, B. Baradaran, J. Mosafer, A. Baghbanzadeh, N. R. deBarros, M. Hashemzaei, K. Lee, J. Lee, S. Zhang, W. Sun, H.-J. Cho, S. Ahadian, N. Ashammakhi, M. R. Dokmeci, A. Mokhtarzadeh and A. Khademhosseini, 'Thrombolytic agents: Nanocarriers in controlled release', *Small*, vol. 16, no. 40, p. e2001647, Oct. 2020, doi: 10.1002/smll.202001647.

[3] 'Biological Applications of Silica-Based Nanoparticles'. Accessed: Sep. 30, 2025. [Online]. Available: https://www.mdpi.com/2312-7481/8/10/131.

[4] A. Zeleňáková, V. Zeleňák, E. Beňová, B. Kočíková, N. Király, P. Hrubovčák, J. Szűcsová, Ľ. Nagy, M. Klementová, J. Mačák, V. Závišová, J. Bednarčík, J. Kupčík, A. Jacková, D. Volavka, J. Košuth and Š. Vilček, "The surface modification of the silica-coated magnetic nanoparticles and their application in molecular diagnostics of virus infection," *Sci Rep*, vol. 14, no. 1, pp. 14427, Jun. 2024, doi: 10.1038/s41598-024-64839-2.

Three-dimensional equivalent circuit network for prediction of electric conductivity of porous composites of complex composition

D. Budac[a], V. Milos[a], M. Carda[a], M. Paidar[a], K. Bouzek[a]*
[a] Department of Inorganic Technology, University of Chemistry and Technology, Prague
Technická 5, 16628 Prague 6, Czech Republic
*bouzekk@vscht.cz

Multiphase electric charge conductors composed of materials with various properties are widely utilized in technical, as well as research practice. These composite materials include porous electrodes and other components utilized mainly in the fuel cell and battery technologies. In this study, a novel equivalent electronic circuit (EEC) network model is presented allowing for accurate prediction of the electrical properties of such materials without time-consuming experimental determination [1]. The distinct attribute of this EEC network model is the fact, it requires only easily obtainable data as input parameters: phase composition, porosity and bulk electrical conductivity of individual constituents. The model generates a large number of cubic artificial specimens based on random distribution of individual phases according to the input composition. Each of the generated specimens is substituted with corresponding EEC network. The EEC networks are solved using the Kirchhoff's laws resulting in impedance response simulation for composite conductivity value prediction. Unlike similar models, the EEC network model is able to account for morphological phenomena such as tortuosity, for more than two present phases in the system and for the interface phenomena. The EEC network model was validated using the lanthanum strontium manganite mixed with yttria-stabilized zirconia. Excellent agreement between the experimentally determined and calculated electrical conductivity for the sample porosity of 0 to 60 % was obtained. The phenomena observed were explained in terms of percolation theory and proven by microscopic observations.
Due to its variability, the EEC network model can be suitable for a wide range of practical applications. This approach has thus high potential to save enormous amount of experimental effort, while maintaining sufficient accuracy, when designing corresponding multiphase electrode structures.

Acknowledgements

This work was supported by the project "The Energy Conversion and Storage", funded as project No. CZ.02.01.01/00/22_008/0004617 by Programme Johannes Amos Comenius, call Excellent Research.

References

[1] D. Budáč, V. Miloš, M. Carda, M. Paidar, J. Fuhrmann, K. Bouzek, „Prediction of Electrical Conductivity of Porous Composites Using a Simplified Monte Carlo 3D Equivalent Electronic Circuit Network Model: LSM-YSZ Case Study," *Electrochim. Acta*, vol. 457, 142512, Jul. 2023, doi: 10.1016/j.electacta.2023.142512.

Spectrophotometric Determination of Aspirin Release from PLA Coating Using a Model Glass Substrate

V. Cakyova[a]*, I. Shepa[b], J. Shepa[a], I. Sisolakova[a], R. Orinakova[a]
[a] Department of Physical Chemistry, Institute of Chemistry, Pavol Jozef Šafárik University in Košice, Moyzesova 11, 041 54 Kosice, Slovak Republic
[b] Institute of Materials Research of SAS, Watsonova 47, 04001 Kosice, Slovak Republic
*viktoria.cakyova@upjs.sk

Drug release is the process by which an active pharmaceutical compound is released from a carrier system and becomes available at the target site. Achieving effective therapy depends not only on the presence of the drug, but also on its concentration, duration of action, and ability to reach specific tissues. Therefore, controlled drug delivery systems have been developed to regulate the rate and extent of drug release, enabling sustained therapeutic levels and targeted delivery [1]. Controlled drug delivery systems can be classified according to their release mechanisms into dissolution controlled, diffusion controlled, osmotic and swelling driven, chemically controlled, and nanoparticle-based systems. Among these, chemically controlled systems based on biodegradable polymers are of particular interest, as they rely on structural changes of the carrier material and degrade under physiological conditions without the need for removal [2], [3].

In polymer-based delivery systems, the active compound is incorporated within a polymer matrix and released as the polymer gradually degrades. Polylactic acid (PLA), a biodegradable and biocompatible aliphatic polyester, is widely used for such applications due to its hydrolytic degradation into lactic acid and its tuneable physicochemical properties [4]. The incorporation of acetylsalicylic acid (ASA), a non-steroidal anti-inflammatory drug, provides additional therapeutic benefits. ASA is widely used in clinical practice due to its anti-inflammatory, analgesic, and anti-coagulant effects. Beyond these conventional roles, some studies indicate that ASA can modulate bone remodelling. It has also been shown to promote angiogenesis by enhancing endothelial cell migration and vascular formation, which are essential processes in bone regeneration and healing. These combined effects make ASA a promising candidate for incorporation into polymer-based delivery systems aimed at improving regenerative outcomes [5], [6], [7].

In this study, a polymer solution composed of 5 wt. % PLA and 5 wt. % ASA (relative to the dry polymer mass) was prepared and applied as a coating onto a zinc substrate. However, to assess the intrinsic degradation behaviour and drug release independent of substrate effects, the system was investigated under simplified conditions using a glass as a substrate. The polymer solution was therefore deposited onto a glass substrate and dried at 37° C to form a dry polymer film. The resulting coating was subsequently immersed in distilled water and incubated at 37° C for 12 and 24 hours in order to monitor the release of ASA.

The release of ASA was determined using an indirect colorimetric UV-VIS method based on the quantification of salicylic acid (SA) using iron (III) chloride ($FeCl_3$) as a complexing agent. $FeCl_3$ reacts with the phenolic hydroxyl group of SA to form a violet coloured tetraaquasalicylic iron (III) complex, which was measured spectrophotometrically at 530 nm. The concentration of SA is directly proportional to the concentration of ASA. The concentration curves obtained after 12 and 24 hours are presented in Figure 1.

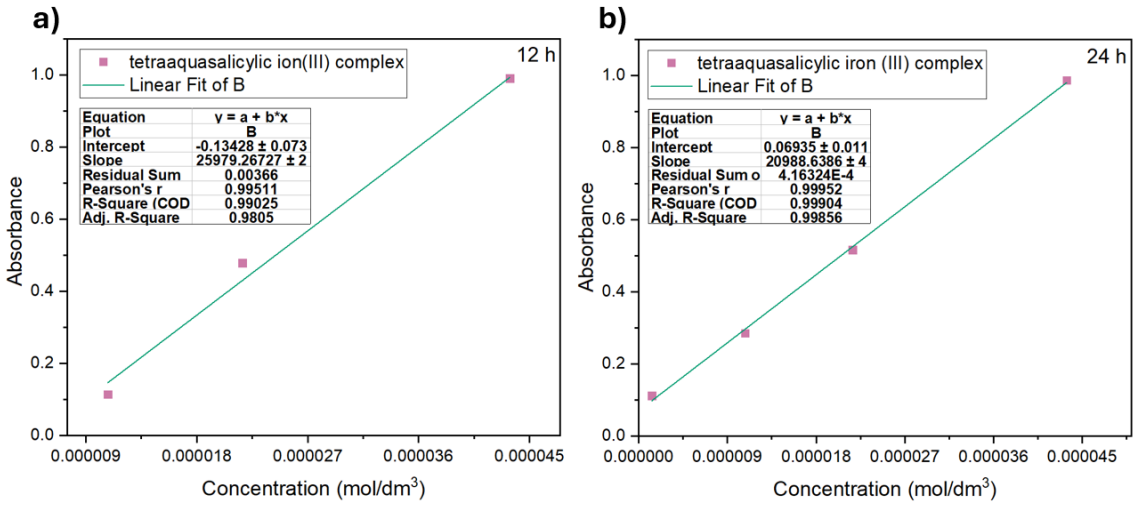

Figure 3 Calibration curves obtained after 12 a) and 24 b) hours.

The calibration curves exhibited excellent linearity (R2 = 0.990 for 12 h and 0.999 for 24 h), ensuring reliable quantification. The concentration of released ASA reached 1.13 × 10-5 mol/dm3 (11.3 μM) after 12 h and 3.65 × 10-5 mol/dm3 (36.5 μM) after 24 h, corresponding to approximately 6.8 % and 22.1 % of the theoretically available ASA, respectively. These findings demonstrate a controlled and sustained release profile of ASA from the PLA matrix and confirm the suitability of the proposed system for future applications in biodegradable zinc-based implant materials.

Acknowledgements

This work was funded by the EU NextGenerationEU through the Recovery and Resilience Plan of the Slovak Republic under project no. 09-I05-03-V02-00047.

References

[1] S. Adepu and S. Ramakrishna, "Controlled drug delivery systems: Current status and future directions," *Molecules,* vol. 26, no. 19, pp. 5905, Oct. 2021, doi: 10.3390/molecules26195905.
[2] H. Lu, Z. Cai, and P. Hu, "Recent Advances in Polymeric Delivery Vehicles for Controlled and Sustained Drug Release," *Multidisciplinary Digital Publishing Institute,* vol. 16, no. 9, pp. 1184, Sep. 2024, doi: 10.3390/pharmaceutics16091184.
[3] B. Olamide Ishola, K. A. Rahaman, S. A. Razzak, M. M. H. Rumon, M. S. Shakil, and S. Uddin, "Advanced mechanisms of polymer-based drug delivery systems for clinical applications," *Royal Society of Chemistry*, vol. 2, Mar. 2026, doi: 10.1039/d5pm00242g.
[4] J. C. Middleton and A. J. Tipton, "Synthetic biodegradable polymers as orthopedic devices," *Biomaterials,* vol. 21, no. 23, pp. 2335-2346m Dec. 2000, doi: 10.1016/S0142-9612(00)00101-0.
[5] R. Fattahi, F. mohebichamkhorami, M. M. Khani, M. Soleimani, and S. Hosseinzadeh, "Aspirin effect on bone remodeling and skeletal regeneration: Review article," *Elsevier Ltd*., vol. 76, pp. 101753, Jun.2022, doi: 10.1016/j.tice.2022.101753.
[6] S. Funke *et al.*, "Aspirin Stimulates the Osteogenic Differentiation of Human Adipose Tissue-Derived Stem Cells In Vitro," *Int. J. Mol. Sci.*, vol. 25, no. 14, Jul. 2024, doi: 10.3390/ijms25147690.
[7] M. Meng *et al.*, "Optimization of surface imprinted layer attached poly(vinylidene fluoride) membrane for selective separation of salicylic acid from acetylsalicylic acid using central composite design," *Chemical Engineering Journal*, vol. 231, pp. 132–145, Sep. 2013, doi: 10.1016/j.cej.2013.07.015.

Mechanochemically Synthesized DOPO-Based Flame Retardants in Polymer Electrolytes for Safer Lithium–Sulfur Batteries

J. Demeterova[a]*, J. Lescinsky[a], V. Niscakova[a], A. Fedorkova[a]
[a] Department of Physical Chemistry, Institute of Chemistry, Pavol Jozef Šafárik University in Košice, Moyzesova 11, 041 54 Kosice, Slovak Republic
*jana.demeterova@student.upjs.sk

Introduction

The commercialization of lithium–sulfur (Li–S) batteries is limited not only by electrochemical instability but also by safety concerns associated with flammable liquid electrolytes [1], [2]. Ether-based systems exhibit high volatility and poor thermal stability, increasing the risk of thermal runaway. In addition, polysulfide dissolution leads to shuttle effects, self-discharge, and capacity fading [2]. Polymer electrolytes represent a promising strategy to mitigate these issues by combining reduced flammability with suppression of polysulfide transport and improved interfacial stability [2].
Recent research highlights the importance of multifunctional additives capable of simultaneously improving safety and electrochemical performance, particularly phosphorus-containing compounds that influence interphase formation and redox chemistry [3].

Experimental

In the SUNFLOWERS project, DOPO-based flame-retardant additives are synthesized via a solvent-free mechanochemical reaction with glycidyl methacrylate, enabling a sustainable and scalable synthesis route. Mechanochemical synthesis conditions (30–90 min milling) directly influence molecular structure and additive dispersion.
The synthesized additives are incorporated into PVDF-HFP-based polymer electrolyte membranes containing LiTFSI. The polymer matrix provides mechanical stability and enables electrolyte uptake, while limiting polysulfide diffusion. Electrochemical characterization includes CV, EIS, and galvanostatic cycling, complemented by thermal and structural analysis.

Results and Discussion

DOPO-derived additives introduce both chemical and physical stabilization mechanisms. Phosphorus functional groups interact with polysulfides, reducing their mobility and suppressing shuttle effects [3]. This interaction improves Coulombic efficiency and stabilizes intermediate species during cycling. Simultaneously, the polymer matrix provides physical confinement, limiting diffusion of soluble species and enhancing redox reversibility. The combination of chemical interaction and physical trapping leads to improved cycling stability and reduced capacity fading, consistent with observations in polymer-based Li–S systems [2].
From an interfacial perspective, DOPO-based additives promote formation of stable cathode electrolyte interphases, reducing parasitic reactions and improving charge-transfer kinetics. These interphases influence impedance evolution and facilitate more uniform Li_2S deposition.
Mechanochemical synthesis plays a key role in determining additive dispersion and reactivity. Improved dispersion enhances interfacial interactions and leads to more homogeneous electrochemical behavior. Additionally, incorporation of phosphorus-based compounds significantly improves thermal stability and reduces flammability, addressing key safety limitations of conventional electrolytes.

Conclusion

This study demonstrates that mechanochemically synthesized DOPO-based additives provide a multifunctional approach to improving both safety and electrochemical performance of Li–S batteries. The integration of polymer electrolytes and phosphorus-based flame retardants enables suppression of polysulfide shuttle, stabilization of interfaces, and enhanced thermal stability, supporting the development of safer and more sustainable Li–S systems within the SUNFLOWERS project.

Acknowledgements

This work was funded by the project EU NextGenerationEU through the Recovery and Resilience Plan for Slovakia under the project SUNFLOWERS No. 09I02-03-V01-00022.

References

[1] A. Manthiram, Y. Fu, S.-H. Chung, C. Zu, and Y.-S. Su, "Rechargeable lithium–sulfur batteries," *Chem. Rev.,* vol. 114, pp. 11751–11787, 2014, doi: 10.1021/cr500062v.
[2] R. Fang, S. Zhao, Z. Sun, D.-W. Wang, H.-M. Cheng, and F. Li, "More reliable lithium–sulfur batteries: Status, solutions and prospects," *Adv. Mater*., vol. 29, Art. no. 1606823, 2017, doi: 10.1002/adma.201606823.
[3] S. S. Zhang, "Liquid electrolyte lithium/sulfur battery: Fundamental chemistry, problems, and solutions," *J. Power Sources,* vol. 231, pp. 153–162, 2013, doi: 10.1016/j.jpowsour.2012.12.102.
[4] T. Friščić, C. Mottillo, and H. M. Titi, "Mechanochemistry for synthesis," *Angew. Chem. Int. Ed.,* vol. 58, pp. 1018–1029, 2019, doi: 10.1002/anie.201906755.

Impact of Pyrolysis Temperature on Hydrogen-Evolution Reaction Activity of High-Entropy Carbides

K. Denk[a]*, M. Plevova[a], I. Shepa[a], K. Nemesh[a,b], D. Kozien[c], M. Streckova[a]
[a] Institute of Materials Research, Slovak Academy of Sciences, Košice, Slovakia
[b] Faculty of Materials, Metallurgy and Recycling, Technical University of Košice, Košice, Slovakia
[c] Department of Ceramics and Refractories, Faculty of Materials Science and Ceramics
AGH University of Krakow, Mickiewicza, 30-059 Krakow, Poland
*kdenk@saske.sk

The European Union has set ambitious climate targets, including achieving climate neutrality by 2050 and substantially reducing greenhouse gas emissions by 2030, which necessitates the transition to low-carbon energy systems. In this context, hydrogen is increasingly recognized as a key energy carrier within the emerging hydrogen economy, enabling efficient energy storage and sector coupling. Among available production methods, water electrolysis plays a central role, particularly proton exchange membrane (PEM) electrolysis, which offers high current densities, rapid response to fluctuating renewable energy inputs, and the production of high-purity hydrogen. These advantages make PEM systems especially suitable for integration with intermittent renewable energy sources such as wind and solar power, thereby supporting grid stability and sustainable energy conversion. Despite these advantages, the widespread deployment of PEM electrolysis is still limited by material-related challenges, especially under the harsh acidic conditions required for operation.

The performance and durability of PEM electrolyzers strongly depend on the electrocatalysts used for the hydrogen-evolution and oxygen-evolution reactions. Currently, platinum group metals (PGM), particularly platinum, are considered the most effective catalysts for the hydrogen-evolution reaction (HER) due to their optimal hydrogen adsorption properties and high stability in acidic environments. However, their high cost and limited availability hinder large-scale implementation. As a result, significant research efforts are focused on developing alternative materials with comparable activity and stability, with high-entropy materials (HEM) emerging as promising candidates to replace PGM-based catalysts.

HEMs are multicomponent systems typically containing four or more elements with comparable atomic radii. This approach promotes the formation of stable single-phase solid materials and leads to properties distinct from those of the individual constituents. High-entropy carbides (HEC), formed by two interpenetrating sublattices of transition metals and carbon, are characterized by high hardness and good electrical conductivity. Their wide distribution of hydrogen adsorption energies enables access to a catalytic "sweet spot" consistent with the Sabatier principle, making them promising materials for HER.

Composite ceramic nanofibers based on TiZrHfNbTaC HEC were prepared from fibres containing the individual components. Nb, Ta, and Hf chlorides with titanium isopropoxide and zirconium propoxide served as ceramic precursors, while polyacrylonitrile acted as the carrier polymer. The fibres were subsequently pyrolyzed in the temperature range of 1100–2100 °C with 200 °C difference for 15 minutes – each temperature represents one sample – producing fibrous ceramic structures. Their phase composition and morphology were analyzed using XRD and SEM/EDS techniques. The electrochemical performance toward HER was investigated in an acidic environment using a three-electrode setup, and the samples were also assessed in terms of long-term stability and electrical conductivity.

An increase in pyrolysis temperature led to gradual carbothermal reduction and enhanced crystallization of the HEC phase. At lower temperatures, XRD patterns showed broad reflections along with residual HfO_2, indicating incomplete phase formation. In contrast, samples treated at temperatures ≥1900 °C exhibited well-defined carbide reflections and the disappearance of oxide phases. Concurrently, the initially amorphous carbon matrix transformed into a more ordered graphitic structure with improved alignment of carbon layers. This structural evolution contributed to higher electrical conductivity and a marked a significant improvement in HER activity in the acidic environment to values overpotential *ca*. −40 mV.

Acknowledgements

This work was funded by the EU Next Generation EU through the Recovery and Resilience Plan for Slovakia under the project No 09I04-03-V02-00006, No. 09I03-03-V02-00013 and No. 09I03-03-V04-00579.

Advancing High-Efficiency Redox Flow and Li-Ion Systems: From Material Modelling to Scalable Hybrid Storage

A. Fedorkova[a]*, N. Podrojkova[a], V. Niscakova[a], J. Lescinsky[a], R. Orinakova[a]
[a] Department of Physical Chemistry, Institute of Chemistry, Pavol Jozef Šafárik University in Košice, Moyzesova 11, 041 54 Kosice, Slovak Republic
*andrea.fedorkova@upjs.sk

Keywords: Hybrid storage systems, Li-ion batteries, Li-S batteries, redox-flow batteries, applied research.

Introduction

The evolution of energy storage technologies, specifically lithium-ion (LIB) and redox flow batteries (RFBs) is a key factor of the global transition to renewable energy. Current research prioritizes the development of advanced materials, high-fidelity modeling, and rigorous empirical testing to enhance performance, safety, and economic feasibility. A critical component of widespread adoption is long-term durability and the integration of ethically sourced materials to minimize environmental impact. To support a circular economy, it is essential that these systems are designed for efficient recycling or repurposing at the end of their lifecycle [1].
While lithium-ion batteries currently dominate the market across electric mobility and stationary storage due to their high energy density, continuous innovation in electrode chemistry and cell architecture remains necessary. Simultaneously, RFBs have emerged as a premier solution for grid-scale storage, offering long-duration discharge, rapid response times, and extended operational lifespans. In these systems, the selection of redox couples and electrolyte compositions is fundamental to determining energy density and cost. This study integrates computational modeling with laboratory validation to develop novel components for both Li-S and redox flow technologies.
The operational efficiency of RFBs is governed by complex electrochemical and mass transport phenomena. Performance degradation is primarily driven by ohmic resistance, a major component of total internal overpotential. This resistance is a multifaceted parameter involving:

- Ionic resistance of the ion-exchange membrane.
- Electronic resistance of bipolar plates and porous carbon electrodes.
- Contact resistance at material interfaces.

In high-performance systems, membrane ionic conductivity often acts as the primary bottleneck. Maximizing the mobility of charge-carrying species (e.g., protons in vanadium systems) while maintaining low crossover rates is vital to preventing self-discharge. During charging, an external power source drives the redox reactions, converting electrical energy into chemical potential stored in external tanks. During discharge, ions flow through the membrane while electrons move through the external circuit. Efficiency is hindered by the ohmic drop ($V = IR$), which causes a linear deviation from the theoretical Nernstian potential, reducing voltage efficiency at high current densities. To address this, advanced diagnostics like Electrochemical Impedance Spectroscopy (EIS) are used to decouple ohmic losses from activation and mass-transport polarizations.

Computational Modelling in Battery Research

Advanced numerical simulations accelerate the discovery of next-generation materials by deciphering electrochemical performance. For Li-ion systems, atomistic tools allow for the precise engineering of cathode, anode, and electrolyte architectures, reducing R&D costs. In the RFB domain, the synergy between Machine Learning (ML) and High-Throughput Computational Screening (HTCS) enables the rapid identification of redox-active species. Current research is increasingly focused on non-aqueous RFBs, which offer broader voltage windows. For example, a recent prototype achieved discharge voltages between 2.25 V and 1.9 V [2]. To assess scalability, a 2D time-transient reactive transport model was developed to predict voltage and ion transport dynamics.
The model distinguishes between laminar flow in open channels and porous media flow in felt regions. Findings suggest that traditional definitions, such as the Kozeny-Carman equation, may be inadequate for these unique setups, necessitating alternative governing equations. Precise calibration of electrolyte permeability using either experimental validation or inlet pressure data is essential for refining these simulations (Figure 1).

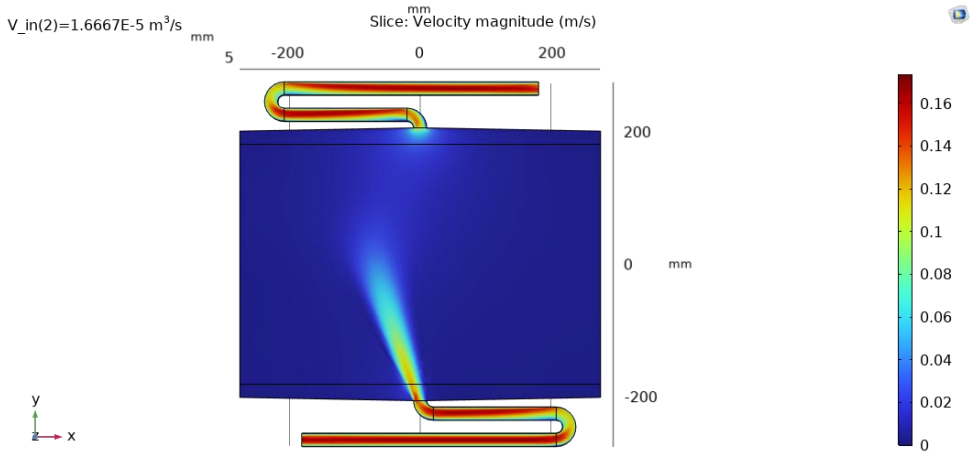

Figure 1 Simulations on velocity in redox flow battery system.

Conclusion

The advancement of RFB technology is a critical milestone for sustainable, grid-scale energy storage. This research highlights that the integration of atomistic modeling and high-throughput screening is vital for overcoming material limitations. By combining simulations with laboratory validation, we have identified new redox-active species that improve both energy density and economic viability.

Key focus areas included:

- Mitigating Ohmic Resistance: Optimizing membrane conductivity and interface architecture to maintain high voltage efficiency.
- Refining Transport Models: Identifying the limitations of the Kozeny-Carman equation in 2D reactive transport models.
- Scalability: Emphasizing the need for precise permeability calibration and refined fluid dynamics.

Ultimately, the transition from theoretical models to industrial prototypes confirms that RFBs are a robust and sustainable alternative to traditional chemistries. By prioritizing ethical sourcing and recyclability, this work ensures that future storage systems are as environmentally responsible as they are technically efficient.

Acknowledgements

This work was funded by the EU NextGenerationEU through the Recovery and Resilience Plan for Slovakia under the project SUNFLOWERS No. 09I02-03-V01-00022.

References

[1] R M. A. S. Al-Saeedi et al., "Challenges and advances in redox flow batteries utilizing sustainable and cost-effective non-vanadium active materials," *J. Mater. Chem. A*, vol. 13, no. 14, pp. 8837–8881, 2025, doi: 10.1039/D5TA00113G.

[2] M. D'Adamo, N. Daub, L. Trilla, J. A. Saez-Zamora, and J. M. Paz-Garcia, "Modeling of a Non-Aqueous Redox Flow Battery for Performance and Capacity Fade Analysis," *Batteries*, vol. 11, no. 1, p. 8, Jan. 2025, doi: 10.3390/batteries11010008.

Novel Design of High-Efficiency Hybrid Storage: An Experimental Study of Redox Flow and Li-S Chemistries

A. Fedorkova[a]*, N. Podrojkova[a], V. Niscakova[a], R. Orinakova[a]
[a] Department of Physical Chemistry, Institute of Chemistry, Pavol Jozef Šafárik University in Košice, Moyzesova 11, 041 54 Kosice, Slovak Republic
*andrea.fedorkova@upjs.sk

Keywords: Hybrid energy storage systems, Li-S batteries, redox-flow batteries, applied research.

Introduction

The global push towards carbon neutrality necessitates the advancement of diverse, high-performance electrochemical energy storage systems (EESS). Lithium-Sulfur (Li-S) and Redox Flow Batteries (RFBs) have emerged as leading candidates, offering distinct yet complementary strengths. This work examines the strategic synergy between these technologies, focusing on their integrated roles in meeting the multi-scale demands of modern power grids and electric mobility.

Li-S batteries represent the frontier of high-energy-density storage, with a theoretical capacity of $2600 Wh/kg far exceeding conventional lithium-ion systems. However, commercialization is currently limited by the "shuttle effect" of soluble polysulfides and significant volume expansion. In contrast, RFBs particularly vanadium and non-aqueous organic systems are ideal for grid-scale storage due to their decoupled energy and power scaling, exceptional cycle life, and inherent safety [1]. The synergy between these two systems is rooted in shared electrochemical principles and innovations in materials science.

Advancements in polysulfide chemistry for Li-S cathodes directly inform the development of high-capacity redox-active species for RFBs. By utilizing advanced atomistic modelling and high-throughput computational screening (HTCS), we have identified novel electrolyte additives and membrane coatings that mitigate parasitic crossover in both technologies. Additionally, the implementation of 2D time-transient reactive transport models enables precise simulation of ion migration and fluid dynamics, creating a unified framework to optimize electrode porosity and minimize ohmic resistance.

A primary objective of this synergistic approach is the development of Hybrid Energy Storage Systems (HESS). These systems combine the rapid response and high density of Li-S cells [2] with the long-duration stability of RFBs, using advanced power electronics to buffer peak loads while maintaining grid stability. By prioritizing ethically sourced materials and circular economy principles, this research ensures the lifecycles of both Li-S and RFB technologies align with global sustainability goals. The convergence of these fields supported by operando diagnostics and real-time data monitoring establishes a robust pathway for the next generation of scalable, cost-effective, and environmentally responsible energy storage.

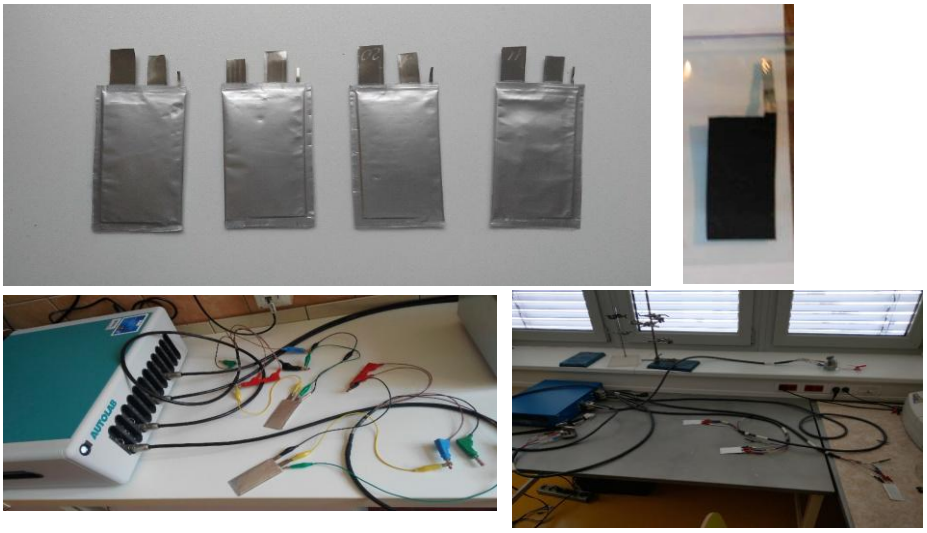

Figure 1 Li-S battery prototypes, cathode coated on Al foil and testing of pouch cells.

Results and Discussion

The electrochemical evaluation of the fabricated pouch cells yielded significant results. By optimizing the electrode architecture, the active surface area of the cathodes was increased approximately 30-fold. The capacities and cycling stability observed in these pouch cells are comparable to results previously obtained in smaller testing formats, such as El-cells and coin cells. To date, the prepared pouch cells have achieved an average lifespan of 200 cycles. Long-term measurements for several units remain ongoing, and the current performance trajectory is promising (Figure 1). The primary objective of this development phase is to achieve 500 cycles with a minimum specific capacity of 400 mAh/g.

A comprehensive safety evaluation was conducted, encompassing both electrochemical and physical stress tests. Several protocols, including overcharging and over-discharging, were successfully performed at room temperature. Destructive nail penetration tests were also carried out under standard laboratory conditions. Notably, no significant heat generation or thermal runaway was observed during these tests, indicating a high degree of inherent safety. During the electrochemical overcharge tests, the pouch cells exhibited significant swelling, which resulted in the interruption of contact between the electrodes effectively acting as a passive safety mechanism.

Conclusion

This research highlights the strategic integration of Lithium-Sulfur (Li-S) and Redox Flow Battery (RFB) technologies as a vital approach to achieving global carbon neutrality. By combining the high energy density of Li-S chemistry with the long-duration stability and inherent safety of RFBs, this study provides a comprehensive framework for both grid-scale storage and electric mobility. The experimental results demonstrate that optimizing electrode architecture to achieve a 30-fold increase in cathode surface area allows pouch cells to match the performance of laboratory-scale testing formats.

The synergy between these two technologies, driven by advanced atomistic modeling and 2D reactive transport simulations, facilitates the rapid identification of novel materials and electrolyte additives. By prioritizing ethically sourced materials and circular economy principles, this work establishes a robust, scalable, and environmentally responsible pathway for the next generation of hybrid energy storage systems.

Acknowledgements

This work was funded by the EU NextGenerationEU through the Recovery and Resilience Plan for Slovakia under the project SUNFLOWERS No. 09I02-03-V01-00022 and by SKEBA platform.

References

[1] X. Qian, D. R. Chang, and S. Jung, "Experimental and computational study on alloxazine derivative based organic redox flow battery," *Chem. Eng. J.*, vol. 429, p. 132420, Feb. 2022.

[2] X. Wang, Z. Song, R. Liu, R. Yu, and J. Wang, "Recent progress in host and electrolyte engineering towards Li2S cathode for lithium-sulfur battery," *Nano Res. Energy*, 2026, Art. no. 9120194, doi: 10.26599/NRE.2025.9120194.

P(OEGMA-co-MAA) copolymer brush coatings combing protein resistance and biogonjugation for biosensing and cell culture

K. Gajos[a]*, O. Lishchynskyi[b], Y. Stetsyshyn[c], A. Budkowski[a]
[a] M. Smoluchowski Institute of Physics, Jagiellonian University,
Łojasiewicza 11, 30-348 Kraków, Poland
[b] Department of Biotechnology, Faculty of Bioscience Engineering, Ghent University,
Proeftuinstraat 86, Ghent 9000, Belgium
[c] Lviv Polytechnic National University, St. George's Square 2, Lviv, Ukraine
*katarzyna.gajos@uj.edu.pl

Bioactive surfaces providing controlled immobilization of functional proteins such as enzymes, antibodies, and extracellular matrix (EMC) proteins are widely used in biosensing, cell culture, or tissue engineering applications. The immobilization process should allow control over the amount of protein, minimize nonspecific adsorption, and ensure the preservation of the biological activity of functional proteins. Substrates modification with polymer brushes, by polymer grafting, is a versatile approach for tailoring the physicochemical properties of the material and providing the necessary conditions for protein immobilization. For bioactive surfaces, stable covalent immobilization of protein is preferred, which can be easily achieved for polymer brushes by incorporation of the protein-reactive side chain functional groups. In turn, anti-fouling properties can be provided by the hydrophilic polymer chain, which are additionally advantageous for preserving the biological activity of immobilized proteins. Therefore, the fabrication of copolymer brush coating is a promising approach combining antifouling properties with high-capacity covalent protein binding [1][2].
In this work [3], we report the fabrication and comprehensive characterization of novel copolymer brush coatings based on 2-(2-methoxyethoxy)ethyl methacrylate (OEGMA) and methacrylic acid (MAA) for controlled protein immobilization. Random P(OEGMA-co-MAA) copolymer brushes were synthesized from silicon substrates using atom transfer radical polymerization (ATRP). Different proportions of OEGMA and MAA monomers are applied to optimize the balance between the antifouling properties of OEGMA and the density of the protein coupling species provided by MAA carboxyl groups after activation with EDC/NHS chemistry. X-ray photoelectron spectroscopy (XPS) and Time-of-flight Secondary Ion Mass Spectrometry (Tof-SIMS) were applied to evaluate the copolymer brush composition. The protein immobilization capacity of EDC/NHS activated brushes was examined for the immunoglobulin IgG antibody for different brush composition and protein solution concentrations. Additionally, nonspecific adsorption was determined for nonactivated brushes. Furthermore, the Tof-SIMS technique was applied for comprehensive characterization of the antibody functionalized copolymer brush coatings. Tof-SIMS depth profiling was applied for the first time to evaluate protein distribution through brush thickness and estimate protein loads per brush volume. The interfacial state of IgG molecules [4], involving dominant orientation and residue involvement in the coupling with MAA segments was investigated with PCA analysis of Tof-SIMS data.

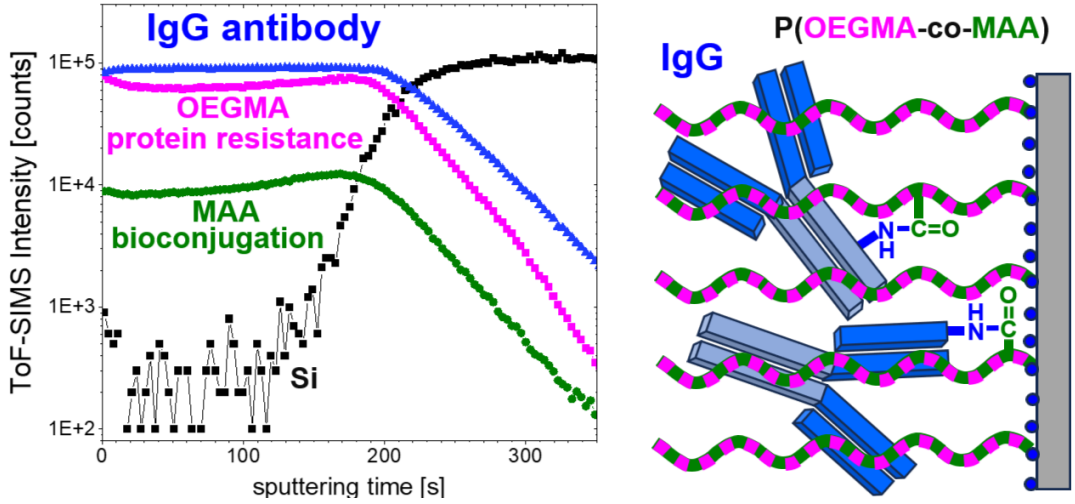

Figure 1 ToF-SIMS depth profiles of P(OEGMA-co-MAA) brush coatings followed by covalent immobilization of the IgG antibody enabled by the EDC/NHS activation of MAA segments. The plotted negative ions are characteristic for the silicon substrate (Si^- , black), OEGMA ($C_4H_5O_2^-$, pink) and MAA (C_4H^-, green) segments of the copolymer brush and the IgG protein (CNO^-, blue).

XPS and Tof-SIMS analysis of P(OEGMA-co-MAA) coating revealed the molar MAA fraction in the copolymer brush equal to that of the reaction mixture and a uniform composition through the brush, confirming a success random copolymerization. An amount of IgG protein covalently attached to EDC/NHS activated brushes and physical adsorbed to nonactivated brushes was compared for different P(OEGMA-co-MAA) composition with fluorescence microscopy and ToF-SIMS, revealing that a 0.25 molar fraction of MAA is optimal with the maximal load of the immobilized IgG antibody, while maintaining low fouling properties. Additionally, ToF-SIMS depth profiling clearly showed a uniform IgG distribution through the brush thickness and provided a total IgG mass per brush volume, reaching ~ 0.4 g/cm3 which is nine times higher than for IgG monolayer. Moreover, an amount of immobilized protein can be controlled by the brush composition and the applied concentration of protein solutions. The interfacial state of antibody was compared for the P(OEGMA-co-MAA) and PMAA brushes with PCA analysis of ToF-SIMS data to explain the enhanced antigen binding ratio for copolymer brush. The third principal component PC3 differentiated IgG-functionalized P(OEGMA-co-MAA) and PMAA brushes in terms of the surface composition of reactive and nonreactive to the EDC/NHS activated MAA segments amino acids, reflecting differences in the MAA segments density. In turn, the fourth principal component PC4 described the dominant antibody orientation, revealing the higher proportion of molecules in active tail-on orientation on copolymer brush, which is related to electrostatic interaction with IgG domain with negatively charged MAA segments. Finally, the biocompatibility of P(OEGMA-co-MAA) brush coatings was demonstrated for human fibroblast cell culture, further promoted by coatings functionalization with fibronectin.

Acknowledgements

This work was financed by the Polish National Science Centre (NCN) under Grant 2021/43/D/ST5/02231 and partially by “Laboratories of the Young” as part of the “Excellence Initiative – Research University” program at the Jagiellonian University in Kraków.

References

[1] M. Badoux, M. Billing, and H. A. Klok, “Polymer brush interfaces for protein biosensing prepared by surface-initiated controlled radical polymerization,” *Polym. Chem.*, vol. 10, no. 23, pp. 2925–2951, 2019, doi: 10.1039/c9py00163h.

[2] Q. Yu, Y. Zhang, H. Wang, J. Brash, and H. Chen, “Anti-fouling bioactive surfaces,” *Acta Biomater.*, vol. 7, no. 4, pp. 1550–1557, Apr. 2011, doi: 10.1016/j.actbio.2010.12.021.

[3] K. Gajos, O. Lishchynskyi, P. Dąbczyński, S. Tymetska, Ł. Bodek, Y. Shymborska, N. Janiszewska, Y. Stetsyshyn and A. Budkowski “Integrating Protein Resistance and Bioconjugation in P (OEGMA- co - MAA) Brushes for Biosensing and Cell Culture : ToF-SIMS Profiling and Antibody Characterization,” *ACS Appl. Mater. Interfaces*, vol. 18, no. 1, pp. 3122–3139, 2026, doi: 10.1021/acsami.5c19592.

[4] K. Gajos, K. Awsiuk, and A. Budkowski, “Controlling orientation, conformation, and biorecognition of proteins on silane monolayers, conjugate polymers, and thermo-responsive polymer brushes: investigations using TOF-SIMS and principal component analysis,” *Colloid Polym. Sci.*, vol. 299, pp. 385–405, 2021, doi: 10.1007/s00396-020-04711-7.

Synchrotron-Based XRD tomography and TEM analysis of 3D-Printed Tool Steels

V. Girman[a,b]*, D. Hrehova[a], S. Michalik[c], J. Bednarcik[a,d]*
[a] P. J. Šafárik University in Košice, Department of Solid State Physics, Park Angelinum 9, Košice
[b] Slovak Academy of Science, Institute of Materials Research, Watsonova 47, Košice
[c] Diamond Light Source Ltd, Harwell Science and Innovation Campus, Oxford, OX11 0DE, United Kingdom
[d] Slovak Academy of Science, Institute of Experimental Physics, Watsonova 47, Košice
*vladimir.girman@upjs.sk

Additively manufactured tool steels represent a technologically important class of materials in which the final performance is strongly governed by the phase composition, microstructural refinement and possible spatial heterogeneity introduced during rapid solidification [1]. In this work, the structure of a high-alloyed high-speed tool steel with the nominal composition Fe–Cr4–Mo1–V1–W8–C1 (wt.%) produced by powder bed fusion (PBF) was investigated using a combination of synchrotron X-ray diffraction, absorption X-ray tomography, X-ray diffraction computed tomography (XRD-CT) and transmission electron microscopy (TEM). The aim was to identify the dominant and minor phases, evaluate their spatial distribution in the cylindrical sample and assess the applicability of tomographic methods for phase-sensitive characterization of a fine PBF microstructure.

Experimental procedure

The studied material was prepared from gas-atomized powder in an argon atmosphere. The powder fraction used for PBF processing had a particle size of 20–63 µm. The cylindrical sample, with dimensions of approximately 2 mm in diameter and 6 mm in length, was manufactured using an SLM250HL system with a laser power of 150 W, a scanning speed of 400 mm s−1, a hatch spacing of 40 µm and a layer thickness of 60 µm. Synchrotron measurements were performed at the I12-JEEP beamline of Diamond Light Source using an X-ray energy of 109.28 keV, corresponding to a wavelength of 0.0113456 nm. Absorption tomography was carried out in transmission geometry using 2400 projections over 180°. XRD-CT was performed with a 50 × 50 µm² incident beam and a translation step of 0.05 mm; more than 11 000 diffraction patterns were collected in a quasi fly-scan mode. Selected diffraction patterns were evaluated by Rietveld refinement, while the tomographic reconstructions were complemented by TEM imaging, selected-area electron diffraction and SEM-EDS line analysis.

Results and discussion

A) Rietveld analysis confirmed that the PBF-processed steel is dominated by two crystalline phases: retained austenite with a FCC lattice and martensite with a BCC lattice. Across 7 representative positions selected along the sample cross-section, the austenite fraction ranged from 51.3 to 73.5 vol.%, whereas martensite was present in the range of 26.5 to 48.7 vol.%. No clear systematic radial gradient in the phase composition was observed. A particularly important result was that the martensitic phase did not exhibit a measurable tetragonal distortion [2].
B) Absorption tomography provided a reliable reconstruction of the macroscopic cylindrical geometry and revealed surface particles attached to the sample, most likely originating from partially fused powder. However, no direct contrast between austenite and martensite was observed (Figure 1). This behaviour is consistent with the calculated attenuation contrast at 109.28 keV. The linear attenuation coefficients were estimated as approximately 4.96 cm−1 for austenite and 4.82 cm−1 for martensite, corresponding to a relative difference of only about 3%. For a material path length of 1 mm, the absolute difference in transmittance was only about 0.009. Therefore, absorption tomography is suitable for visualizing the sample morphology and larger heterogeneities, but not for directly distinguishing the two structurally different yet chemically similar matrix phases [2].

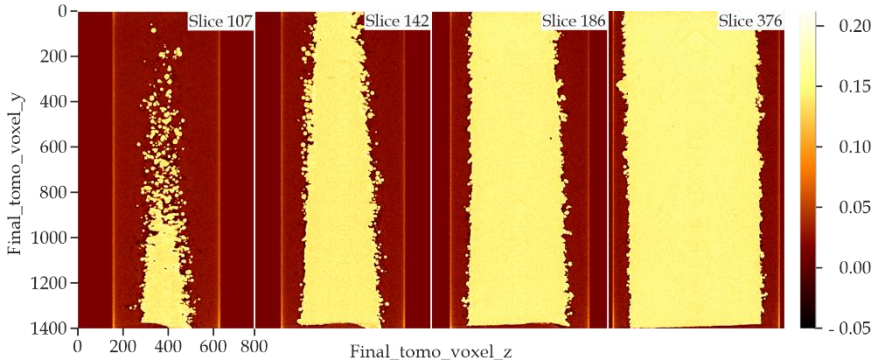

Figure 1 Selected slices from the reconstructed model of the sample volume segment, showing regions beneath the surface (107) and within the central area (376).

C) XRD-CT provided phase-sensitive diffraction information; however, its quantitative interpretation was limited by the overlap of austenite and martensite reflections, absorption effects, and the spatial averaging caused by the 50 × 50 µm² beam size. Initially, the tomographic reconstruction was carried out using the complete diffraction profiles. Although this approach preserved the overall diffraction response of the irradiated volume, it did not prove to be suitable for distinguishing subtle spatial variations in the phase-related signal, most likely due to the superposition of multiple diffraction contributions within the reconstructed intensity. A more meaningful indication was obtained by reconstructing the signal from selected diffraction peaks, specifically the austenite (200) reflection and the martensite (211) reflection. These peak-based reconstructions showed enhanced reconstructed intensity near the sample edges and revealed a weak indication of a changed relative contribution of the two phases in the radial direction. However, the semiquantitative analysis of masked central and edge regions indicated only a very small difference in the relative phase-related signal. The estimated austenite/martensite signal contribution was approximately 49.3/50.7% in the centre and 48.5/51.5% near the edge. These values should be interpreted only as relative reconstructed diffraction signal contributions rather than absolute phase fractions. The reconstructed intensity is influenced not only by the amount of the corresponding phase, but also by the selected reflections, structure factors, multiplicity, local texture, absorption effects, spatial averaging, and possible reconstruction artefacts. Therefore, the observed radial variation should be considered as a qualitative to semiquantitative indication of a slight change in the austenite/martensite-related diffraction response, rather than as a direct quantitative determination of the local phase fractions [2].

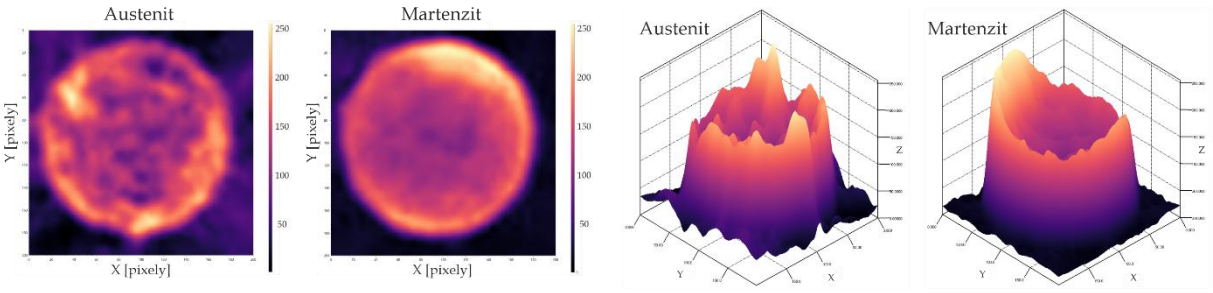

Figure 2 Reconstruction of 2D cross-sections of the investigated sample using one diffraction peak from each phase (left), together with their 3D representation, in which the Z-axis represents image intensity (right).

D) TEM analysis confirmed the coexistence of austenite and martensite and revealed a strongly refined microstructure. Although the initial powder particles had sizes of 30–60 µm, the final microstructure contained polyhedral grains with an average size of approximately 1 µm (Figure 3). Martensite occurred as lath-like and plate-like features inside prior austenitic grains. In the central part of the sample, coarser martensitic plates were observed, whereas near-surface regions contained finer and more densely distributed martensitic features, including locally observed burst-type athermal martensite (Figure 4). These morphological differences indicate a thermal gradient during solidification and cooling. Electron diffraction and SEM-EDS further showed the presence of minor carbide precipitates located preferentially at grain boundaries (Figure 5). These precipitates were interpreted as (W,Mo)6C and VC carbides, supporting the interpretation of weak unidentified reflections observed in the synchrotron diffraction patterns. Sporadic square plate-like amorphous features, shown on Figure 6, were also observed, although their chemical composition could not be determined [2].

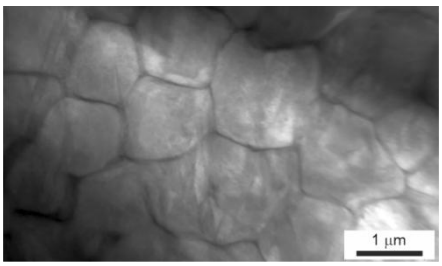

Figure 3 Typical microstructure of the analysed sample, showing austenitic grains containing martensitic plates. The grain boundaries are decorated by carbide phases, namely $(W,Mo)_6C$ and VC.

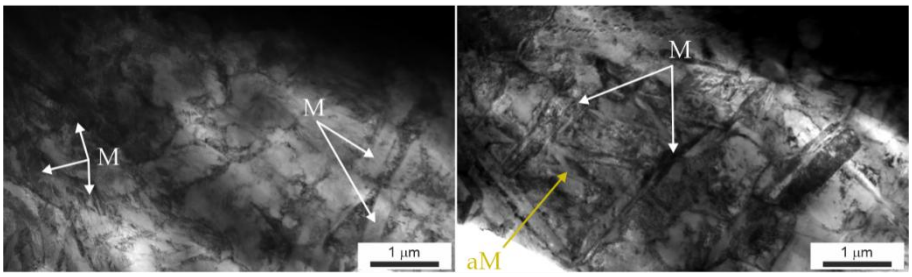

Figure 4 Characteristic microstructure observed in the centre of the sample (left) and near the edge (right). In the central region, the martensite plates (M) are thicker, whereas near the edge they become narrower and athermal martensite (aM) is also observed.

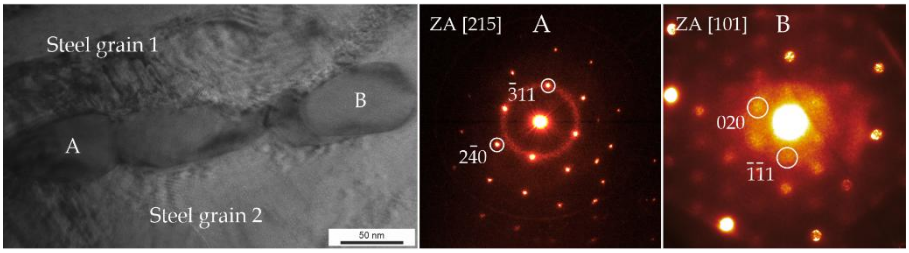

Figure 5 Detailed view of the grain boundaries. The nanoprecipitates were identified by electron diffraction. A - $(W,Mo)_6C$ and B – VC phases.

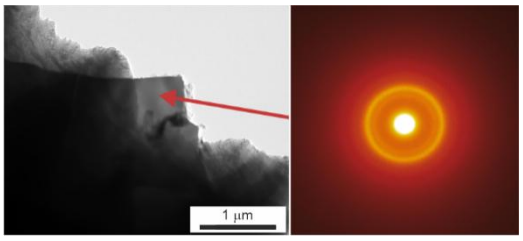

Figure 6 Unidentified amorphous plate-like features occasionally observed within the sample microstructure.

Conclusions

The combined use of synchrotron diffraction, X-ray tomography and TEM demonstrated that PBF processing of the investigated high-speed tool steel results in a complex, strongly refined, multiphase microstructure. Synchrotron diffraction confirmed austenite and martensite as the dominant phases, while TEM identified additional carbide precipitates of the $(W,Mo)_6C$ and VC types, as well as unidentified amorphous phase. Absorption tomography was effective for morphological inspection but insufficient for direct phase discrimination because of the weak attenuation contrast between the two main phases. XRD-CT provided spatially resolved phase-related information, although the present experimental configuration did not allow fully quantitative phase mapping due to peak overlap and spatial averaging. The results show that correlative characterization combining bulk synchrotron methods with local TEM analysis is essential for understanding the microstructure formation of PBF-processed tool steels.

Acknowledgements

This research was funded by the EU NextGenerationEU through the Recovery and Resilience Plan for Slovakia under the project No. 09I03-03-V03-00034, and co-funded by the research project VEGA 1/0638/24. Authors also acknowledge Diamond Light Source for time on the I12-JEEP beamline (cm40628-2).

References

[1] D. Herzog, V. Seyda, E. Wycisk, and C. Emmelmann, “Additive manufacturing of metals,” Acta Materialia, vol. 117, pp. 371–392, 2016.
[2] D. Hrehová, “ Structural study of 3D-printed tool steel using X-ray tomography.” Diploma Thesis, Pavol Jozef Šafárik University in Košice, 2026.

Refinement of Production of Biomimetic Ceramic Coating on Zinc Powder Grains for Biomaterial Preparation

R. Gorejova[a]*, I. Mojzisova[a], R. Orinakova[a]
[a] Department of Physical Chemistry, Institute of Chemistry, Pavol Jozef Šafárik University in Košice, Moyzesova 11, 041 54 Kosice, Slovak Republic
*radka.gorejova@upjs.sk

Zinc-based biodegradable materials represent a promising class of next-generation biomaterials due to their balanced corrosion behavior for temporary biomedical applications [1,2]. Their controlled degradation rate and essential physiological role of zinc make them particularly attractive for use in bioresorbable implants and tissue engineering [3]. Despite these advantages, the physical-chemical and biological properties of zinc-based biodegradable materials are still not fully optimal for all clinical applications, as they may exhibit insufficient mechanical strength, non-uniform degradation, or initial toxicity [4]. Therefore, surface and structural modifications are often required to enhance their performance, with ceramic coatings representing an effective strategy to improve corrosion resistance, biocompatibility, and overall functional stability. Calcium phosphates are particularly suitable coating materials due to their excellent biocompatibility, osteoconductivity, and chemical similarity to natural bone tissue, making them highly effective for improving the biological and protective performance of zinc-based biodegradable implants. Moreover, calcium phosphate coatings can be prepared biomimetically under mild conditions, enabling the formation of bone-like mineral layers that closely mimic natural biological processes and enhance surface integration [5].
The aim of this work was to biomimetically coat zinc powders with calcium phosphate layers and optimize the preparation methodology in order to obtain surface-modified powders suitable for subsequent use as precursor materials in the fabrication of biodegradable composites. Hydroxyapatite (HAp) layers were biomimetically deposited on zinc powders under controlled pH conditions (Figure 1) to promote uniform surface mineralization, followed by SEM and EDX analyses to verify the morphology, composition, and successful formation of the calcium phosphate coating (Figure 1b,c). The results demonstrated the successful preparation of particles with a homogeneously deposited coating layer on individual zinc grains, while EDX analysis confirmed the presence and uniform distribution of the calcium phosphate phase on the powder surface. Moreover, corrosion behavior of cold-pressed samples prepared from previously obtained powders was sutdied using potentiodynamic polarization method at constant temperature (37° Celsius) and pH (7.4) at Hank's balanced salt solution. Corrosion rates of the samples was calculated using Tafel extrapolation method (Figure 1d).

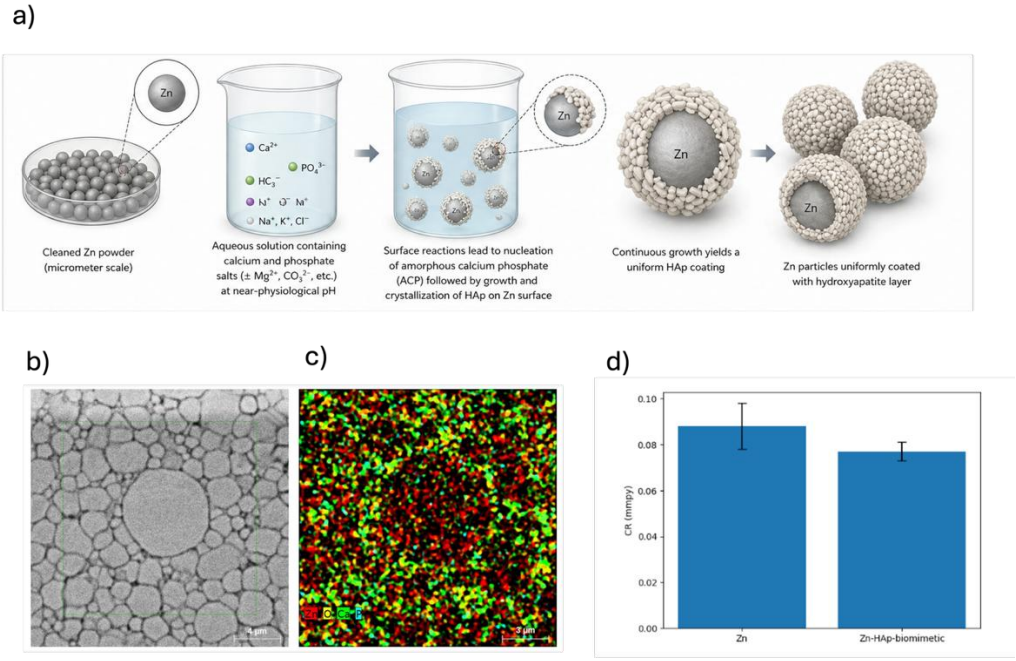

Figure 1 Biommimetic preparation of ceramic-coated zinc powder (a). Zinc powder with ceramic layer mostl found on the outer perifery (b,c). Corrosion rate comparison of pure Zn and Zn-ceramic cold-pressed samples obtained from PDP measurements (d).

Acknowledgements

This work was funded by the EU NextGenerationEU through the Recovery and Resilience Plan for Slovakia under the project ZETA no. 09I03-03-V04-00010.

References

[1] A. R. Khan, N. S. Grewal, C. Zhou, K. Yuan, H.-J. Zhang and Z. Jun, "Recent advances in biodegradable metals for implant applications: Exploring in vivo and in vitro responses," *Results in Engineering*, vol. 20, pp. 101526, Dec. 2023, doi: 10.1016/j.rineng.2023.101526.

[2] J. Cheng, B. Liu, Y. H. Wu, and Y. F. Zheng, "Comparative in vitro study on pure metals (Fe, Mn, Mg, Zn and W) as biodegradable metals," *J Mater Sci Technol*, vol. 29, no. 7, pp. 619–627, Jul. 2013, doi: 10.1016/j.jmst.2013.03.019.

[3] P. K. Bowen, J. Drelich, and J. Goldman, "Zinc Exhibits Ideal Physiological Corrosion Behavior for Bioabsorbable Stents," *Advanced Materials*, vol. 25, no. 18, pp. 2577–2582, May 2013, doi: 10.1002/adma.201300226.

[4] G. Katarivas Levy, J. Goldman, and E. Aghion, "The prospects of zinc as a structural material for biodegradable implants—a review paper," *Metals*, vol. 7, no. 10, p. 402, Oct. 2017, doi: 10.3390/met7100402.

[5] P. Habibovic, F. Barrère, C. A. Van Blitterswijk, K. de Groot and P. Layrolle, "Biomimetic hydroxyapatite coating on metal implants," *Journal of the American Ceramic Society*, vol. 85, no. 3, pp. 517–522, Mar. 2002, doi: 10.1111/j.1151-2916.2002.tb00126.x.

Electrolyte-Dependent Bifunctional Activity and Surface Reconstruction of MoNiP for Water Splitting

A. Guboova[a,b]*, Y. Katayama[a], Q. Su[a], M. Streckova[b]
[a] SANKEN, The University of Osaka, 8-1 Mihogaoka, Ibaraki City, Osaka, 567-0047 Japan
[b] Institute of Materials Research, Slovak Academy of Sciences, Watsonova 47, 040 01 Kosice, Slovak Republic
*a.guboova@sanken.osaka-u.ac.jp

Hydrogen evolution reaction (HER) and oxygen evolution reaction (OER) are the two key half-reactions in water electrolysis, offering a clean and sustainable pathway for hydrogen production. However, the widespread deployment of electrolyzers is hindered by the high cost and scarcity of precious metal catalysts such as Pt, Ru, and Ir [1], which exhibit the best activity and stability [2]. Consequently, significant research efforts have been devoted to developing efficient and durable alternatives based on earth-abundant transition metals [3].
Among non-noble metal catalysts, Ni-Mo compounds have emerged as highly efficient materials for water splitting due to their synergistic electronic interactions and structural versatility [4], [5].
In this work, a MoNiP catalyst was synthesized via a simple citric-acid assisted sol-gel route (complexation) followed by controlled calcination and reduction. It was systematically investigated as a non-precious electrocatalyst for HER and OER with a focus on its electrolyte-dependent electrochemical behaviour. Structural characterization confirmed the formation of the phosphide phase along with a minor contribution of molybdenum dioxide species. The catalyst was deposited on a glassy carbon electrode, and electrochemical measurements were carried out in acidic (0.5 M H_2SO_4, pH 0.3), neutral (0.5 M Na_2SO_4, pH 6), and alkaline media (0.1 M and 1 M KOH, pH 13 and 14 respectively).
The HER activity (Figure 1b) of the catalyst exhibited a strong dependence on the electrolyte. The highest performance was observed in acidic media, followed by alkaline conditions, while significantly lower activity was obtained in neutral electrolyte and diluted alkaline solution. This behaviour reflects the distinct mechanistic requirements of HER across different pH environments and highlights the role of electrolyte composition in governing hydrogen evolution kinetics. In contrast, the OER performance (Figure 1c) revealed a markedly different trend, with significant catalytic activity observed exclusively in alkaline media.

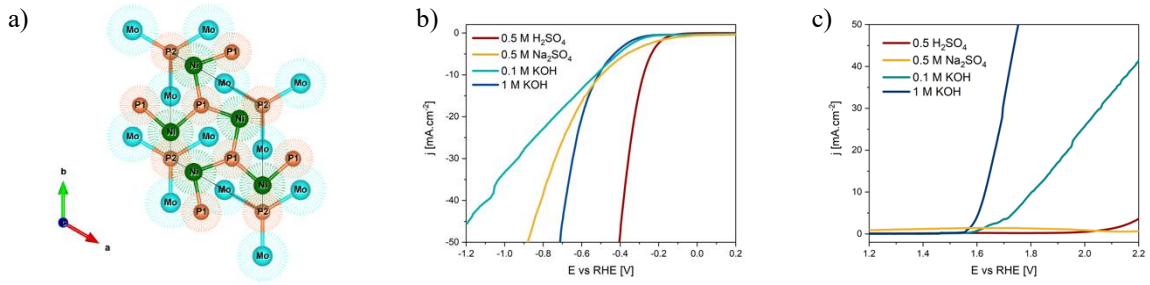

Figure 4 a) Structural representation of the MoNiP catalyst. b) linear sweep voltammetry (LSV) curves for HER, and c) LSV curves for OER in 0.5 M H_2SO_4 (pH 0.3), 0.5 M Na_2SO_4 (pH 6), 0.1 M KOH (pH 13), and 1 M KOH (pH 14).

Cyclic voltammetry (CV) provided key insights into the underlying processes (Figure 2). In KOH, the initial cycle exhibited broad oxidation features accompanied by elevated current densities indicative of irreversible surface processes and catalyst activation. In subsequent cycles, well-defined and reversible redox peaks emerged, corresponding to the Ni^{2+}/Ni^{3+} transition. These features are attributed to the formation of a NiOOH-like phase, which is widely recognized as the active species for OER in Ni-based systems. The stabilization of these redox peaks upon cycling confirms the establishment of a stable electrochemically active surface.
In neutral and acidic media, only large oxidation currents were observed during the initial cycle, followed by a rapid decrease in current and the absence of distinct redox features in subsequent scans. This indicates that the processes are predominantly irreversible and do not result in the formation of a stable redox-active phase. In acidic conditions, this behaviour can be associated with the dissolution of Ni species, while in neutral media the limited availability of hydroxide ions inhibits the formation of the NiOOH active phase. Differences in the observed capacitive current between different electrolytes are attributed to variations in double-layer structure arising from electrolyte composition, including ion identity, specific adsorption effects, and differences in surface chemistry.
These results demonstrate that MoNiP acts as a precatalyst, undergoing in situ surface reconstruction in alkaline media to form a NiOOH-based active phase responsible for OER activity. While the electrochemical response is dominated by nickel redox transitions, the presence of molybdenum, including minor oxide contributions, is

expected to influence the electronic structure and facilitate charge transfer, thereby contributing indirectly to catalytic performance.

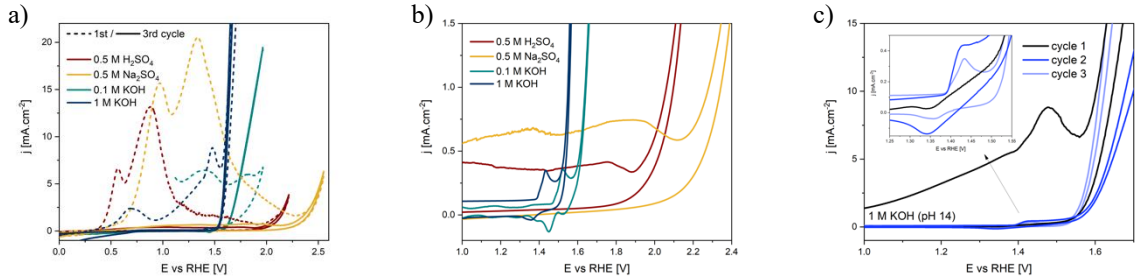

Figure 5 a) OER CV curves recorded in different electrolytes. Dashed lines correspond to the first cycle, while solid line represent the third cycle, b) enlarged CV curves of 3rd cycle in the OER region highlighting the appearance of readox peaks corresponding to Ni^{2+}/Ni^{3+} redox transitition, indicative of in situ surface reconstruction into a NiOOH-like active phase c)CVs in 1 M KOH over three consecutive cycles. The inset highlights the second and third cycle.

In situ Raman spectroscopy (Figure 3) revealed progressive surface reconstruction during the first cycle, characterized by the emergence of NiOOH bands (~495 and ~568 cm^{-1}), Mo-O vibrations (~745 cm^{-1}), and increased low-frequency intensity associated with Ni-O lattice formation. In the second cycle, the reconstructed surface persists and exhibits enhanced Raman intensity predominantly during the reduction sweep, indicating continued structural reorganization. By the third cycle, the catalyst reaches a stable state, with Raman activity localized in the oxidation region, corresponding to reversible Ni^{2+}/Ni^{3+} redox transitions.

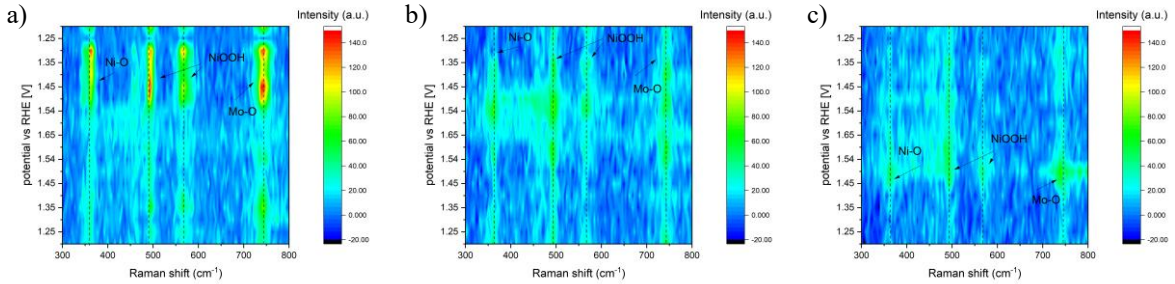

Figure 3 Heatmaps of in situ Raman spectra collected over three cycles, illustrating catalyst activation in the first cycle and the transition to stable redox behavior in subsequent cycles.

Overall, this study highlights the electrolyte-dependent dual functionality of MoNiP, combining efficient HER activity with a reconstruction-driven OER mechanism. The findings emphasize the critical role of in situ transformation in determining catalytic behaviour and provide insights into the rational design of transition metal phosphide-based electrocatalysts for water splitting. Ongoing operando spectroscopic studies aim to directly probe the formation of the active phase under reaction conditions and further elucidate the reconstruction mechanism.

Acknowledgements

This work was supported by JSPS KAKENHI Grant Number JP 25KF0149.

References

[1] M. M. H. Rocky, I. M. M. Rahman, M. Endo, and H. Hasegawa, “Comprehensive insights into aqua regia based hybrid methods for efficient recovery of precious metals from secondary raw materials,” *Chemical Engineering Journal*, vol. 495, pp. 153537, Sep. 2024, doi: 10.1016/j.cej.2024.153537.

[2] R. Qin, G. Chen, X. Feng, J. Weng and Y. Han, “Ru/Ir-Based Electrocatalysts for Oxygen Evolution Reaction in Acidic Conditions: From Mechanisms, Optimizations to Challenges,” *Advanced Science*, vol. 11, no. 21, pp. 2309364, Jun. 2024, doi: 10.1002/advs.202309364.

[3] J. Guo, Y. Haghshenas, Y. Jiao, P. Kumar, B. I. Yakobson, A. Roy, Y. Jiao, K. Regenauer-Lieb, D. Nguyen and Z. Xia, “Rational Design of Earth-Abundant Catalysts toward Sustainability,” *Advanced Materials*, vol. 36, no. 42, pp. 2407102, Oct. 2024, doi: 10.1002/adma.202407102.

[4] B. Qiu, D. Zhang, R. Fang, Y. Wang, B. Shen, J. Dai and H. Chu, “In situ synthesis of Ni, Mo bimetallic crystalline-amorphous co-existing heterostructures for efficient hydrogen evolution reaction,” *Compos B Eng*, vol. 307, pp. 112956, Nov. 2025, doi: 10.1016/j.compositesb.2025.112956.

[5] S. Sarfraz, N. Khan, M. Zahra, Manzar, K. H. Shah, M. Javed, Mohsin, A. Zidan, Ammar, A. Bahadur, S. Iqbal, S. Mahmood, A.-E. Farouk and S. Aloufi, "Toward Efficient Hydrogen Generation Using Nickel-Molybdenum Catalyst and Its Environmental Sustainability," *Microsc Res Tech*, vol. 88, no. 4, pp. 999–1006, Apr. 2025, doi: 10.1002/jemt.24762.

Lithium-Sulfur Batteries: An Overview of Advantages and Disadvantages

F. Chovancova[a]*, V. Niscakova[a], I. Sisolakova[a], A. Fedorkova[a]
[a] Department of Physical Chemistry, Institute of Chemistry, Pavol Jozef Šafárik University in Košice, Moyzesova 11, 041 54 Kosice, Slovak Republic
*frederika.chovancova1@student.upjs.sk

Lithium-ion batteries have dominated the portable electronics and electric vehicle markets for decades because of their high energy density, long cycle life, and mature manufacturing infrastructure. However, conventional intercalation-based lithium-ion chemistries are approaching practical limits in gravimetric and volumetric energy density, creating the need for alternative electrochemical storage systems capable of meeting future demands in transportation, grid storage, and high-performance portable devices. Among the most promising post-lithium-ion technologies, lithium–sulfur (Li–S) batteries have attracted sustained attention due to their exceptionally high theoretical specific capacity and energy density, low material cost, and the natural abundance of sulfur [1,2].

Li–S batteries employ a metallic lithium anode and a sulfur-based cathode operating through multistep conversion reactions involving soluble lithium polysulfide intermediates. Sulfur offers a theoretical specific capacity of 1675 mAh g^{-1}, while lithium metal provides 3860 mAh g^{-1}, enabling projected energy densities substantially higher than those of state-of-the-art lithium-ion systems. In addition to their electrochemical advantages, sulfur is inexpensive, widely available, and environmentally benign, which makes Li–S technology particularly attractive for large-scale and sustainable energy storage applications [3,4].

Despite these advantages, the practical deployment of Li–S batteries remains constrained by several fundamental materials and interfacial challenges. The intrinsically low electronic conductivity of sulfur and its final discharge products (Li_2S/Li_2S_2) limits active material utilization and rate capability. A major issue is the polysulfide shuttle effect, caused by dissolution of long-chain lithium polysulfides into the electrolyte and their migration between electrodes, resulting in active material loss, low coulombic efficiency, and rapid capacity fading. Furthermore, sulfur undergoes significant volume expansion during lithiation, which can compromise cathode structural integrity and electrode contact. On the anode side, lithium dendrite growth and unstable solid-electrolyte interphase formation create substantial safety risks and shorten cell lifetime [1,5].

Addressing obstacles requires integrated materials engineering strategies targeting both electrodes and the electrolyte. Considerable attention has been directed toward conductive and polar sulfur host matrices, porous carbon architectures, catalytic additives, separator modifications, and multifunctional interlayers capable of physically confining and chemically adsorbing polysulfides. In parallel, electrocatalytically active materials can accelerate the redox conversion of sulfur species, reducing polarization and improving sulfur utilization. Advanced electrolyte formulations, including high-concentration electrolytes, localized high-concentration systems, and solid-state or quasi-solid-state electrolytes, also represent promising routes for suppressing shuttle phenomena while enhancing interfacial stability [6,7,8].

Future progress in Li–S batteries will likely depend on synergistic optimization of cathode architecture, lithium metal protection strategies, electrolyte chemistry, and scalable manufacturing approaches. With continued advances in interfacial science and functional materials design, Li–S technology remains a strong candidate for next-generation rechargeable batteries with significantly enhanced energy-storage capability [9].

However, several key challenges still need to be addressed before widespread commercialization, such as the inherent electrical insulating nature of sulfur and its discharge products, significant volume changes during cycling, and the notorious "shuttle effect" of lithium polysulfides [10]. These issues contribute to low active material utilization, rapid capacity decay, and safety concerns, hindering the practical application of liquid electrolyte-based Li-S batteries [11].

Acknowledgements

This work has been funded by the Recovery and Resilience Plan for Slovakia under the project SUNFLOWERS no. 09I02-03-V01-00022.

References

[1] X. Yang, X. Li, K. R. Adair, H. Zhang, and X. Sun, “Structural Design of Lithium–Sulfur Batteries: From Fundamental Research to Practical Application,” *Electrochem. Energy Rev.* , vol. 1, no. 3, p. 239, Jun. 2018, doi: 10.1007/s41918-018-0010-3.

[2] C. Wu, T.-C. Chan, and S. Chung, “Metal-based composite sulfur cathodes for lithium–sulfur electrochemical cells,” *Commun. Mater.* , vol. 6, no. 1, Jun. 2025, doi: 10.1038/s43246-025-00835-x.

[3] A. Manthiram, S. Chung, and P. Chen, “Lithium–Sulfur Batteries: Progress and Prospects,” *Adv. Mater.* , vol. 27, no. 12, p. 1980, Feb. 2015, doi: 10.1002/adma.201405115.

[4] B. B. Gicha, L. T. Tufa, N. Nwaji, X. Hu, and J. Lee, "Advances in All-Solid-State Lithium–Sulfur Batteries for Commercialization," *Nano-Micro Lett.* , vol. 16, no. 1. Springer Science+Business Media, Apr. 15, 2024. doi: 10.1007/s40820-024-01385-6.
[5] P. B. T, S. Choudhury, and E. E. Marinero, "Polymer-Based Solid-State Electrolytes For Lithium–Sulfur Batteries," *ACS Appl. Polym. Mater.*, Jun. 2025, doi: 10.1021/acsapm.5c01559.
[6] J. Li, L. Gao, F. Pan, C. Gong, L. Sun, H. Gao, J. Zhang, Y. Zhao, G. Wang, H. Liu, *et al.* , "Engineering Strategies for Suppressing the Shuttle Effect in Lithium–Sulfur Batteries," *Nano-Micro Lett.* , vol. 16, no. 1. Springer Science+Business Media, Nov. 10, 2023. doi: 10.1007/s40820-023-01223-1.
[8] G. D. Donato, T. Ates, H. Adenusi, A. Varzi, M. A. Navarra, and S. Passerini, "Electrolyte Measures to Prevent Polysulfide Shuttle in Lithium-Sulfur Batteries," *Batter. Supercaps* , vol. 5, no. 7, Apr. 2022, doi: 10.1002/batt.202200097.
[9] J. Ke, Z. Wang, H. Zhu, M. Chen, R. Song, Q. Ji, D. Liu, S. Lan, "Suppression strategies for the polysulfide shuttle effect in electrolyte systems," *Commun. Mater.*, vol. 6, no. 1, Nov. 2025, doi: 10.1038/s43246-025-00953-6.
[10] E. T. Gedif, "Addressing the Key Challenges of Lithium-Sulfur Batteries: A Comprehensive Overview and Future Perspectives," *ECS Meet. Abstr.* , no. 2, p. 309, Aug. 2024, doi: 10.1149/ma2024-012309mtgabs.
[11] H. Pan, Z. Cheng, Z. Zhou, S. Xie, W. Zhang, N. Jan, W. Guo, J. Fransaer, J, Luo, A. Cabot, M. Wubbenhorst, "Boosting Lean Electrolyte Lithium–Sulfur Battery Performance with Transition Metals: A Comprehensive Review," *Nano-Micro Lett.* , vol. 15, no. 1. Springer Science+Business Media, Jun. 29, 2023. doi: 10.1007/s40820-023-01137-y.
[12] B. Qi, X. Hong, Y. Jiang, J, Shi, M. Zhang, W. Yan, C. Lai, "A Review on Engineering Design for Enhancing Interfacial Contact in Solid-State Lithium–Sulfur Batteries," *Nano-Micro Lett.* , vol. 16, no. 1. Springer Science+Business Media, Jan. 04, 2024. doi: 10.1007/s40820-023-01306-z.

Molecularly Imprinted Electrochemical Sensor for Vancomycin: Performance Comparison with Non-Imprinted Counterparts

N. Jasnakova[a]*, J. Shepa[a], I. Sisolakova[a], R. Orinakova[a]
[a] Department of Physical Chemistry, Institute of Chemistry, Pavol Jozef Šafárik University in Košice, Moyzesova 11, 041 54 Kosice, Slovak Republic
*nikola.jasnakova@upjs.sk

Introduction

Vancomycin (VAN) has been used for several decades in the treatment of severe bacterial infections, during which a gradual selection of resistant bacterial strains has been observed in clinical practice [1]. For this reason, therapeutic drug monitoring of vancomycin plasma concentrations is essential, primarily for two key reasons: (i) prevention of adverse toxic effects in patients and (ii) minimisation of the risk of emergence and spread of antimicrobial resistance [2].

In recent years, considerable research attention has been devoted to the development of electrochemical biosensors based on molecularly imprinted polymers (MIP), which represent a promising platform for rapid, cost-effective, and highly selective detection of vancomycin. MIP systems exhibit significant potential due to their ability to selectively rebind target molecules that serve as templates during their synthesis [2, 3, 4]. This characteristic makes them suitable for analytical applications requiring high selectivity in complex biological matrices.

Experiment

A Metrohm DropSens SPCE was functionalized with a polypyrrole-based MIP layer prepared via in situ electropolymerization. The precursor solution consisted of pyrrole (0.2 M; 2.5 mL) and vancomycin (0.016 g) dissolved in 7.5 mL acetate buffer. Electropolymerization was carried out using cyclic voltammetry in the potential range of – 0.1 to 1.2 V at a scan rate of 50 $mV \cdot s^{-1}$ for 25 cycles.

Template removal was achieved by controlled overoxidation in 0.1 M NaOH (− 1.3 V to +1.2 V; 100 $mV \cdot s^{-1}$; 20 cycles), resulting in the formation of specific binding cavities complementary to the vancomycin molecule. In parallel, a non-imprinted polymer (NIP) was prepared under identical conditions but in the absence of the template molecule to evaluate the selectivity of the imprinting process.

Electrochemical response was evaluated in phosphate-buffered saline (PBS), adjusted with 1 M NaOH, within a potential window of –0.6 to 1.0 V at concentrations of 500, 250, and 125 μM.

Results and discussion

The electrochemical response of molecularly imprinted polymer (MIP) and non-imprinted polymer (NIP) sensors toward VAN shows clear differences in the low-potential region around E ≈ 0.15 V. In this region, a weak but reproducible signal is observed, which is significantly more pronounced and concentration-dependent for the MIP sensor compared to the NIP control. For the MIP, the current increases systematically with increasing VAN concentration (125–500 μM), indicating preferential analyte binding within the imprinted sites.

This response occurs before the onset of dominant faradaic processes at higher potentials, suggesting that the signal is primarily governed by interfacial effects associated with molecular recognition. In contrast, the NIP sensor exhibits only a weak and poorly defined response, comparable to the blank electrolyte (NaOH/PBS), reflecting the absence of specific binding sites.

The distinct behaviour of MIP and NIP sensors in this low-potential region identifies E ≈ 0.15 V as a sensitive window for detecting imprinting effects. In this regime, the signal arises mainly from interfacial capacitive contributions rather than direct analyte oxidation, enabling efficient transduction of binding events into measurable electrochemical responses [5].

Overall, these results demonstrate that molecular imprinting enhances both the selectivity and sensitivity of the sensor and allows reliable discrimination between different analyte concentrations. The observed differences between MIP and NIP systems confirm the successful formation of functional binding sites essential for vancomycin detection.

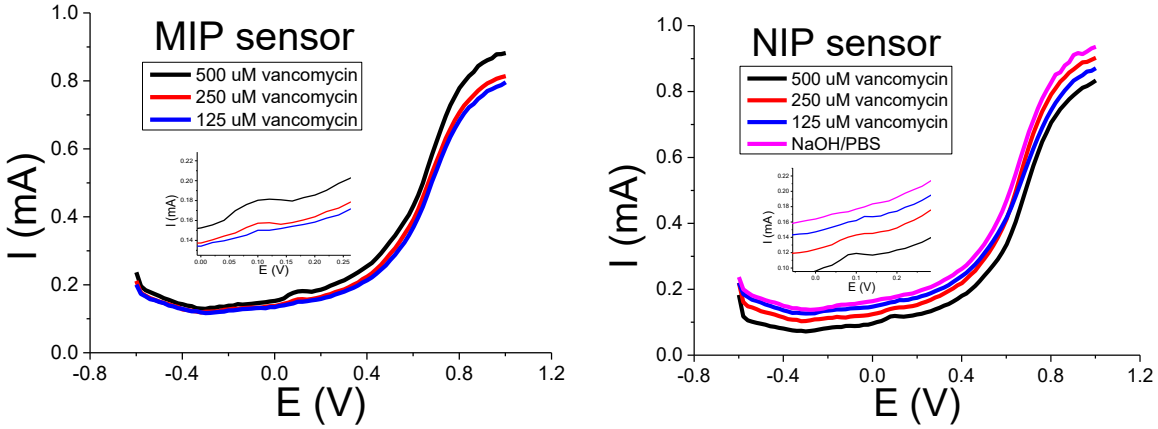

Figure 1 Electrochemical response of NIP and MIP sensors toward vancomycin.

Acknowledgements

This work was funded by the EU NextGenerationEU through the Recovery and Resilience Plan of the Slovak Republic under project no. 09-I05-03-V02-00047

References

[1] K. Sisodia, A. Panda, H. Haridas, D. Rynga, D. Kumar, and R. Gaind, "Vancomycin MIC creep and the emergence of oxacillin-susceptible MRSA: A three-year surveillance study from a tertiary care centre," *New Microbes New Infect.*, vol. 71, p. 101742, Jun. 2026, doi: 10.1016/j.nmni.2026.101742.

[2] A. M. Gaber, H. M. Emara, and N. K. Allam, "Electrochemical biosensors for vancomycin monitoring in blood: advances, strategies, and future perspectives," *RSC Adv.*, vol. 15, no. 49, pp. 41418–41431, 2025, doi: 10.1039/D5RA07262J.

[3] L. Díaz-Villavicencio, A. N. Baeza-Fonte, M. D. Luaces-Alberto, A. C. Valdés-González, Y. E. Milián-Rodríguez, and A. R. Lazo-Fraga, "Vancomycin selective electrode based on molecularly imprinted polymer," *Chemical Papers*, vol. 78, no. 1, pp. 165–172, Jan. 2024, doi: 10.1007/s11696-023-03051-4.

[4] C. Ye *et al.*, "Study on the properties and reaction mechanism of polypyrrole@norfloxacin molecularly imprinted electrochemical sensor based on three-dimensional CoFe-MOFs/AuNPs," *Electrochim. Acta*, vol. 379, p. 138174, May 2021, doi: 10.1016/j.electacta.2021.138174.

[5] S. El-Akaad, M. A. Mohamed, N. S. Abdelwahab, E. A. Abdelaleem, S. De Saeger, and N. Beloglazova, "Capacitive sensor based on molecularly imprinted polymers for detection of the insecticide imidacloprid in water," *Sci. Rep.*, vol. 10, no. 1, p. 14479, Sep. 2020, doi: 10.1038/s41598-020-71325-y.

Phase Evolution and Cell–Material Interactions in a Composite Calcium Phosphate System

A. Jelonek[a]*, M. Martyniak[b]
[a,b] Biovico Sp. z o. o., ul. Hutnicza 15 B, 81-061 Gdynia, Poland
*agnieszka.jelonek@biovico.com

Introduction

Calcium phosphate bone cements (CPCs) are widely used as biomaterials for bone defect filling due to their biocompatibility and osteoconductive properties [1], [2]. Their clinical usefulness, however, is limited by relatively slow remodeling *in vivo*, making modification of their composition desirable to promote faster mineral conversion and a more favorable cellular response [1]. In the present work, a composite setting paste (CSP) containing octacalcium phosphate (OCP) [3], lecithin-modified nanohydroxyapatite [4,5], and a methacrylate derivative of 4-aminosalicylic acid (PHMA) [6,7] was developed. OCP can act as a precursor of apatite calcium phosphates under physiological conditions [3], while lecithin-modified nHAp may improve the biological activity of the CSP [4], [5]. In turn, the PHMA composite additive may interact with Ca^{2+} ions and facilitate apatite nucleation through complexation phenomena [6], [7] and improve the washout resistance of the CSP. The proposed formulation was evaluated with respect to phase evolution, osteogenic gene expression, and mineralization potential.

Materials and methods

CSP formulations were allowed to set for 72 h in PBS (37 °C, with daily medium exchange). After rinsing with distilled water and ethanol, the samples were dried and ground into powder. Phase composition was analyzed by powder X-ray diffraction (XRD). The effect of 10% cement extracts on osteogenic response was investigated in MG-63 cells after 10 days of exposure by quantitative PCR. Expression of osteonectin, osteocalcin, osterix, RUNX2, BMP4, and BMP7 was normalized to reference genes. Mineralization potential was assessed in Saos-2 cells using Alizarin Red S staining to detect calcium-rich deposits and quantify the progression of mineral formation. The effect of PHMA polymer addition on washout resistance of the CSP was evaluated by measuring the static and dynamic disintegration coefficients (according to ISO/DIS 18531).

Results and discussion

XRD analysis demonstrated progressive phase transformation of CPS toward a hydroxyapatite-dominated structure during incubation under physiological conditions (37 °C, PBS), consistent with a dissolution–reprecipitation maturation pathway. This behavior indicates that the designed formulation remains chemically active under physiological conditions and evolves toward a more stable apatite phase. (Figure 1).

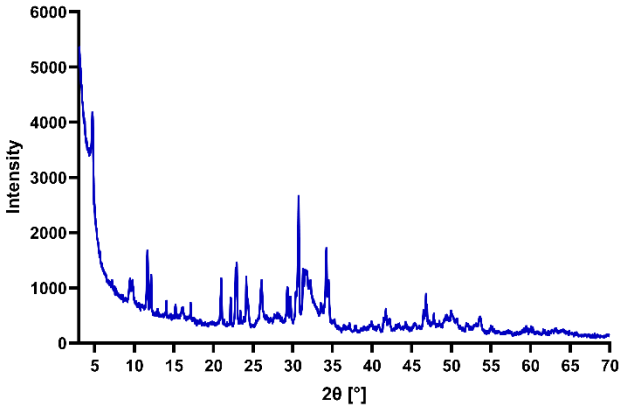

Figure 1 Example diffractogram of a CSP sample after 72 hours of incubation in PBS (37°C).

In MG-63 cells cultured with cement extracts, the expression of osteogenic markers remained comparable to the control, indicating no inhibitory effect on osteogenic activity. A trend toward higher expression of osteonectin, RUNX2, and BMP4 was observed for the formulation containing lecithin-modified nanohydroxyapatite compared with the corresponding formulation without lecithin. Mineralization assays further demonstrated enhanced calcium deposition in Saos-2 cultures exposed to CSP extracts relative to control conditions and reference hydroxyapatite bone cement with chitosan (Reference material 2), which supports the pro-mineralizing character of the composite system (Figure 2).

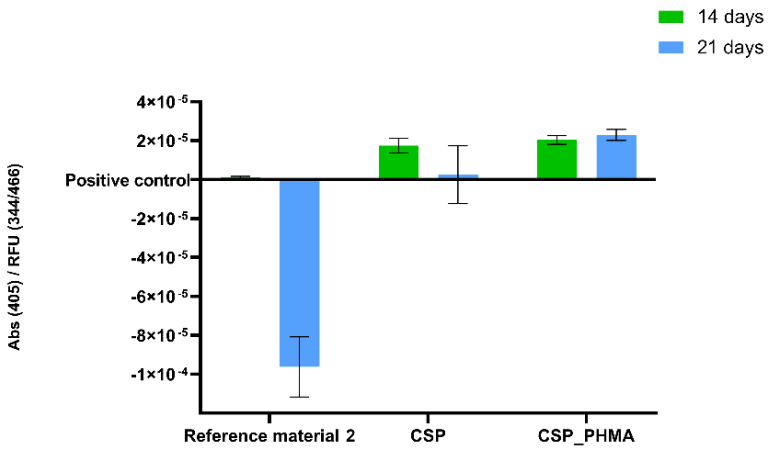

Figure 2 Effect of 10% CP cement extracts on the mineralization of Saos-2 cells after 14 and 21 days of incubation. Results presented as absorbance normalized to DNA quantity.

Washout test showed that composite setting paste with PHMA (CSP_PHMA) exhibit a lower static disintegration coefficient and a higher dynamic disintegration coefficient compared to composition without PHMA (CSP) and two reference cements: hydroxyapatite bone cement (Reference material 1) and hydroxyapatite bone cement with chitosan (Reference material 2). The obtained results indicate that the cement containing PHMA essentially did not undergo disintegration under the test conditions (Figure 3).

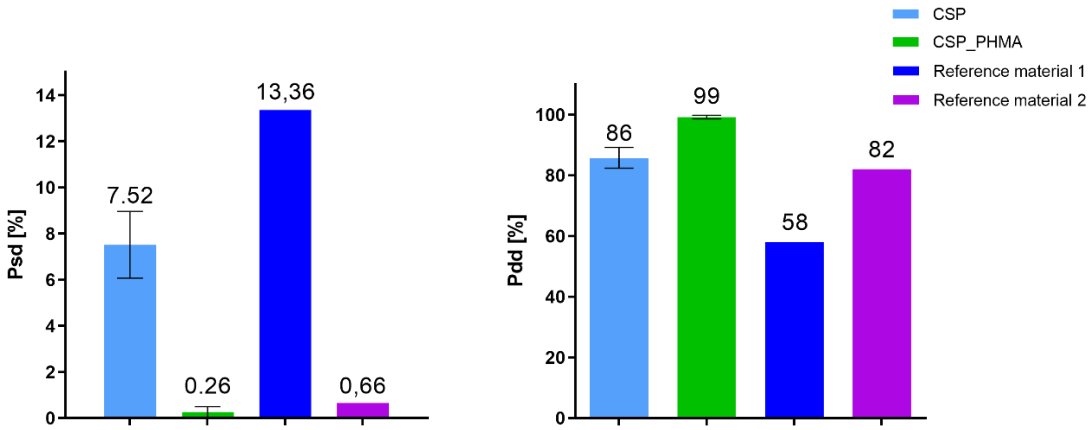

Figure 3 Static (Psd) and dynamic (Pdd) disintegration coefficients of tested Composite Setting Pastes with PHMA (CSP_PHMA), without PHMA (CSP), and reference cements.

Conclusions

The developed composite setting paste undergoes controlled phase transformation toward a hydroxyapatite-dominated structure under physiological conditions, confirming its chemically active and metastable character. The incorporation of lecithin-modified nanohydroxyapatite was associated with a tendency toward enhanced expression of selected osteogenic markers, indicating modulation of cell–material interactions. In parallel, the composite system promoted mineral deposition and exhibited high resistance to disintegration in the presence of PHMA, demonstrating the role of compositional design in tuning both physicochemical stability and biological response. These findings highlight the potential of engineered calcium phosphate composites as multifunctional materials with controllable phase evolution and bioactivity.
The solution described in the abstract is part of a patent application PL P.448989.

Acknowledgements

Research co-financed under the Smart Growth Operational Program (POIR) for the years 2014–2020, grant no. POIR.04.01.04-00-0133/15 entitled Innovative polymer composites for filling bone defects.

References

[1] M. Bohner, U. Gbureck, and J. E. Barralet, "Technological issues for the development of more efficient calcium phosphate bone cements: a critical assessment," *Biomaterials*, vol. 26, no. 33, pp. 6423–6429, Nov. 2005, doi: 10.1016/j.biomaterials.2005.03.049.

[2] N. Eliaz and N. Metoki, "Calcium Phosphate Bioceramics: A Review of Their History, Structure, Properties, Coating Technologies and Biomedical Applications," *Materials*, vol. 10, no. 4, pp. 334, 2017, doi: 10.3390/ma10040334.

[3] O. Suzuki, Y. Shiwaku, and R. Hamai, "Octacalcium phosphate bone substitute materials: Comparison between properties of biomaterials and other calcium phosphate materials," *Dent. Mater. J.*, vol. 39, no. 2, pp. 187–199, Mar. 2020, doi: 10.4012/dmj.2020-001.

[4] M. Wojasiński, E. Duszyńska and T. Ciach, "Lecithin-based wet chemical precipitation of hydroxyapatite nanoparticles," *Colloid Polym. Sci.*, vol. 293, pp. 1561–1568, Mar. 2015, doi: 10.1007/s00396-015-3557-0.

[5] B. Han, B. Tang, and M. E. Nimni, "Combined effects of phosphatidylcholine and demineralized bone matrix on bone induction," *Connect. Tissue Res.*, vol. 44, no. 3–4, pp. 160–166, 2003, doi: 10.1080/03008200390215863.

[6] C. Elvira and J. San Roman, "Complexation of polymeric drugs based on polyacrylic chains with aminosalicylic acid side groups," *J. Mater. Sci. Mater. Med.*, vol. 8, no. 12, pp. 743–746, Dec. 1997, doi: 10.1023/A:1018504410878.

[7] B. L. Rivas, "Analysis of the interactions of biologically active poly(methacrylic-aminosalicylic acid) supports with Ca2+ and Zn2+ by ultrafiltration," *J. Membr. Sci.*, vol. 192, no. 1-2, pp. 187–191, Oct. 2001, doi: 10.1016/S0376-7388(01)00497-5.

Metal-Modified GaTCPP MOFs: Structure Preservation and Application in Electrochemical Sensing

N. Kiraly[a]*, P. Obsatnik[a], J. Shepa[b], J. Demeterova[b], S. Kiraly[b], I. Sisolakova[b]
D. Volavka[c], M. Almasi[a], R. Orinakova[b], V. Zelenak[a]
[a] Department of Inorganic Chemistry, Institute of Chemistry, Pavol Jozef Šafárik University in Košice, Moyzesova 11, 041 54 Kosice, Slovak Republic
[b] Department of Physical Chemistry, Institute of Chemistry, Pavol Jozef Šafárik University in Košice, Moyzesova 11, 041 54 Kosice, Slovak Republic
[c] Department of Condensed Matter Physics, Pavol Jozef Šafárik University in Košice, Jesenná 9, 041 54 Kosice, Slovak Republic
*nikolas.kiraly@upjs.sk

Metal–organic frameworks (MOFs) are a versatile class of crystalline porous materials formed by the coordination of metal ions or clusters with multifunctional organic ligands. Their high surface area, tunable porosity, and chemical versatility make them attractive for applications in catalysis, sensing, energy storage, and biomedicine [1]. In electrochemical sensing, MOFs are particularly promising due to their accessible active sites and ability to promote selective host–guest interactions, which can significantly enhance detection performance [2].
In this work, a porphyrin-based MOF, GaTCPP, was synthesized and further modified via post-synthetic metalation to obtain M(II)-functionalized materials (M = Cu, Zn, Co). The parent framework, constructed from Ga(III) ions and tetrakis(4-carboxyphenyl)porphyrin (H_6TCPP), was prepared solvothermally and structurally confirmed by SC-XRD. Subsequent incorporation of transition metal ions into the porphyrin core was achieved under controlled conditions, yielding stable microporous materials.
Comprehensive characterization by PXRD, FTIR, XPS, microscopy, and gas adsorption confirmed the preservation of structural integrity and porosity after post-synthetic modification, together with homogeneous metal distribution. Cyclic voltammetric measurements showed that post-synthetic metalation changes the electrochemical response of GaTCPP-MOF in PBS and in the presence of ciprofloxacin.

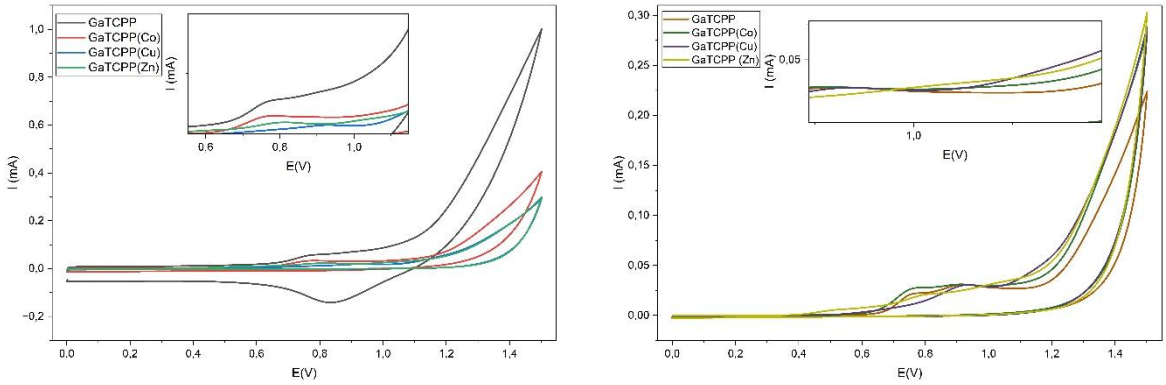

Figure 6 Cyclic voltammograms of GaTCPP-MOF and post-synthetically metal-modified analogues recorded in PBS (left) and in the presence of ciprofloxacin (right), showing the effect of metalation on the electrochemical response of the framework.

In PBS, the parent GaTCPP-MOF showed a much higher current response than the post-synthetically metalated analogues and also displayed a visible reductive peak. This suggests that the non-metalated framework contains electroactive sites that become partly occupied or affected after metalation, which changes its original electrochemical response. In the presence of ciprofloxacin, the voltammetric response showed two peaks. First around 0.75 V, related mainly to the MOF framework, and second around 0.95 V, related to the ciprofloxacin oxidation. In this region, the Zn-functionalized material showed the highest response, suggesting that Zn modification improves the sensing performance toward ciprofloxacin.

Acknowledgements

This work was supported by VEGA 1/0058/25, 1/0442/25 and Funded by the EU NextGenerationEU through the Recovery and Resilience Plan for Slovakia under the project No. 09I03-03-V05-00008 (VVGS-ESGV-2923).

References

[1] H. Zhou and S. Kitagawa, „Metal–Organic Frameworks (MOFs),“ *Chem. Soc. Rev*., vol. 43, pp. 5415-5418, Jul 2014, doi: 10.1039/C4CS90059F.

[2] M. Yin, L. Zhang, X. Wei, J. Sun and D. Xu, „Detection of antibiotics by electrochemical sensors based on metal-organic frameworks and their derived materials,“ *Microchem. J.,* vol. 183, pp.107946, Dec. 2022, doi: 10.1016/j.microc.2022.107946.

[3] N. Király, D. Capková, M. Almáši, T. Kazda, O. Čech, P. Čudek, A. Straková Fedorková, M. Lisnichuk, V. Meynen and V. Zeleňák, „Post-synthetically modified metal–porphyrin framework GaTCPP for carbon dioxide adsorption and energy storage in Li–S batteries,“ *RSC Adv*., vol. 12, pp. 23989-24002, Aug. 2022, doi: 10.1039/D2RA03301A.

Chromium-Based MIL-101 for Sensitive Electrochemical Sensing of Antibiotic Compounds

S. Kiraly[a]*, J. Shepa[a], J. Demeterova[a], I. Sisolakova[a], M. Almasi[b], R. Orinakova[a], V. Zelenak[b], N. Kiraly[b]
[a] Department of Physical Chemistry, Institute of Chemistry, Pavol Jozef Šafárik University in Košice, Moyzesova 11, 041 54 Kosice, Slovak Republic
[b] Department of Inorganic Chemistry, Institute of Chemistry, Pavol Jozef Šafárik University in Košice, Moyzesova 11, 041 54 Kosice, Slovak Republic
*sona.kiraly@upjs.sk

Metal–organic frameworks (MOFs) represent a versatile class of crystalline porous materials composed of metal nodes interconnected by organic linkers, characterized by high surface areas, tunable pore architectures, and adjustable chemical functionalities. Among these, MIL-101(Cr), a chromium(III)-based MOF constructed from terephthalate ligands, is one of the most extensively investigated systems due to its outstanding physicochemical properties. It exhibits an exceptionally high specific surface area (often exceeding 3000 $m^2 \cdot g^{-1}$), large mesoporous cages, and excellent thermal, chemical, and hydrolytic stability, making it suitable for a wide range of applications. In recent years, MIL-101(Cr) has attracted increasing attention in sensing applications, particularly for the detection of environmental pollutants, biomolecules, and pharmaceutical compounds. Its stability in aqueous environments, high porosity, and compatibility with electrode materials make it especially promising for electrochemical sensing, enabling high sensitivity, selectivity, and long-term operational stability [1,2].
In this work, MIL-101(Cr) was synthesized via a solvothermal method using chromium(III) nitrate nonahydrate and terephthalic acid (H_2BDC) as precursors. The organic linker was initially dissolved in an alkaline medium containing tetramethylammonium hydroxide (TMAOH) under ambient conditions, followed by the addition of the chromium salt. The pH of the reaction mixture was adjusted to 6.0–6.5, and the resulting solution was transferred into a Teflon-lined autoclave and heated at 453 K (180 °C) for 24 h. After gradual cooling to room temperature, the resulting green solid was collected by centrifugation, thoroughly washed with distilled water, and dried at ambient conditions, yielding the product with high efficiency (~88% based on chromium content).

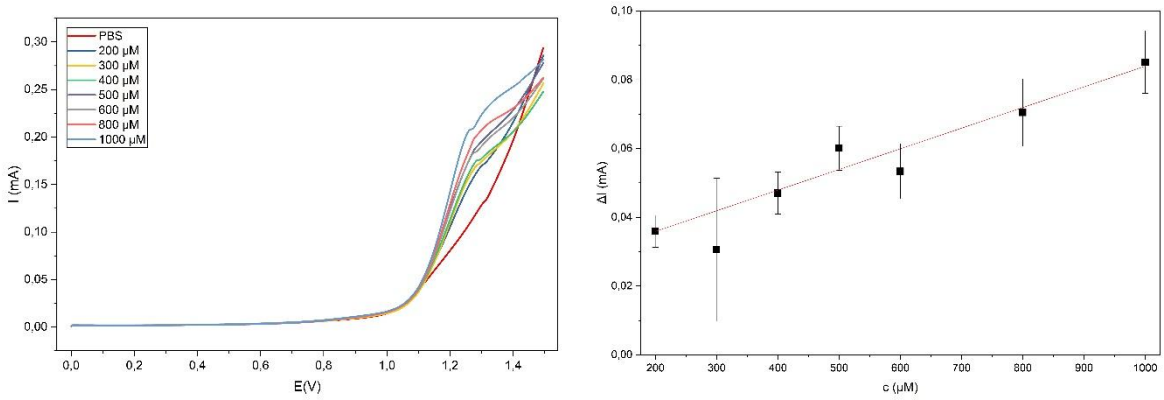

Figure 7 Differential pulse voltammograms of gentamicin (200–1000 µM) recorded at the CrMOF/MWCNTs/Nafion:ethanol (1:4, v/v)/SPCE in PBS (pH ≈ 7.4). The calibration plot was constructed from the blank-corrected current response measured at 1.30 V; error bars represent standard deviations obtained from three independent series.

The SPCE working electrode was modified by drop-casting a dispersion of MIL-101(Cr) and MWCNTs prepared in Nafion:ethanol (1:4, v/v). To evaluate the relationship between the current response and gentamicin concentration, differential pulse voltammetry was performed in gentamicin solutions prepared in phosphate-buffered saline (PBS, pH ≈ 7.4) using the modified electrode. The blank-corrected current response at 1.30 V increased with increasing gentamicin concentration in the range of 200–1000 µM, yielding a calibration plot with moderate linearity ($R^2 = 0.94$), a sensitivity of 0.060 µA μM^{-1}, and a limit of detection (LOD) of 87 µM. These findings highlight the potential of the developed electrode as a promising platform for gentamicin sensing.

Acknowledgements

Funded by the EU NextGenerationEU through the Recovery and Resilience Plan for Slovakia under the project No. 09-I05-03-V02-00047.

References

[1] Q. Xia, X. Li, X. Xiao, W. Deng and Y. Yang, "Peroxidase-like NH_2-MIL-101(Cr)-enabled fluorescence sensing of ofloxacin in honey through charge transfer modulation," *Food Chem.*, vol. 510, pp. 148692, May 2026, doi: 10.1016/j.foodchem.2026.148692.

[2] R. T. Massah, S. L. Z. Jiokeng, J. Liang, E. Njanja, T. M. M. Ntep, A. Spiess, L. Rademacher, C. Janiak and I. K. Tonle, "Peroxidase-like NH_2-MIL-101(Cr)-enabled fluorescence sensing of ofloxacin in honey through charge transfer modulation," *ACS Omega*, vol. 7, no. 23, pp. 19420–19427, Jun. 2022, doi: 10.1021/acsomega.2c01106.

Fe-based soft magnetic composites for electromagnetic energy conversion: Characterization of powders and green compacts

V. Kostiuk[a]*, S. Ravi[a], Z. Bircakova[a], R. Bures[a], M. Faberova[a], V. Koval[a], J. Fuzer[b], P. Kollar[b]

[a] Institute of Materials Research, Slovak Academy of Sciences, Košice, Slovakia
[b] Institute of Physics, Faculty of Science, P.J. Safarik University in Kosice, Park Angelinum 9, Košice, Slovakia
*vkostiuk@saske.sk

Introduction

The transition towards renewable energy sources, electrified transport, and distributed energy-storage systems requires increasingly efficient power-electronic converters capable of managing energy flow among generation units, storage devices, and electrical loads [1]. In these systems, passive magnetic components, particularly inductors, transformers, and chokes, are essential for energy transfer, voltage conversion, filtering, and electromagnetic interference suppression. Their efficiency, power density, thermal stability, and operating-frequency range are strongly governed by the properties of the soft magnetic core material.

Soft magnetic composites (SMCs) are a promising class of magnetic core materials for electromagnetic energy-conversion applications. They typically consist of ferromagnetic powder particles electrically insulated by thin interparticle layers. This microstructural design combines high magnetic response with increased electrical resistivity, thereby suppressing eddy-current losses and improving the frequency stability of magnetic properties [2]. Compared with conventional laminated steels, SMCs also offer nearly isotropic magnetic behaviour and enable the fabrication of complex three-dimensional magnetic circuits via powder-metallurgical processing. These features make them attractive for compact, high-frequency inductive components used in power converters, electric drives and power-electronic interfaces connected to energy-storage systems [2,3].

A critical aspect in the development of Fe-based SMCs is the formation of a continuous, stable insulating phase on the surface of iron particles while maintaining sufficient compressibility, densification, and magnetic permeability after compaction. The balance among electrical insulation, particle deformation, interparticle magnetic coupling, and final compact density is therefore decisive for achieving favourable functional properties. Natural or ceramic insulating phases, such as mica-based minerals, may offer an effective way to increase interparticle electrical resistance while preserving the advantages of Fe-based powder cores.

In this work, Fe-based soft magnetic composites containing biotite as an insulating phase were prepared by Resonant Acoustic Mixing, followed by high-pressure uniaxial compaction. The study examines how biotite content and processing time influence powder compressibility, compact formation and complex permeability spectra. By correlating processing conditions with the magnetic response of green compacts, the work aims to clarify the role of the insulating-phase distribution in tailoring Fe-based SMCs for electromagnetic energy-conversion applications.

Materials and Methods

The starting material was a water-atomized iron powder ABC 100.30 (Höganäs AB, Sweden). Prior to further processing, the powder was sieved and only the particle size fraction above 45 μm was selected for the experiments. As an insulating phase, a high-purity biotite powder (99.999%, US Research Nanomaterials) with particle size below 45 μm was used. The morphology of the initial powders, including iron particles and biotite, is illustrated in Figure 1. The biotite was added to the iron powder in amounts ranging from 1 to 5 wt.%, and the mixtures were processed using a LabRAM mixer. Two different processing regimes were applied, namely short-term mixing for 15 minutes and extended processing corresponding to 24 hours of self-milling [4].

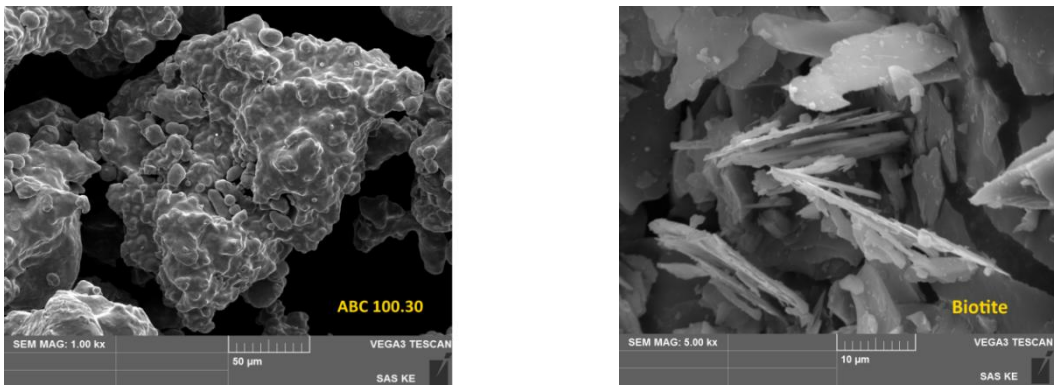

Figure 1 SEM images of ABC 100.30 powder (fraction >45 µm) and biotite particles.

The prepared powder mixtures were subsequently compacted using a uniaxial hydraulic press (LabTest 5.600 ZL). For all experiments, a constant powder volume of 0.5 cm³ was used and pressed in a cylindrical die under a maximum pressure of 2000 MPa with a holding time of 15 s at peak pressure. A punch displacement rate of 1 mm/min was applied for all samples to ensure consistent compaction conditions. To evaluate the magnetic properties, samples with appropriate geometries were prepared. Ring-shaped specimens with an outer diameter of 24 mm and an inner diameter of 13.5 mm were used for magnetic measurements. The morphology of the powder mixtures was analyzed using scanning electron microscopy (SEM) with a TESCAN Vega3 LMU microscope (TESCAN Brno, Czech Republic). The powders were mounted on aluminium holders using double-sided carbon tape and examined in high vacuum mode (≤ 0.018 Pa) at an accelerating voltage of 15 kV. Data acquisition and processing were carried out using Esprit 1.9 software (Bruker Nano GmbH, Berlin, Germany). The complex permeability (μ′ and μ″) was measured using an impedance analyzer HP4194A in the frequency range from 500 Hz to 40 MHz.

Results and Discussion

The results presented in Figure 2 show that both the biotite content and the RAM processing time have a clear influence on the compressibility of the investigated powder mixtures.

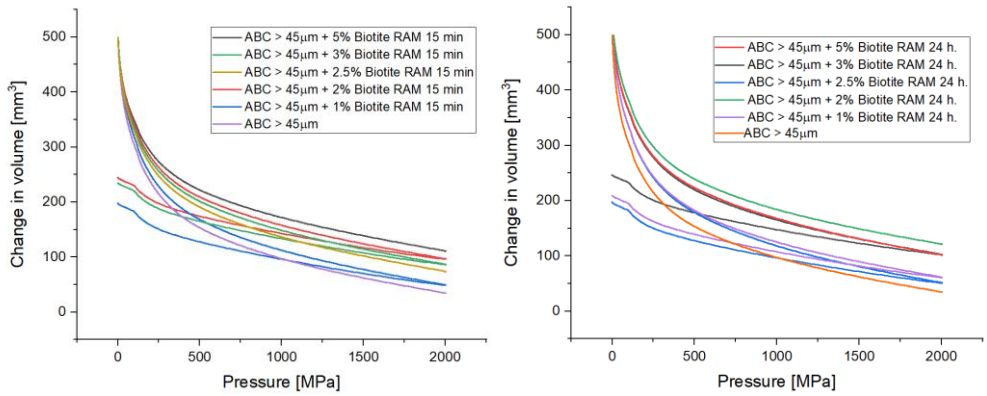

Figure 2 Compaction curves of Fe/biotite powder mixtures RAM mixed for 15 min (left) and for 24 h (right).

With increasing biotite content, a gradual decrease in compressibility is observed, which indicates that the presence of the insulating phase limits particle rearrangement and plastic deformation during pressing. This behavior can be explained by the fact that biotite particles form a non-metallic layer on the surface of iron particles, which reduces direct contact between them and thus increases resistance to compaction. As a result, the powders require higher pressure to achieve the same level of densification, and their overall compressibility decreases. At the same time, the effect of processing time is also noticeable. Samples subjected to longer RAM processing time 24 h generally show a better compaction compared to short-term processing 15 min. This can be attributed to a more uniform distribution of biotite on the particle surfaces, which reduces local agglomeration and allows more homogeneous deformation during pressing. However, this effect is strongly dependent on the biotite content. At lower concentrations, longer processing can slightly improve compressibility, while at higher contents the insulating phase becomes dominant, limiting particle deformation and leading to reduced overall compaction efficiency.

Magnetic Properties

In order the differences in magnetic properties between the materials and the compaction pressures to be best visible, the complex relative permeability spectra vs. magnetizing frequency of green samples with the lowest (1 wt.%) and the highest (5 wt.%) content of biotite are shown in Figure 3 and Figure 4, respectively, for RAM mixing for 15 min and 24 h. The complex permeability has the real and the imaginary part, and is used to evaluate the dynamic magnetization process [2,5]. We can see a quite high frequency stability of the real parts in case of all green compacts, together with their relatively high initial values. The real permeability reflects the domain wall movability and hence depends on number of any structural defects hindering the domain wall motion, but on the other hand, it is also significantly dependent on inner demagnetizing fields, arising from the interrupted magnetic flux causing free magnetic charges at the surfaces of insulated ferromagnetic particles in case of composite materials [2,3]. Therefore, we see higher values of the initial real parts for 1 % of mica compared to 5 %, as well as slightly higher for 15 min RAM mixing time, indicating that Fe particles in samples with 5% are covered with thicker non-ferromagnetic (biotite) coating layers interrupting the magnetic flux and weakening magnetic interactions between particles, making the magnetization process more difficult [2]. Similarly, the magnetic response is lower for longer 24 h RAM mixing, indicating better quality of mica coating layer, i.e. better insulation of Fe particles from each other and elimination of electrical contacts between them. Although this has a negative effect on real parts values, the good insulation of particles is required for the frequency stability enhancement and eddy currents elimination [2,5].

We see that samples of 5% biotite and 24 h RAM exhibit higher resonant frequencies than 1% and 15 min samples. The tendency of lower real part permeability with higher frequency stability for lower pressing pressures is approximately obeyed, due to the higher amount of air gaps (porosity) acting also as a non-ferromagnetic component diluting the magnetic filler content and weaking magnetic interactions between particles [2].

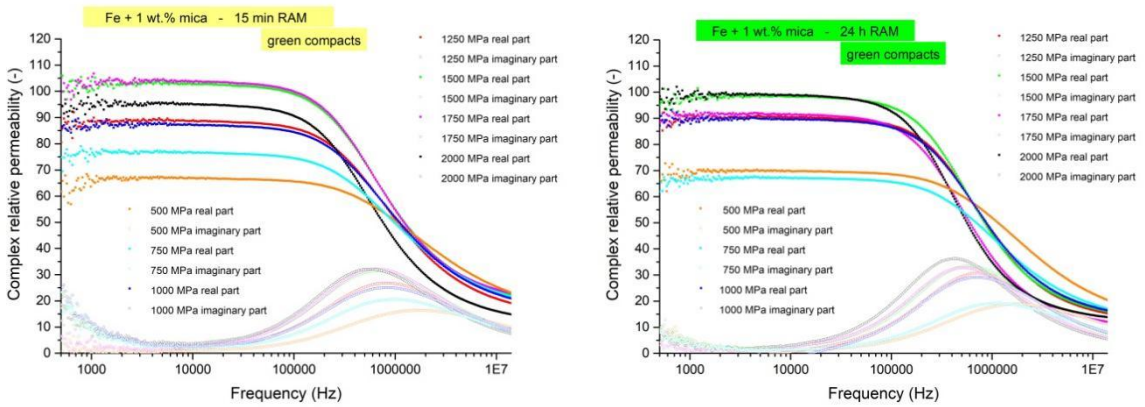

Figure 3 Complex relative permeability spectra vs. magnetizing frequency of green soft magnetic composite samples Fe@mica-biotite (1 wt.%), RAM mixed for 15 min (left) and for 24 h (right), compacted at different pressures.

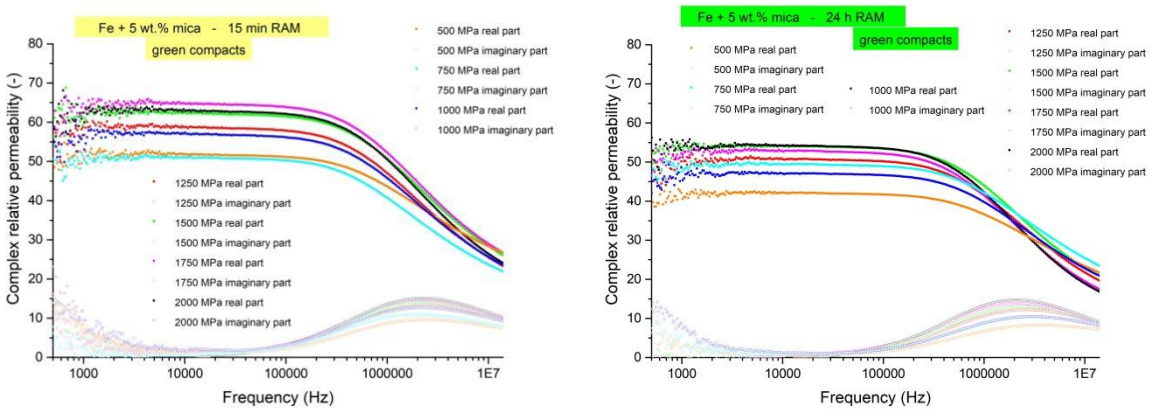

Figure 4 Complex relative permeability spectra vs. magnetizing frequency of green soft magnetic composite samples Fe@mica-biotite (5 wt.%), RAM mixed for 15 min (left) and for 24 h (right), compacted at different pressures.

Conclusions

Fe-based soft magnetic composites with biotite as the insulating phase were successfully prepared by Resonant Acoustic Mixing and high-pressure compaction. The results show that both biotite content and processing time significantly affect powder compressibility and the magnetic response of green compacts. Increasing the biotite content reduces compressibility and the real part of the complex permeability but improves particle insulation and improves the frequency stability of magnetic response. Longer RAM processing promotes a more uniform distribution of the insulating phase, leading to better electrical separation of Fe particles and higher resonant frequencies. These findings indicate that Fe/biotite composites are promising candidates for high-frequency magnetic cores in electromagnetic energy-conversion applications.

Acknowledgements

This work was financially supported by the Slovak Research and Development Agency (a Grant no. SK-CN-23-0014), EU NextGenerationEU (PO R1, No. 09103-03-V02-00013) and VEGA 2/0099/24, VEGA 1/0132/24.

References

[1] J. M. Silveyra, E. Ferrara, D. L. Huber and T. C. Monson, „Soft magnetic materials for a sustainable and electrified world,“ *Science,* vol. 362, no. 6413, pp. eaao0195 / 418–427, Oct. 2018, doi: 10.1126/science.aao0195.
[2] E. A. Périgo, B. Weidenfeller, P. Kollár and J. Füzer, „Past, present, and future of soft magnetic composites,“ *Applied Physics Reviews,* vol. 5, no. 3, pp. 031301 Sep. 2018, doi: 10.1063/1.5027045.
[3] J. He, H. Yuan, M. Nie, H. Guo, H. Yu, Z. Liu and R. Sun, Soft magnetic materials for power inductors: State of art and future development,“ *Materials Today Electronics*, vol. 6, pp. 100066, Dec. 2023, doi: 10.1016/j.mtelec.2023.100066.
[4] R. Bureš and M. Fáberová, “Method for production of composite magnetic powders by selfmilling,” SK Patent SK132021A3, 2021.
[5] S. Chikazumi, *Physics of ferromagnetism*, 2nd ed., Oxford University Press Inc., New York, 1999.

The Use of a Customized PDO Implant to Close a Ventral Tracheal Defect with Absent Annular Support in the Presence of a Multidrug-resistant Infection

M. Kozar[a]*, B. Siskova[a]
[a]Small Animal Clinic, University of Veterinary Medicine and Pharmacy in Košice,
Komenského 73, 040 01, Košice, Slovak Republic
*martin.kozar@uvlf.sk

Laryngotracheal injuries represent a relatively rare yet potentially life-threatening clinical entity in small animal practice. This report describes a complex case of a chronic ventral tracheal defect associated with persistent contamination by multidrug-resistant (MDR) bacterial pathogens, significantly compromising the patient's prognosis and survival.

Microbiological analysis revealed a polymicrobial infection involving *Klebsiella pneumoniae*, *Staphylococcus intermedius*, and *Staphylococcus haemolyticus*. All isolates exhibited extensive antimicrobial resistance profiles consistent with chronic wound colonisation. The formation of a structured, multilayered biofilm likely contributed to impaired antibiotic penetration, perpetuation of chronic inflammation, and delayed epithelialisation.

Initial surgical management, performed at a referring private practice, consisted of layered closure of the ventral cervical soft tissues. However, due to the absence of tracheal annular support (tracheal rings), complete defect closure was not achievable, resulting in persistent respiratory compromise. Tracheal tissue demonstrates limited regenerative capacity, primarily due to the avascular nature of hyaline cartilage. Furthermore, continuous biomechanical stress associated with respiratory motion (cyclic distension and collapse) contributes to instability of defect margins, favouring chronicity, necrosis, impaired perfusion, and failure to progress to the proliferative phase of wound healing.

Considering increasing interest in biodegradable biomaterials as adjuncts in regenerative medicine, a decision was made to utilise polydioxanone (PDO) as a synthetic, resorbable scaffold to bridge the tracheal defect. A patient-specific, three-dimensional (3D)-printed implant was designed and applied directly to the defect site.

The implant was secured using simple interrupted sutures placed through both the implant material and the adjacent tracheal cartilaginous structures, achieving complete mechanical bridging of the defect. Postoperative management focused primarily on close monitoring of respiratory function and early detection of potential complications.

Long-term observations of biodegradable polymers commonly used in tissue engineering, such as polycaprolactone (PCL) and polylactic acid (PLA), indicate that PDO exhibits distinct advantages in terms of degradation kinetics, modulation of the inflammatory response, and integration within host tissue.

Macroscopic evaluation of the implant site was performed from the intraluminal perspective at 1, 5, and 12 months postoperatively. Clinical assessment included continuous monitoring of respiratory function, auscultation for pathological sounds, radiographic imaging, and endoscopic examination.

The most significant epithelial ingrowth through the PDO scaffold was observed between days 30 and 90 post-implantation. By this stage, the implant was fully covered by newly formed epithelium, with minimal inflammatory response and negligible scar tissue formation. Progressive resorption of the implant occurred over the subsequent 60 days, with near-complete degradation corresponding to the absence of native tracheal rings.

During the follow-up period, normal respiratory function was restored, and spontaneous resolution of bacterial contamination was observed without the need for prolonged antimicrobial therapy. The targeted application of a PDO-based implant enabled rapid defect closure, restoration of tracheal integrity, resolution of clinical signs (including coughing), and an optimal cosmetic outcome.

Polydioxanone proved to be a rapidly resorbable material providing sufficient temporary mechanical support while facilitating effective tissue integration. Complete degradation occurred within approximately 180–210 days, eliminating the need for secondary implant removal.

This clinical case highlights the potential of customised biodegradable implants in the management of complex tracheal defects involving loss of structural support. The findings support the role of PDO as a promising material in regenerative surgical approaches following traumatic tissue loss.

Acknowledgements

This war was supported by a KEGA 012UVLF-4/2025 research project.

References

[1] A. Findrik Balogová, M. Kožár, R. Staroňová, M. Schnitzer, G. Dancáková, J. Živčák, and R. Hudák, "Therapy of extensive chronic skin defects after a traumatic injury due to microbial contamination using a surface implant made of a biocompatible polycaprolactone—a pilot case study," *Polymers*, vol. 14, no. 23, p. 5293, 2022, doi: 10.3390/polym14235293.

[2] S. L. Debs, R. S. Petersson, and S. J. Wong, “Management of dog-related penetrating laryngotracheal trauma in a pediatric patient,” *Cureus*, vol. 15, no. 11, p. e48470, Nov. 2023, doi: 10.7759/cureus.48470.
[3] B. Šišková, M. Kožár, R. Staroňová, I. Shepa, V. Hajdučková, P. Hudecová, M. Kaduková, and M. Schnitzer, “Antibacterial effect and therapy of chronic skin defects using the composite bioscaffold polycaprolactone/GelitaSpon/povidone-iodine in domestic dogs,” *Polymers*, vol. 15, no. 21, p. 4201, 2023, doi: 10.3390/polym15214201.

Engineering Ionic Liquid–Modified Electrolytes for Enhanced Stability and Interfacial Control in Lithium–Sulfur Batteries

J. Lescinsky[a]*, V. Niscakova[a], A. Fedorkova[a]
[a] Department of Physical Chemistry, Institute of Chemistry, Pavol Jozef Šafárik University in Košice, Moyzesova 11, 041 54 Kosice, Slovak Republic
*jakub.lescinsky@student.upjs.sk

Introduction

Lithium–sulfur (Li–S) batteries are considered one of the most promising next-generation electrochemical energy storage systems due to their high theoretical specific capacity (1675 mAh g^{-1}) and energy density. Despite these advantages, their practical implementation is limited by fundamental physicochemical challenges, including polysulfide dissolution, non-ideal electrolyte thermodynamics, and unstable electrode–electrolyte interfaces [1],[2]. The redox mechanism of sulfur involves multiple electron-transfer steps coupled with dissolution and precipitation reactions, where the distribution of polysulfide species (Li_2S_x) is strongly dependent on the solvation environment and ionic interactions in the electrolyte [1], [3].
In conventional ether-based electrolytes, Li^+ ions are solvated by DOL/DME molecules, forming dynamic solvation shells that influence ionic conductivity, viscosity, and redox kinetics. Deviations from ideal solution behavior become significant at higher salt concentrations or in the presence of strongly interacting species, requiring consideration of activity coefficients rather than simple concentration-based descriptions. These non-idealities directly affect electrode potentials, polarization, and charge-transfer kinetics, making electrolyte design a key factor in controlling overall battery performance.

Experimental

Within the SUNFLOWERS project, a systematic electrolyte engineering strategy is implemented based on LiTFSI/$LiNO_3$ in DOL:DME, modified by pyrrolidinium-based ionic liquids and dual-salt systems. Ionic liquid concentration is varied in the range of 5–20 vol%, enabling controlled transition from dilute to quasi-concentrated electrolyte regimes. In parallel, dual-salt formulations combining LiTFSI and LiFSI are investigated to modify Li^+ coordination structures and improve transport properties.
LiBOB is introduced as a functional additive to promote early-stage SEI/CEI formation and stabilize electrode interfaces, consistent with strategies described in advanced electrolyte design frameworks. Electrochemical characterization includes cyclic voltammetry, galvanostatic cycling, and electrochemical impedance spectroscopy, enabling separation of bulk resistance, charge-transfer resistance, and diffusion contributions.

Results and Discussion

The incorporation of ionic liquids significantly alters the electrolyte structure by enhancing ion–ion interactions and modifying Li^+ solvation shells. As ionic liquid content increases, the system transitions toward a regime characterized by ion aggregates and reduced solvent-separated ion pairs, leading to decreased polysulfide solubility and suppression of shuttle processes [3], [4]. These observations are consistent with experimentally observed relationships between electrolyte composition and electrochemical response in Li–S systems .
From a thermodynamic perspective, increased ionic strength leads to deviations of activity coefficients from unity, affecting the effective electrochemical potential of reacting species. As shown in previous studies, activity-controlled behavior becomes dominant in concentrated systems, influencing both plateau potentials and polarization behavior .
Dual-salt systems further enhance performance by modifying Li^+ coordination and promoting formation of inorganic-rich SEI layers (e.g., LiF), which reduce interfacial resistance and improve mechanical stability [5]. The addition of LiBOB supports formation of stable interphases, reducing electrolyte decomposition and enhancing Coulombic efficiency [6].
Electrochemical impedance spectroscopy can be used to assess the influence of electrolyte composition on charge-transfer resistance, while cyclic voltammetry may provide insight into the reversibility of sulfur redox reactions. Such an approach enables discussion of the interplay between ion transport, interfacial kinetics, and electrolyte non-ideality.

Conclusion

This work provides a comprehensive framework linking electrolyte molecular design with thermodynamic, transport, and interfacial phenomena in Li–S batteries. By integrating ionic liquid modification, dual-salt

strategies, and functional additives, a pathway toward stable, high-performance, and safer Li–S systems is established, fully aligned with the SUNFLOWERS project objectives.

Acknowledgements

This work was funded by the project EU NextGenerationEU through the Recovery and Resilience Plan for Slovakia under the project SUNFLOWERS No. 09I02-03-V01-00022

References

[1] Q. Pang, X. Liang, C. Y. Kwok, and L. F. Nazar, "Advances in lithium–sulfur batteries based on multifunctional cathodes and electrolytes," *Nat. Energy*, vol. 1, no. 16132, 2016, doi: 10.1038/nenergy.2016.132.
[2] A. Manthiram, Y. Fu, S.-H. Chung, C. Zu, and Y.-S. Su, "Rechargeable lithium–sulfur batteries," *Chem. Rev*., vol. 114, pp. 11751–11787, 2014, doi: 10.1021/cr500062v.
[3] S. S. Zhang, "Liquid electrolyte lithium/sulfur battery: Fundamental chemistry, problems, and solutions," *J. Power Sources*, vol. 231, pp. 153–162, 2013, doi: 10.1016/j.jpowsour.2012.12.102.
[4] Y. Yamada, J. Wang, S. Ko, E. Watanabe, and A. Yamada, "Advances and issues in developing salt-concentrated battery electrolytes," *Nat. Energy*, vol. 4, pp. 269–280, 2019, doi: 10.1038/s41560-019-0336-5.
[5] H.-J. Peng, J.-Q. Huang, X.-B. Cheng, and Q. Zhang, "Review on high-loading and lean-electrolyte lithium–sulfur batteries," *Adv. Energy Mater*., vol. 7, no. 24, Art. no. 1700260, 2017, doi: 10.1002/aenm.201700260.
[6] K. Xu, "Electrolytes and interphases in Li-ion batteries and beyond," *Chem. Rev*., vol. 114, pp. 11503–11618, 2014, doi: 10.1021/cr500003w.

Determination of Texture Characteristics of Clay Minerals

M. Lhotka[a]*, L. Mastný[b]
[a] Department of Inorganic Technology, Faculty of Chemical Technology, University of Chemistry and Technology, Prague, Technická 5, 166 28, Prague 6, Czech Republic
[b] Department of Inorganic Chemistry, Faculty of Chemical Technology, University of Chemistry and Technology, Prague, Technická 5, 166 28, Prague 6, Czech Republic
*miloslav.lhotka@vscht.cz

Porous substances occur in many areas of chemical technology, most often as catalysts, membranes, adsorbents. Clay minerals can also be considered porous materials and therefore the knowledge of textural properties is one of the important characteristics of these materials. Clay materials are divided into several groups, which differ in their structure and also have different textural properties. Therefore, the knowledge of the basic textural characteristics of these substances, such as the shape, width, pores volume and classification, porosity, specific surface area (S_{BET}), true and apparent density, as well as the appropriate methods for their determination are necessary for the processing and use of clay materials. The methods for examining porous materials vary according to the size of the pores. The adsorption methods are preferably used for micro and mesoporous materials, while the Hg-porosimetry for macroporous materials. The methods of studying the structure of solids are mostly based on adsorption phenomenon. The goal of all adsorption theories is to predict the amount of adsorbate needed to covering the surface with the monolayer of gas molecules and to determine the area required to the adsorption of one molecule of adsorbate. From the number of theories the "BET" isotherm is currently used to the S_{BET} calculation. As the example of clays characterization, the determination of structural characteristics of kaolinite, bentonite, montmorillonite and rehydroxylated kaolinites using the adsorption methods. The adsorption isotherms were measured on an 3Flex surface analyser (Micromeritics, Norcross, GA, USA) using the gas sorption technique (N_2 at 77 K). These adsorption isotherms were fitted according the Brunauer-Emmett-Teller (S_{BET}) method and t-plot method ($S_{t\text{-}plot}$) for specific surface area, the micropore volume by the t-plot method and the pore-size distribution by the Barrett-Joyner-Halenda (BJH) method and Density Functional Theory (DFT) method. In addition, the scanning adsorption isotherms of all the mentioned samples were measured. Scanning isotherms provide important information about the pore network geometry, including its connectivity and pore size distribution, which cannot be revealed from the main adsorption and desorption isotherms.
In this study, results concerning complex clay textural analysis were obtained. In conclusion, although there is a wide variety of methods applicable to the clay texture characterization, each method has the limitations, which must be taken into account when evaluating the results.

References

[1] S. Brunauer, P. H. Emmet a E. Teller, „Adsorption of Gases in Multimolecular Layers," *J. Am. Chem. Soc*., vol. 60, no. 2, pp. 309-319, Feb. 1938, doi: doi.org/10.1021/ja01269a023.
[2] R. Cimino, K. A. Cychosz, M. Thommes, A. V. Neimark, "Experimental and theoretical studies of scanning adsorption–desorption isotherms," *Colloids and Surfaces A: Physicochem. Eng. Aspects,* vol. 437, pp. 76–89, Nov. 2013, doi: 10.1016/j.colsurfa.2013.03.025.

Advanced Hydroxyapatite Coatings for Hard Tissue Biomedical Applications

I. Mojzisova[a]*, R. Orinakova[a]
[a] Department of Physical Chemistry, Institute of Chemistry, Pavol Jozef Šafárik University in Košice, Moyzesova 11, 041 54 Kosice, Slovak Republic
*ivana.mojzisova@student.upjs.sk

Ceramic materials like hydroxyapatite (HAp) are widely used in biomedical applications due to their excellent biocompatibility, osteoconductive properties, and chemical similarity to the inorganic components of human bone. Hydroxyapatite has been widely applied as bone fillers, tissue engineering scaffolds, drug delivery systems, and bioactive coatings for metallic implants [1]. Synthetic hydroxyapatite is one of the most used coatings on implantable metallic prostheses to improve the biological response of the host's surrounding tissue. Previous studies have demonstrated that HAp coatings can significantly enhance implant stability, promote osseointegration and accelerate osteogenesis directly at the bone-implant interface [2]. Stoichiometric HAp, with chemical formula of $Ca_{10}(PO_4)_6(OH)_2$ and a Ca/P ratio of 1.67, represents one of the most stable calcium phosphate salts across a wide pH range (4-12) at room temperature. Its stability arises from its molecular framework, which consists of a phosphate tetrahedral network held together by a distributed calcium ions [1]. However, the hydroxyapatite in the human body is not stoichiometric and Ca^{2+} ions are substituted by other ions present in the body fluids.

Ion doping is also often preferred in the biological application research of HAp. Numerous studies have demonstrated that the incorporation of ions such as Cu^{2+}, Ag^{+} and Zn^{2+}, into the hydroxyapatite lattice can effectively modulate its biological and physicochemical properties. Among these, silver ion substitution is particularly attractive, as it enhances the material's properties while providing strong antimicrobial activity. Hydroxyapatite is suitable host matrix for such modification due to its ability to accommodate ionic substitutions without significant structural disruption [3].

Silver-doped hydroxyapatite coatings have been fabricated using various techniques, including wet chemical precipitation followed by coating deposition, hydrothermal processing, plasma spraying, sol–gel methods, and electrochemical deposition. Among these approaches, electrochemical deposition (ED) has emerged as a particularly promising method due to its relatively mild processing conditions, low cost, and ability to produce coatings with controlled thickness, morphology, and composition on substrates with complex geometries. In contrast to high-temperature techniques such as plasma spraying and hydrothermal processing, electrochemical deposition minimizes the risk of thermal degradation, thermomechanical mismatch, and undesirable modifications of the substrate surface. ED allows to deposition of ceramic coatings on wide range of inert metallic substrates like titanium or degradable metal like zinc [4].

The ED of silver-doped hydroxyapatite (HAp-Ag) coatings is commonly performed using a three-electrode system operated under galvanostatic or potentiostatic conditions. During the deposition process, cathodic reactions occurring at the surface of the working electrode led to a local increase in pH in the vicinity of the substrate. This localized alkalization promotes the precipitation of calcium phosphate species and the subsequent formation of hydroxyapatite directly on the metallic surface. Simultaneously, silver ions present in the electrolyte can be incorporated into the growing HAp structure through partial substitution of Ca^{2+} ions (Figure 1) [5].

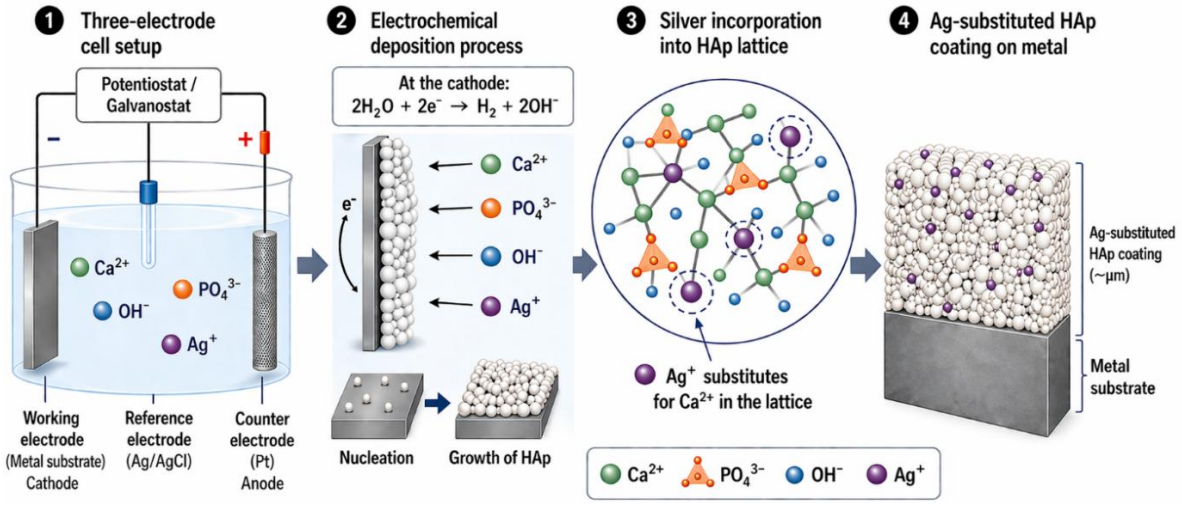

Figure 1 Electrochemical deposition of Ag^{+}-substituted hydroxyapatite coating on a metallic substrate [AI generated].

The incorporation of dopant ions into the HAp structure can induce some changes in the phase composition and crystal structure of the resulting coating, depending on the chemical nature and concentration of the incorporated dopants. These modifications are often reflected in X-ray diffraction (XRD) patterns as shifts of the characteristic HAp diffraction peaks toward lower or higher diffraction angles, corresponding to expansion or contraction of the HAp unit cell. Whether the dopant ions induce lattice expansion or contraction depends primarily on their ionic radius relative to that of Ca2+. For example, ions with smaller ionic radii than Ca2+, such as Zn2+, may lead to contraction of the HAp lattice following substitution within the crystal structure [5]. In contrast, due to the larger ionic radius of Ag+ compared to Ca2+, the substitution of calcium ions by silver ions within the HAp lattice may result in lattice expansion and corresponding shifts in diffraction peaks toward lower diffraction angles (Figure 2) [6].

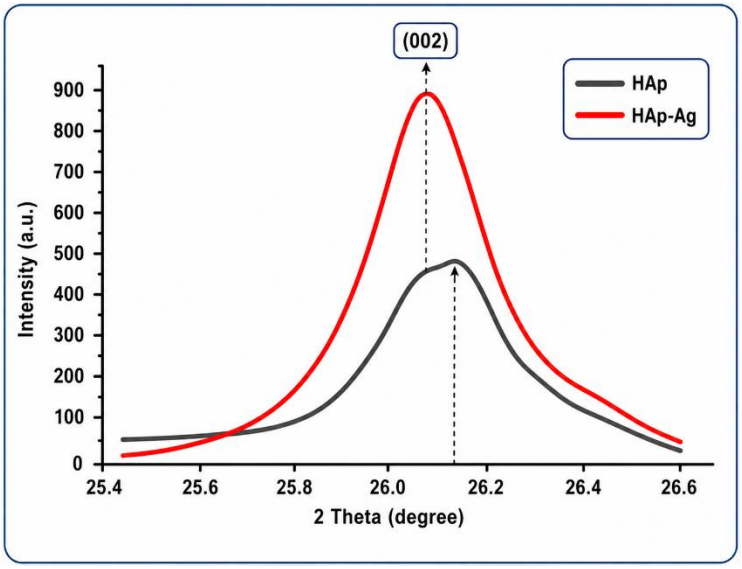

Figure 2 Comparison of X-ray diffraction patterns between HAp and HAp-Ag [6].

In addition to structural modifications, silver incorporation may also influence the electrochemical and protective properties of hydroxyapatite coatings. Several studies have suggested that ion-doped HAp coatings can enhance the corrosion resistance of metallic substrates through the formation of denser and more homogeneous coating structures, thereby limiting ionic diffusion toward the substrate surface. Furthermore, changes in grain size and surface passivation behaviour induced by ionic substitution may contribute to improved surface stability and enhanced protective performance of the coating. However, excessive dopant incorporation may adversely affect coating properties by increasing porosity and promoting the formation of structural defects within the deposited layer [5].

The combination of the bioactive properties of hydroxyapatite with the antimicrobial activity of silver represents a promising strategy for the development of multifunctional biomedical coatings. Electrochemical deposition offers significant potential for the fabrication of Ag-doped HAp coatings due to its low processing temperature, versatility, and ability to control coating composition and morphology. Furthermore, this method enables the deposition of bioactive coatings on various metallic substrates. Such coatings may contribute to improved implant performance by promoting osseointegration while simultaneously reducing the risk of implant-associated infections

Acknowledgements

This work was supported by the Slovak Research and Development Agency under the project APVV-24-0033.

References

[1] M. Mirzaee, M. Vaezi, and Y. Palizdar, “Synthesis and characterization of silver doped hydroxyapatite nanocomposite coatings and evaluation of their antibacterial and corrosion resistance properties in simulated body fluid,” *Materials Science and Engineering: C*, vol. 69, pp. 675–684, Dec. 2016, doi: 10.1016/J.MSEC.2016.07.057.

[2] S. L. Iconaru, D. Predoi, C. S. Ciobanu, M. Motelica-Heino, R. Guegan and C. Bleotu, “Development of Silver Doped Hydroxyapatite Thin Films for Biomedical Applications,” *Coatings*, vol. 12, no. 3, pp. 341, Jan. 2022, doi: 10.3390/coatings12030341.

[3] N. Méndez-Lozano, M. Apatiga-Castro, A. de J. Ruíz-Baltazar, M. de la Luz-Asunción, and E. E. Pérez-Ramírez, "Characterization and Evaluation of Silver Concentrations in Hydroxyapatite Powders," *J. Funct. Biomater.*, vol. 14, no. 9, Sep. 2023, doi: 10.3390/jfb14090467.
[4] M. Ehlert, A. Radtke, M. Bartmański, and P. Piszczek, "Evaluation of the Cathodic Electrodeposition Effectiveness of the Hydroxyapatite Layer Used in Surface Modification of Ti6Al4V-Based Biomaterials," *Materials*, vol. 15, no. 19, Oct. 2022, doi: 10.3390/ma15196925.
[5] M. S. Safavi, F. C. Walsh, M. A. Surmeneva, R. A. Surmenev, and J. Khalil-Allafi, "Electrodeposited hydroxyapatite-based biocoatings: Recent progress and future challenges," *Coatings*, vol. 11, no. 1, pp. 110, Jan. 2021, doi: 10.3390/coatings11010110.
[6] Y. Yan, X. Zhang, Y. Huang, Q. Ding, and X. Pang, "Antibacterial and bioactivity of silver substituted hydroxyapatite/TiO2 nanotube composite coatings on titanium," *Appl. Surf. Sci.*, vol. 314, pp. 348–357, Sep. 2014, doi: 10.1016/J.APSUSC.2014.07.027.

Hydrogen Production over NiCoS via a Mechanochemically Induced Self-Propagating Reaction

T. Mudrinic[a], M. Balaz[b], A Guboova[c], M. Streckova[c]*
[a] University of Belgrade, Institute of Chemistry, Technology and Metallurgy, National Institute of the Republic of Serbia, Njegoševa 12, 11000 Belgrade, Republic of Serbia
[b] Institute of Geotechnics Slovak Academy of Sciences, Watsonova 45, 040 01 Košice, Slovak Republic
[c] Institute of Materials Research, Slovak Academy of Sciences, Watsonova 47,040 01Košice
*mstreckova@saske.sk

Water electrolysis enables the electrochemical splitting of water into hydrogen and oxygen, with overall efficiency governed by the activity and durability of electrocatalysts for the hydrogen evolution reaction (HER) at the cathode and the oxygen evolution reaction (OER) at the anode. For large-scale hydrogen production, it is essential to develop efficient, earth-abundant catalysts that can be synthesized rapidly and in a cost-effective manner.
In this work, we present a rapid and environmentally benign mechanochemical route for the synthesis of transition metal sulfide catalysts. This approach enables the direct formation of Ni–Co sulfide materials from elemental precursors within seconds, eliminating the need for high-temperature processing or solvent-based synthesis. As a result, the method significantly lowers the carbon footprint and aligns with the principles of green chemistry. Evaluation of ignition across different Ni:Co:S ratios indicated that mechanochemical reactivity is highly dependent on the initial particle size of Ni and Co and increases with higher Co content.
By tuning the Ni-to-Co ratio, a series of compositions with distinct catalytic properties were obtained. The structural and morphological characterization was performed using X-ray diffraction (XRD), X-ray photoelectron spectroscopy (XPS), scanning electron microscopy (SEM), and high-resolution transmission electron microscopy (HR-TEM). Samples with intermediate Co content exhibited diffraction patterns indicative of a multiphase system composed of Co_9S_8-, CoS-, and Ni_9S_8-type structures. Considering the cation substitution behavior observed at both low and high Co concentrations, these phases are more appropriately described as mixed Ni–Co sulfides rather than distinct Co and Ni sulfide phases.
Electrochemical performance was done in tree-electrode set up in 1M KOH condition. The optimized ternary sulfide system exhibited superior HER performance in alkaline media, characterized by low overpotential, excellent stability, and sustained long-term activity. The enhanced catalytic behavior is attributed to synergistic interactions between multiple sulfide phases and the optimized metal composition, which collectively improve electronic conductivity, increase active surface area, and promote a favorable balance between water dissociation and hydrogen adsorption steps.
The combination of rapid, scalable synthesis, environmentally friendly processing, and strong electrocatalytic performance highlights the potential of these materials for practical application in cost-effective alkaline water electrolysis systems.

Acknowledgements

This work was funded by the EU Next Generation EU through the Recovery and Resilience Plan for Slovakia under the project No. 09I03-03-V04-0006, the Ministry of Science, Technological Development and Innovation of the Republic of Serbia (Contract No. 451-03-33/2026-03/200026).

Electrochemical Evaluation of Organic Redox Molecules: Kinetics and Transport in Redox Flow Batteries

V. Niscakova[a]*, N. Kiraly[b], M. Almasi[b], J. Lescinsky[a], A. Fedorkova[a], R. Orinakova[a]
[a] Department of Physical Chemistry, Institute of Chemistry, Pavol Jozef Šafárik University in Košice, Moyzesova 11, 041 54 Kosice, Slovak Republic
[b] Department of Inorganic Chemistry, Institute of Chemistry, Pavol Jozef Šafárik University in Košice, Moyzesova 11, 041 54 Kosice, Slovak Republic
*veronika.niscakova@upjs.sk

Introduction

The increasing penetration of renewable energy sources into modern energy systems has intensified the demand for efficient and scalable energy storage technologies [1]. Among the available solutions, redox flow batteries (RFBs) have emerged as promising candidates for large-scale applications due to their flexible architecture, decoupled energy and power capacities, and long operational lifetime [2]. In recent years, organic redox flow batteries (ORFBs), employing redox-active organic molecules as electrochemical charge carriers, have attracted significant attention. Their appeal lies in the abundance of organic materials, potential cost-effectiveness, and the high degree of structural tunability, which enables precise control over electrochemical properties such as redox potential, solubility, and stability [3]. In particular, aqueous organic redox flow batteries have been widely explored as environmentally friendly and safe alternatives for grid-scale energy storage [1]. The overall performance of ORFBs is strongly governed by the physicochemical and electrochemical characteristics of the redox-active species. Key parameters include redox kinetics, diffusion coefficients, and chemical stability, which collectively determine the efficiency, energy density, and cycling stability of the system [4]. Despite considerable advances in molecular design, challenges such as limited reaction kinetics, mass transport constraints, and degradation mechanisms continue to restrict the practical deployment of organic electrolytes [1], [3]. A detailed understanding of the interplay between electron transfer kinetics and mass transport processes is therefore essential for optimizing the performance of organic redox systems. Electrochemical characterization techniques provide valuable insight into these processes and enable the establishment of structure–property relationships critical for the rational design of advanced materials.

In our study, we specifically target two well-established classes of organic molecules—anthraquinones and viologens—which represent archetypal systems for multi-electron and single-electron redox processes, respectively. Rather than treating these systems separately, we approach them comparatively, with the aim of identifying how their intrinsic differences translate into electrochemical performance under identical experimental conditions.

Experimental Approach

In order to systematically evaluate the electrochemical behavior of selected organic electrolytes, we employed cyclic voltammetry (CV) as our primary characterization technique. All measurements were performed in a conventional three-electrode configuration consisting of a glassy carbon working electrode, a platinum counter electrode, and an Ag/AgCl reference electrode. Particular attention was paid to electrode preparation, as reproducibility of surface conditions proved to be critical for obtaining reliable kinetic parameters. The investigated compounds were dissolved in an aqueous supporting electrolyte (1 M NH_4Cl), chosen to ensure sufficient ionic conductivity while maintaining compatibility with both quinone- and viologen-based systems. Prior to each measurement, the electrolyte solutions were thoroughly deaerated with high-purity argon in order to eliminate interference from dissolved oxygen. Our experimental workflow was designed in two steps. First, wide-range voltammograms were recorded to identify the electrochemically active regions of each molecule. Subsequently, detailed measurements were performed at varying scan rates (5–500 $mV \cdot s^{-1}$), allowing us to assess both the reversibility of the redox processes and the dominant mass transport regime. This approach enabled us to directly compare electron-transfer kinetics and diffusion behavior across the studied systems.

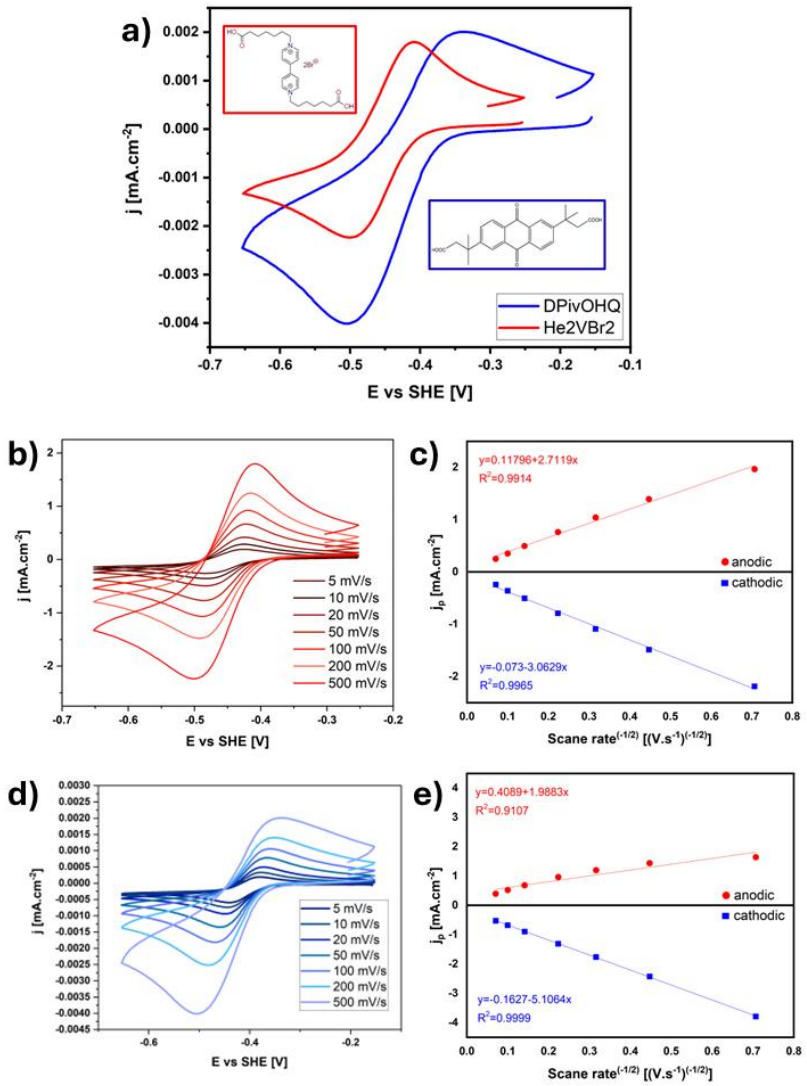

Figure 8 Electrochemical characterization of the investigated organic redox-active molecules. (a) Comparison of cyclic voltammograms of He_2VBr_2 (red) and DPivOHQ (blue) recorded at a scan rate of 500 $mV \cdot s^{-1}$. (b) Cyclic voltammograms of He_2VBr_2 recorded at different scan rates (5–500 $mV \cdot s^{-1}$). (c) Dependence of anodic and cathodic peak current densities on the square root of the scan rate for He_2VBr_2, indicating diffusion-controlled behavior. (d) Cyclic voltammograms of DPivOHQ at different scan rates (5–500 $mV \cdot s^{-1}$). (e) Corresponding linear dependence of peak current densities on the square root of the scan rate for DPivOHQ.

Results and Discussion

The cyclic voltammetric response of the investigated systems clearly reflects the fundamental differences between anthraquinone and viologen derivatives. The anthraquinone-based molecule exhibits a characteristic two-electron redox process corresponding to the quinone/hydroquinone transformation. This multi-electron transfer is advantageous from the perspective of charge storage, as it enables higher theoretical capacity. However, in our measurements, this process was accompanied by broader peaks and increased peak-to-peak separation, indicating somewhat slower electron-transfer kinetics. In contrast, the viologen derivative displays a well-defined and highly reversible one-electron reduction to the radical cation. The corresponding voltammograms are characterized by sharp peaks and minimal peak separation, suggesting fast electron-transfer kinetics and good electrochemical reversibility.

A key aspect of our analysis was the dependence of peak current on the square root of the scan rate. For both systems, a linear relationship was observed, indicating that the redox processes are predominantly diffusion-controlled. Using the Randles–Ševčík relationship, we estimated diffusion coefficients on the order of 10^{-6} $cm^2 \cdot s^{-1}$ for the viologen derivative, which is in excellent agreement with literature values. The anthraquinone derivative exhibited slightly lower and less symmetric diffusion behavior, likely reflecting the more complex nature of its two-electron redox mechanism. From a practical perspective, these results highlight the complementary advantages of the two molecular systems. The viologen derivative combines fast kinetics with favorable transport properties, making it particularly suitable for neutral aqueous electrolytes. On the other hand, the anthraquinone

derivative offers higher charge density due to its multi-electron redox process, although at the cost of slower kinetics and increased susceptibility to side reactions, especially under neutral conditions.

Perspective and Ongoing Work

Building on these findings, our ongoing work is focused on targeted structural modifications aimed at improving the stability of both molecular systems without compromising their electrochemical performance. In the case of anthraquinones, we are exploring the introduction of sterically hindering substituents to suppress nucleophilic attack and enhance chemical robustness. For viologens, our efforts are directed toward increasing molecular size and introducing charged functional groups in order to reduce membrane crossover, which remains a critical challenge in practical RFB operation. At the same time, we are expanding our experimental methodology to include long-term cycling tests and complementary analytical techniques, such as UV–Vis spectroscopy, in order to better understand degradation mechanisms at the molecular level. We believe that combining detailed electrochemical analysis with rational molecular design will be essential for advancing organic RFB systems toward real-world applications.

Conclusion

In this work, we have demonstrated that anthraquinone and viologen derivatives represent two fundamentally different, yet complementary approaches to organic redox-active electrolytes for aqueous flow batteries. Through systematic electrochemical characterization, we have shown that viologens provide fast and reversible redox behavior with excellent transport properties, while anthraquinones offer higher charge storage capacity through multi-electron processes. Rather than identifying a single “optimal” system, our results emphasize the importance of matching molecular properties to the intended operating conditions. This perspective will guide our future research, which aims to bridge the gap between molecular design and practical battery performance.

Acknowledgements

This work was funded by the EU NextGenerationEU through the Recovery and Resilience Plan for Slovakia under the project SUNFLOWERS No. 09I02-03-V01-00022.

References

[1] F. Zhu, Q. Chen, and Y. Fu, “Perspectives on aqueous organic redox flow batteries,” *Green Energy & Environment*, vol. 9, no. 11, Nov. 2024, pp. 1641–1649, 10.1016/j.gee.2024.08.003.
[2] G. S. Nambafu, “Organic molecules as bifunctional electroactive materials for symmetric redox flow batteries : A mini review,” *Electrochemistry Communications,* vol. 127, pp. 107052, Jun. 2021, doi: 10.1016/j.elecom.2021.107052.
[3] V. Singh, S. Kim, J. Kang, and H. R. Byon, “Aqueous organic redox flow batteries,” *Nano Research*, vol. 12, no. 9, pp. 1988–2001, Mar. 2019, doi: 10.1007/s12274-019-2355-2.
[4] C. G. Cannon, P. A. A. Klusener, N. P. Brandon, and A. R. J. Kucernak, “Aqueous Redox Flow Batteries : Small Organic Molecules for the Positive Electrolyte Species,” *Chem Sus Chem*, vol. 16, no. 18, 2023, doi: 10.1002/cssc.202300303.

Synthesis and Physicochemical Characterization of Lanthanide-Based MOF series Derived from H_4MTA for Photovoltaic Applications

P. Obsatnik[a]*, J. Shepa[b], R. Filip[b], S. Kiraly[b], M. Almasi[a], V. Zelenak[a], N. Kiraly[a]
[a] Department of Inorganic Chemistry, Institute of Chemistry, Faculty of Science UPJS,
Moyzesova 11, 041 54 Kosice, Slovak Republic
[b] Department of Physical Chemistry, Institute of Chemistry, Faculty of Science UPJS,
Moyzesova 11, 041 54 Kosice, Slovak Republic
*peter.obsatnik@studnet.upjs.sk

Introduction

Metal–organic frameworks (MOFs) have recently emerged as one of the most dynamic and promising fields within materials science, with over 100,000 structures reported to date. Their exceptional properties, including high specific surface area, tunable pore dimensions, and remarkable structural diversity, make them highly attractive for a broad range of applications such as gas adsorption, catalysis, sensing, and energy-related technologies [1]. In recent years, increasing attention has been directed toward the use of MOFs in photovoltaic systems and solar energy conversion. The hybrid nature of MOFs, combining inorganic nodes with organic linkers, enables fine-tuning of their electronic band structure, which is crucial for optimizing light-harvesting properties. Among the various MOF classes, materials incorporating azo-carboxylate ligands have shown particular promise in photovoltaic applications. The presence of azo linkages allows reversible trans–cis photoisomerization, enabling dynamic modulation of both the structural geometry and electronic properties of the framework in response to light stimuli. Furthermore, multidentate azo-based ligands facilitate the formation of extended coordination networks with enhanced stability and unique optoelectronic characteristics. These features position azo-functionalized MOFs as promising candidates for next-generation photovoltaic materials, where controlled light–matter interactions can be effectively translated into improved energy conversion efficiency [2].

Experimental

In this work, we report the synthesis and comprehensive characterization of a series of fourteen lanthanide-based metal-organic frameworks. The coordination polymers were synthesized via a solvothermal approach involving the tetratopic organic linker H4MTA [3] (0.09 mmol) and lanthanide nitrate precursors Ln(NO3)3·xH2O (0.045 mmol) in a mixed solvent system of N,N′-dimethylformamide and water (6:1, v/v) at 80 °C for seven days. This synthetic protocol enabled the formation of a complete and structurally stable series of LnMTA frameworks spanning the entire range of stable lanthanide elements.

Result and discussion

The LnMTA (Ln= Ln^{3+} lanthanide cations) materials were characterized using infrared infrared spectroscopy, CHN elemental analysis, thermogravimetric analysis (TGA), powder X-ray diffraction (PXRD), and single-crystal X-ray diffraction (SC-XRD). Both single-crystal and powder diffraction analyses confirmed that all synthesized frameworks are isostructural and crystallize in an orthorhombic system. The presence of accessible cavities within the structures motivated further investigation of their gas adsorption properties. The sorption behaviour of LnMTA frameworks was evaluated by CO2 adsorption measurements conducted at 1 bar and temperatures of 0 °C and 20 °C, revealing a high affinity toward CO2 across all samples. Among the studied materials, HoMTA, {[Ho4(MTA)3]·13DMF·14H2O}n, exhibited the highest uptake under low-pressure conditions, reaching 3.98 $mmol \cdot g^{-1}$ at 1 bar and 0 °C. In addition, PrMTA ({[Pr4(MTA)3]·13DMF·14H2O}n) and GdMTA ({[Gd4(MTA)3]·13DMF·14H2O}n) were further investigated under high pressures measurements to 40 bar and at temperatures of 0 °C, 10 °C, and 25 °C (Figure 1). The maximum adsorption capacities were observed at 0 °C and 21 bar, where PrMTA and GdMTA adsorbed 3.31 and 4.38 $mmol \cdot g^{-1}$ of CO_2, respectively.

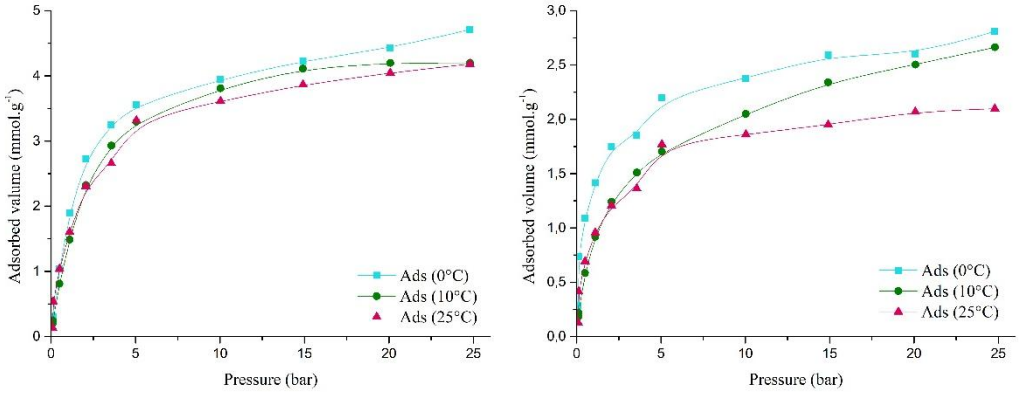

Figure 1 CO_2 adsorption isotherms of GdMTA (a) and PrMTA (b).

To preliminarily evaluate the applicability of the prepared materials in photovoltaic-related systems, the GdMTA material was subjected to chronoamperometric measurements of current response as a function of time, as shown in Figure 2. The obtained curves reveal a pronounced change in current response upon illumination of the electrode, manifested by distinct current increases at defined time intervals. Compared to the reference SPCE electrodes (dark/light), the MOF-modified electrodes exhibit significantly enhanced responses, confirming the photoactivity of the prepared material. With respect to the deposited amount, the most pronounced effect was observed for a loading of 4 µL, representing an optimal balance between the density of photoactive sites and efficient charge transport. A further increase to 5 µL resulted in a decreased response, which can be attributed to increased layer resistance due to the intrinsically low conductivity of the MOF material. Overall, the results demonstrate that the prepared MOF exhibits a measurable photoelectrochemical response and shows promise for applications in light-activated sensing platforms, although further optimization of the immobilization strategy will be required to improve stability and reproducibility.

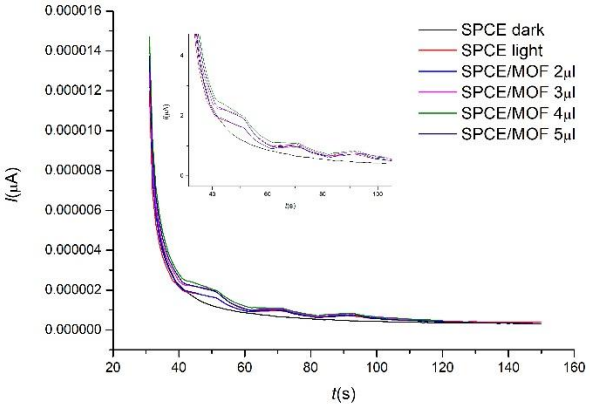

Figure 2 Chronoamperometric response of bare and GdMTA-modified SPCE electrodes under illumination.

Acknowledgements

This work was supported by VEGA 1/0058/25, 1/0442/25 and Funded by the EU NextGenerationEU through the Recovery and Resilience Plan for Slovakia under the project No. 09I03-03-V05-00008 (VVGS-ESGV-2923).

References

[1] O. Cheung, S. Tokuda, D. Jędrzejowski, E. Ploetz, B. Baumgartner, M. Pander, F. Yang, J. D. Evans, R. Ettlinger, S. Wuttke, and D. Matoga, "Material Preparation Information File (MPIF): A Community-Driven Standard for Reporting MOF Syntheses," *Adv. Mater.*, vol. 38, e21420, Feb. 2026, doi: 10.1002/adma.202521420.
[2] S. A. A. Razavi and A. Morsali, "Metal ion detection using luminescent-MOFs: Principles, strategies and roadmap," *Coord. Chem. Rev.*, vol. 415, pp. 213299, Jul. 2020, doi: 10.1016/j.ccr.2020.213299.
[3] M. Almáši, N. Király, V. Zeleňák, M. Vilková, and S. Bourrelly, "Zinc(II) and cadmium(II) amorphous metal–organic frameworks (aMOFs): study of activation process and high-pressure adsorption of greenhouse gases," *RSC Adv.*, vol. 11, pp. 20137–20150, Jun. 2021, doi: 10.1039/D1RA02938J.

Analysis of Battery Storage Implementation Rules in Slovakia

A. Orinak[a]*
[a] Department of Commercial Law and Business Law, Faculty of Law,P.J. Šafárik University in Košice, Kováčska 26, 040 75 Košice, Slovakia
*andrej.orinak@student.upjs.sk

Introduction

The Slovak energy sector is undergoing a transformation driven by the rise of renewable energy sources (RES) and the need for greater grid flexibility. Electricity storage systems (ESS) play a pivotal role in this modernization. To meet climate targets and reduce fossil fuel dependency, the EU will require over 100 GW of battery storage capacity by 2030. In Slovakia, the need for ESS is increasingly urgent due to the boom in photovoltaics, characterized by intermittent generation. Without effective storage, the resulting imbalance between production and consumption threatens grid stability. Battery storage addresses this by balancing supply fluctuations and providing essential ancillary services, such as frequency regulation. Integrating ESS is also financially viable. By optimizing consumption and supporting the transmission system, these assets generate significant cost savings and positive cash flow. The strategic importance of smart storage is further underscored by the Slovak Recovery and Resilience Plan, which aims to reach 68 MW of storage capacity by 2026 [1].

Legislative Framework

Directive (EU) 2019/944 of 5 June 2019 on common rules for the internal market for electricity and amending Directive 2012/27/EU - It defines the term "energy storage" as a standalone activity, allowing battery systems to be operated as independent sources, separate from generation and distribution. It ensures that ESS have equal opportunities to participate in the market for ancillary services.
Directive (EU) 2024/1711 of 13 June 2024 amending Directives (EU) 2018/2001 and (EU) 2019/944 - It addresses the improvement of the Union's electricity market design.
Regulation (EU) 2019/943 on the internal market for electricity - It regulates the principles of electricity market operation, including the integration of energy storage; ESS (Energy Storage Systems) can provide flexibility and ancillary services and participate in balancing markets.
Act No. 251/2012 Coll. on Energy and on amendments to certain acts, as amended - It governs the definition of terms, conditions for obtaining a permit or confirmation of notification requirements for electricity storage activities, and the obligations of such license holders.
Decree of the Regulatory Office for Network Industries (ÚRSO) No. 207/2023 Coll., laying down rules for the operation of the internal electricity market, the content of the operational rules of the system operator and the short-term electricity market organizer, and the scope of commercial terms within the system operator's rules. - It provides further details concerning new market participants, including holders of electricity storage licenses.
Decree of the Regulatory Office for Network Industries (ÚRSO) No. 154/2024 Coll., laying down price regulation in the electricity sector and certain conditions for performing regulated activities in the electricity sector. - It regulates price control in the energy sector and includes provisions related to energy storage facilities.

Current State in Slovakia

In the context of the ongoing energy transition, Slovakia, like many other European Union countries, is intensively focusing on energy transformation and increasing the flexibility of its power system. Battery storage systems play a key role in this process. Their ability to respond rapidly to fluctuations in electricity supply and demand makes them a vital tool for integrating RES and ensuring grid stability.
According to the Slovak Electricity Transmission System (SEPS), the installed capacity of battery storage is expected to reach approximately 250 MW by 2030 and nearly 700 MW by 2040. This growth is anticipated primarily in connection with the development of solar power plants and the overall trend of increasing the share of RES in the country's energy mix [2].
Ancillary Services (AS) are services procured by SEPS to ensure the provision of system services necessary for maintaining supply quality and operational reliability. Their activation results in the delivery of balancing energy. To guarantee technical compliance, every providing facility must hold a valid certificate for each specific ancillary service. Ancillary services provided by certified facilities include:

- Frequency Containment Reserve (FCR): Provides an immediate, automatic response to frequency deviations. Its primary purpose is to stabilize the frequency and maintain the balance between generation and demand within the synchronous area.

- Automatic Frequency Restoration Reserve (aFRR±): Activated automatically via dispatch instructions to restore the system balance and release FCR reserves. It typically reacts within minutes of a frequency deviation to bring the frequency back to its nominal value.
- Manual Frequency Restoration Reserve (mFRR±): Activated manually by the TSO to address larger or longer-term imbalances, such as generation outages or significant demand surges. Its role is to restore the frequency and free up the automatic reserves (aFRR) [3].

To provide ancillary services, the ESS must be certified for the respective service. Most ESS units providing ancillary services are certified for FCR and aFRR±, while some are also certified for mFRR±.
Since 2023, there has been a growing interest in providing FCR services from battery storage systems. This has been positively reflected in the procurement of sufficient FCR volumes between 2023 and 2025, with minimal instances where availability dropped below 80% of the required FCR capacity. Below this threshold, SEPS is mandated, under the rules of the European Awareness System (EAS), to indicate a shortage of FCR regulatory resources.
The current technical conditions of SEPS do not allow ancillary service providers to aggregate ESS for the provision of aFRR (also applicable to mFRR) in various combinations with generation or load facilities [2].
Following the study "Impact of ESS-type Battery Facilities on the Provision of aFRR and mFRR Ancillary Services for SEPS" [4] and its results published on the SEPS website on 30 April 2025, SEPS is currently preparing amendments to the technical conditions and requirements. These will establish rules for battery storage technology and its combination with other technologies [2]. The study concludes that the currently set rules for the provision of FCR ancillary services are sufficient and in line with European Network of Transmission System Operators for Electricity (ENTSO-E) methodologies. Furthermore, the study states that if FCR-type ancillary services were not also provided by operators of Energy Limited Resources (ELR), which include ESS, the total procurement cost for this type of ancillary service would be higher.
The study primarily focused on the provision of FRR services by ESS and the impact of utilizing ESS facilities for SEPS requirements in the following configurations:

- Standalone ESS;
- ESS plus another power source (synchronous generator/load), where AS are provided by the ESS;
- ESS plus another power source (synchronous generator/load), where services are primarily provided by the rotating source and the ESS serves only to maintain the regulation quality of the respective ancillary service (booster).

The conclusions of the study [4] for SEPS resulted in recommendations regarding the expansion of procurement and volumes of FRR services from ESS:

- In the case of standalone ESS: based on analyses of the Intraday Market (IDM) for 2023 and 2024 for 60-minute and 15-minute products, it is impossible to continuously procure power on the IDM for periods longer than 4 hours. This may change with the introduction of 15-minute IDM products; therefore, the study recommends re-analysing the fulfilment of buy and sell orders on the IDM 12 months after the introduction of 15-minute products across all profiles in the region. Based on this, a recommendation to approve or reject standalone ESS for FRR provision can be made.
- The volume of services procured from ESS should not exceed 15% of the total required volume of ancillary services for any FRR-type service. This is due to the need to verify FRR provision from "ESS plus another power source" without risking grid security, significantly deteriorating regulation quality, or negatively impacting current IDM trading trends.
- Following a minimum one-year period of experience with FRR provision from ESS, SEPS should conduct an analysis of FRR delivery quality and IDM trading possibilities. Subsequently, based on these findings, SEPS should re-evaluate the volumes of FRR procured from ESS.
- Legislation should establish clear certification rules and define the scope of these services, including penalties for rule violations—not only regarding charging strategies but also for failures in service delivery.

The implementation of ESS for the provision of FRR-type ancillary services within the transmission system will also impact the regulatory framework of the Slovak Republic, primarily in the following areas:

- **Legislative Area:** This involves amending Acts No. 250/2012 Coll. and 251/2012 Coll., Decrees No. 154/2024 Coll. and 207/2023 Coll., and the SEPS Operational Rules (Grid Code) to explicitly include and define ESS as potential ancillary service providers. These amendments should define ESS facilities, their technical requirements, conditions for ESS certification as AS providers, and their participation in the ancillary services market. Furthermore, they should define the rights and obligations of ESS operators and establish the Authority's jurisdiction in this field.
- **Regulatory Approach of the Authority:** This entails accounting for the specific characteristics of ESS, primarily by adjusting the methods for determining AS prices and tariffs and creating new regulatory tools for ESS monitoring.

- **Economic Area:** Given the financial impact of providing ancillary services via ESS, it will be necessary to re-evaluate remuneration mechanisms for AS provision. Additionally, the methodology for calculating the costs of providing ancillary services, which serve as the basis for calculating end-user tariffs, must be adjusted.

In Slovakia, ESS operators primarily utilize energy storage facilities to provide ancillary services for the transmission system, which include system stabilization, frequency stability maintenance, and rapid response to demand fluctuations. Furthermore, they provide backup power during outages, peak shaving (reduction of reserved capacity), energy arbitrage, imbalance optimization at the balance group level, self-consumption, and sales on the spot market.
One example of battery storage utilization is cost-saving on imbalances at a delivery point where the BESS is installed directly on-site. In this scenario, the storage operator installs the entire system, including the battery and control software, at their own expense to optimize imbalance management at the given delivery point based on their own dispatch instructions rather than the requirements of the delivery point itself. Any evaluated profit from the financial settlement of the optimized imbalance remains with the storage operator, who in turn pays the owner of the delivery point a fixed fee for the right to use their premises.

Based on the ownership data provided by the surveyed operators, market participants can be categorized into two groups: owner-operators and those utilizing lease-based models.
The cost of leasing Battery Energy Storage Systems (BESS) and associated services fluctuates significantly based on capacity, lease duration, and the scope of the service package. These systems are highly versatile, serving applications ranging from microgrids to industrial consumption optimization; their pricing directly reflects this modularity and the inclusion of comprehensive support services. For utility-scale or industrial BESS, lease terms vary from several weeks to several years. Due to the highly customizable nature of these solutions, specific pricing is rarely disclosed publicly, and quotes are typically tailored to the individual technical requirements of each client.
The majority of ESS operators primarily leverage battery storage to provide ancillary services for SEPS, manage self-consumption, and optimize imbalances at the balance group level, as well as to capitalize on spot market volatility during peak price periods. Currently, six operators utilize BESS assets owned by third parties under formal lease agreements. Monthly lease payments range from approximately €1,478 to €33,000, or are structured as a profit-sharing model based on the revenue generated from ancillary services.
These lease rates are contingent upon the system's technical specifications, its operational mode, and the contract duration. When normalized against the installed capacity of the facility, the average lease rate stands at approximately €18,500/MW/month.

Conclusions

Driven by the national Recovery and Resilience Plan and the growing need for grid flexibility, Slovakia’s ESS capacity for ancillary services is projected to reach 250 MW by 2030 and 700 MW by 2040. This rapid expansion positions ESS as a primary economic stimulus and a key provider of FCR and aFRR services, with operators increasingly scaling into secondary and tertiary control. Ultimately, energy storage serves as a cornerstone of modern infrastructure, enabling seamless RES integration and flexible grid management tailored to the specific operational requirements of the Slovak transmission system operator.

Acknowledgements

This work was funded by the EU NextGenerationEU through the Recovery and Resilience Plan for Slovakia under the project SUNFLOWERS No. 09I02-03-V01-00022.

References

[1] Plán obnovy Cestovná mapa k lepšiemu Slovensku. Retrieved March 23, 2026, https://www.planobnovy.sk/site/assets/files/1019/kompletny-plan-obnovy.pdf.
[2] Slovenská elektrizačná prenosová sústava: Stratégia zabezpečenia dostatočného objemu podporných služieb pre rok 2026, Bratislava, 19.06.2025. Retrieved March 23, 2026, https://www.sepsas.sk/engine/wp-content/uploads/2025/06/Strategia-zabezpecenia-PpS-na-2026_final.pdf.
[3] Batériové úložiská, podporné a regulačné služby. Smart energetické riešenia novej generácie. Retrieved March 23, 2026, https://www.sse.sk/velkoodberatelia/energeticky-efektivne-riesenia/bateriove-uloziska-podporne-a-regulacne-sluzby?page_id=14518.
[4] Výsledky štúdie „Vplyv batériových zariadení typu BESS na poskytovanie podporných služieb typu aFRR a mFRR pre SEPS“, 30.4.2025. Retrieved March 23, 2026, https://www.sepsas.sk/aktuality/vysledky-studie-vplyv-bateriovych-zariadeni-typu-bess-na-poskytovanie-podpornych-sluzieb-typu-afrr-a-mfrr-pre-seps/.

Assessment of European Energy Regulations for Clean Energy

A. Orinak[a]*
[a] Department of Commercial Law and Business Law, Faculty of Law, P.J. Šafárik University in Košice, Kováčska 26, 040 75 Košice, Slovakia
*andrej.orinak@student.upjs.sk

Introduction

Renewable energy's transition to a global reality is powered by a cross-sector shift toward sustainable consumption and carbon reduction targets initiated by international agreements in the 1990s. Solar-photovoltaic (PV) and wind are the leading clean energy sources, yet their intermittency, driven by weather variability, requires integration with battery energy storage systems (BESS). This hybridization, supported by research and market trends, ensures a stable supply that mimics the reliability of synchronous generators like hydroelectric power plants (HPP) and thermoelectric power plants (TPP) [1]. BESS, demand-side management (DSM), vehicle-to-grid (V2G) strategies, and combined heat and power (CH&P) plants are classified as renewable energy resources (RER) rather than primary sources, as they facilitate bidirectional energy flow between load and source [2]. Global regulatory frameworks often lag in BESS integration due to a lack of technical clarity. While BESS acts as a load when charging, it is a distinct asset class. Effective regulation requires acknowledging its specific power electronics and bidirectional dynamics to move beyond legacy energy definitions. Europe's experience with battery regulation is a blueprint for establishing robust green hydrogen frameworks under the Renewable Energy Directive [3]. By aligning these regulatory environments, the EU can foster an integrated storage ecosystem that enhances the overall effectiveness of the "Fit for 55" objectives [4]. Drawing on scientific research and international distributed energy resources (DER) legislation, this study identifies best practices for BESS hybridization to support European countries in their transition toward advanced renewable integration.

European Regulatory Framework for Clean Energy

Europe is consolidating energy storage system (ESS) regulatory guidelines through initiatives like the STORE Project, the "Clean Energy for All Europeans" package, the Green Deal, and the 2020 Climate Law [5-9]. While these have reshaped national regulations, barriers such as inadequate project support and undefined regulatory frameworks persist.

The EU electricity sector is driven by normative instruments, such as European Parliament Directives and Communications, which establish renewable energy targets and implementation mechanisms. Key initiatives shaping this landscape include Energy 2020, the 2050 Roadmap, the Clean Energy Package, and the European Green Deal, supported by specific directives like (EU)2018/2001 and (EU)2019/944 [10–12]. To advance its renewable energy and efficiency goals, the EU (2020) published a study on energy storage, identifying critical barriers to both behind-the-meter (BTM) and front-of-the-meter (FTM) solutions. These include a lack of clear definitions, legal provisions for hybridization, and policy coherence among Member States. The report outlines best practices and regulatory status across the EU, covering market access, grid connection, and taxation [13].

National Case Studies: Implementation and Obstacles

Spain is aggressively targeting storage, planning for 6 GW of capacity (3.5 GW pumped hydro, 2.5 GW batteries). While the government recently instituted a "Regulatory Sandbox" (May 2023) to foster BESS innovation, the sector faces a major hurdle: double charging. Because the framework does not distinguish storage from traditional generation or consumption, ESS owners are often charged network access tariffs twice, once when buying energy to charge and again when selling it back to the grid.

The UK has led the way by explicitly amending its regulatory framework to include legal definitions for "energy storage" and "energy storage facilities." This provides much-needed clarity for license applications. Furthermore, the "Storage at Scale" competition has successfully funded innovative lithium-ion and sodium-sulphur projects. However, loopholes regarding double charging for final consumption fees persist, and the role of network operators in owning storage remains a point of debate.

Faced with high renewable penetration, Greece authorized a complete regulatory framework in 2020. It has launched a robust auction scheme aiming to award 1000 MW of capacity by 2025. Greece is a prime example of market-driven storage, where participation in the Frequency Containment Reserve (FCR) can yield significant revenue (approx. €100,000/MW/year), incentivizing utility-scale BESS.

Finland utilizes its "Energy Aid" program to co-finance battery facilities, provided costs do not exceed 50% of the total investment. While Finland allows BESS to provide FCR services, it lacks specific storage-only regulations, often requiring large-scale projects to undergo complex public licensing. Similarly, Denmark and Norway focus

on short-term heat storage and gas coupling, though they still treat ESS agents as "ordinary consumers" regarding taxes.

Germany focuses on avoiding renewable curtailment by integrating ESS directly into power plants. The updated Federal Battery Law and modern building codes have simplified the installation of local storage. This is particularly evident in the residential sector, where low feed-in tariffs have driven users to combine PV with BESS, increasing self-consumption (autarky) from 30% to 80%.

Ireland utilizes a Capacity Remuneration Mechanism (CRM) to support storage based on its operational timing. While they have successfully launched pilot schemes for home-BESS, the regulatory environment is still evolving. Like its peers, Ireland struggles with a lack of legal distinction between generation and storage, hindering the transition to a fully decarbonized supply.

Table 1 Summarization of the regulatory environment of the selected European countries [2].

Country	Regulatory Framework	Market Participation	Specific Challenges And Initiatives	Strengths	Weaknesses
Spain	Lacks ESS regulation.	Limited by double charging.	Ministry instituted regulatory sandbox environment in 2023 for research and innovation; aims to address regulatory gaps.	Potential for regulatory improvement and innovation; increasing research and development opportunities.	Current double charging issue; regulatory uncertainty.
UK	Clear regulatory framework.	Well-defined regulations.	"Storage at Scale" contest funded innovative large-scale ESS projects; addresses licensing and operational issues.	Regulatory clarity; support for large-scale ESS projects; competitive funding opportunities.	Licensing requirements for large-scale projects; no exemption from taxes and fees.
Greece	New regulatory framework.	Voluntary participation.	Market includes various balancing capacity products; emphasizes co-location with PV for energy storage projects.	Regulatory framework for ESS; opportunities for diverse energy storage projects.	Voluntary participation in the market; potential need for clearer incentives.
Finland	Regulatory framework not specific.	Limited by double charging.	Energy Aid program offers co-financing; regulatory framework for large-scale projects involves public audiences.	Financial support for clean energy projects; potential for innovative solutions.	Double charging issue; complex licensing process for large-scale projects.
Denmark and Norway	ESS in expansion planning.	Ordinary consumers with no tax exemption.	Funding for ESS development; specific grid codes for battery connection and access.	Integration into expansion planning; funding support; clear grid codes.	No tax exemption for ESS applications; limited regulatory incentives.
Ireland	Evolving regulation.	Participation depending on technology used.	Supports small-scale BTM ESS; trends toward legal certainty for end consumers and transition to a decarbonized supply.	Evolving regulatory framework; support for small-scale ESS; transition to decarbonized supply.	Lack of distinction between generation technologies and ESS; ongoing regulatory development.
Germany	Strengthened regulation.	Various market participation.	Germany integrates ESS into renewable energy plants; market incentive programs; participation in the	Integration into renewable energy systems; market incentives; participation in	Limited primary frequency control for BESS; complex regulatory landscape.

			frequency market.	frequency market.	

Table 1 summarizes the regulatory status, market participation, challenges, and institutional initiatives of the European countries analysed in this study. While European nations are aligned on climate neutrality, the practical deployment of BESS is hindered by antiquated classification. Most frameworks still struggle to treat BESS as a unique "third resource," leading to:

- Financial Penalties: Double charging remains the most common and counterproductive obstacle.
- Market Restrictions: Limited participation in secondary ancillary services (like FRR) for battery assets.
- Technical Lag: Regulation is often slower to evolve than the power electronics and control systems that define modern BESS performance.

Conclusions

The study highlights the importance of ESS, particularly BESS, as critical power system components. Defined by advanced power electronics and control systems, BESS exhibits a dualistic behaviour during charge and discharge. This versatility defies traditional classification as either a load or a generator, establishing BESS as a distinct third resource. Experiences from pioneering storage markets offer critical best practices for mitigating business risks in emerging clean-technology sectors.

Current regulations that fail to recognize this dualistic behaviour (charging and discharging) result in financial penalties that undermine the business case for green hydrogen and battery projects. For the "Fit for 55" objectives to succeed, these nations must harmonize their definitions to allow ESS to function as a versatile, integrated element of the modern power grid.

Acknowledgements

This work was funded by the EU NextGenerationEU through the Recovery and Resilience Plan for Slovakia under the project SUNFLOWERS No. 09I02-03-V01-00022.

References

[1] J. Mitali, S. Dhinakaran and A. Mohamad, “Energy storage systems: A review”, *Energy Storage Sav.,* vol. 1, no. 3, pp. 166–216, September 2022, doi: 10.1016/j.enss.2022.07.002.

[2] R. Dias Filho, A. C. M. Monteiro, T. Costa, A. Vasconcelos, A. C. Rode, M. Marinho, “Strategic Guidelines for Battery Energy Storage System Deployment: Regulatory Framework, Incentives, and Market Planning”, Energies, vol. 16, no. 21, pp. 7272, October 2023, doi: 10.3390/en16217272.

[3] Renewable Energy Directive, Directive (EU) 2023/2413, 18 October 2023, Retrieved March 30, 2026, https://energy.ec.europa.eu/topics/renewable-energy/renewable-energy-directive-targets-and-rules/renewable-energy-directive_en#the-revised-directive.

[4] Regulation (EU) 2021/119, 30 June 2021, Retrieved March 30, 2026, https://eur-lex.europa.eu/legal-content/EN/TXT/?uri=CELEX%3A32021R1119.

[5] European Commission. Study on Energy Storage—Contributions to the Security of the Electricity Supply in Europe; Publications Office: Luxembourg, 2020. Retrieved March 30, 2026, https://energy.ec.europa.eu/publications/study-energy-storage_en.

[6] European Commission. In Focus: Renewable Energy in Europe. 2020. Retrieved March 30, 2026, https://ec.europa.eu/info/news/focusrenewable-energy-europe-2020-mar-18_en.

[7] stoRE. European Regulatory and Market Framework for Electricity Storage Infrastructure—Analysis and Recommendations for Improvements Based on a Stakeholder Consultation, Deliverable 4.2; stoRE: Munich, Germany, 2013.

[8] stoRE. stoRE—Final Publishable Report, stoRE Project; stoRE: Munich, Germany, 2014.

[9] stoRE. stoRE Project. 2019. Retrieved March 30, 2026, https://www.store-project.eu.

[10] European Parliament and of the Council. Renewable Energy Directive (EU)2018/2001. 2018. Retrieved March 30, 2026, https://eur-lex.europa.eu/legal-content/EN/TXT/PDF/?uri=CELEX:32018L2001.

[11] European Union. Common Rules for the Internal Electricity Market (EU)2019/944. 2019. Retrieved Mar. 30, 2026, https://eur-lex.europa.eu/legal-content/EN/TXT/PDF/?uri=CELEX:32019L0944.

[12] European Commission. European Climate Law (2020); European Commission: Brussels, Belgium, 2020.

[13] K. Moorthy, N. Patwa, Y. Gupta, Y. Breaking barriers in deployment of renewable energy. Heliyon, vol. 5, no. 1, pp. e01166, Jan. 2019, doi: 10.1016/j.heliyon.2019.e01166.

Reproducibility of Electrochemical Response of Carbon Paste Electrodes Based on Commercial and Recycled Graphite

R. Orinakova[a]*, I. Sisolakova[a], S. Vanchak[a], R. Filip[a], J. Shepa[a]
[a] Department of Physical Chemistry, Institute of Chemistry, Pavol Jozef Šafárik University in Košice, Moyzesova 11, 041 54 Kosice, Slovak Republic
*renata.orinakova@upjs.sk

Electrochemical sensors represent an important class of analytical devices widely used for the detection of chemical and biological species due to their high sensitivity, rapid response, and potential for miniaturization. Among various electrode materials, carbon-based systems, particularly carbon paste electrodes (CPEs), have attracted considerable attention owing to their low cost, ease of preparation, and versatile surface modification possibilities [1]. In recent years, increasing emphasis has been placed on the use of recycled carbon materials as sustainable alternatives to conventional commercial sources, in line with the principles of the circular economy [2]. However, the broader application of recycled materials in electrochemical sensing is often limited by concerns related to variability and reproducibility, which are critical parameters determining the reliability of analytical measurements.

In this work the reproducibility of carbon paste electrodes (CPEs) prepared from commercial (samples KG and SP) and recycled graphite (samples A and B) was evaluated using cyclic voltammetry in the ferri/ferrocyanide redox system (Figure 1).

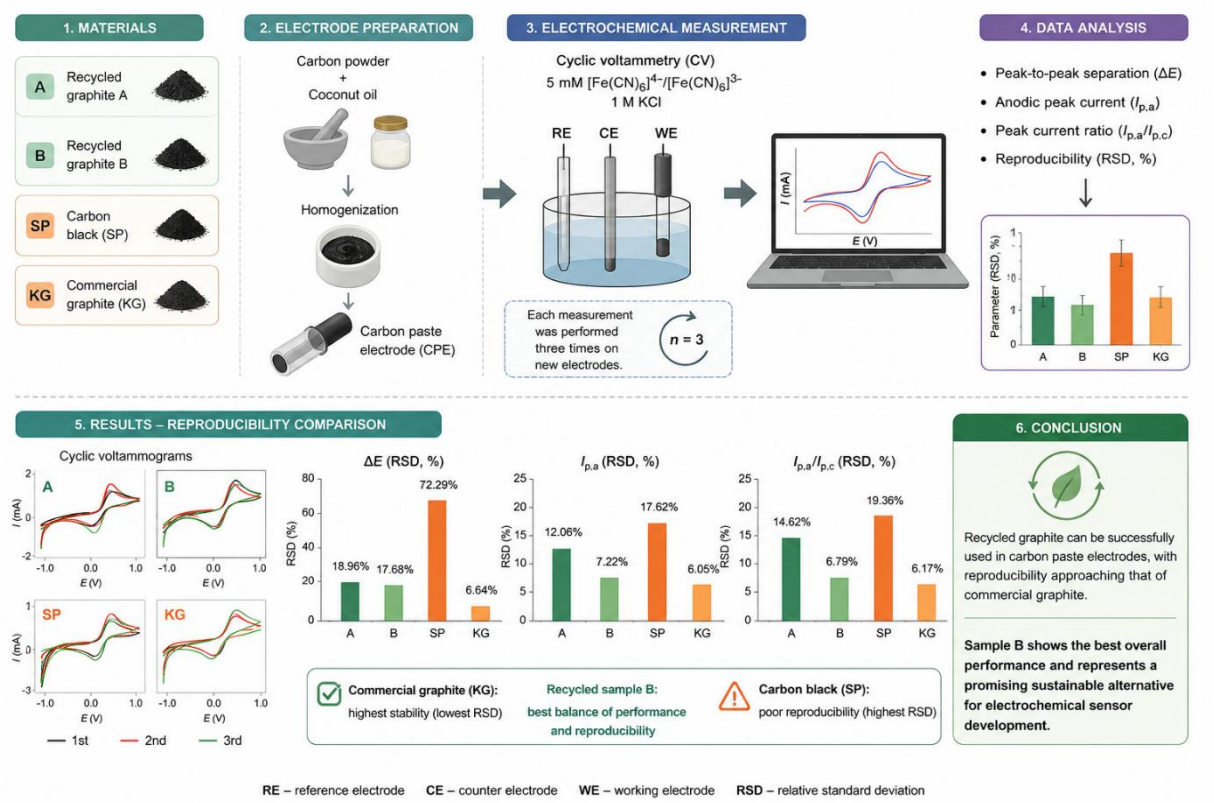

Figure 2 Schematic overview of the experimental workflow used for the evaluation of reproducibility of carbon paste electrodes (CPEs) prepared from commercial and recycled graphite materials (samples A, B, SP, and KG).

While commercial graphite exhibited the lowest variability, selected recycled samples showed comparable reproducibility. In particular, recycled sample B demonstrated a favorable balance between electrochemical performance and measurement consistency, highlighting its potential as a sustainable alternative electrode material. The cyclic voltammograms recorded for individual samples (A, B, SP, KG) in Figure 2 show clear differences in both signal intensity and reproducibility. For each material, three independently prepared electrodes were measured. Sample A exhibits relatively high peak currents but noticeable variability between replicates, particularly in the cathodic branch. Sample B shows significantly better overlap of curves, indicating improved reproducibility. In contrast, sample SP demonstrates the largest deviations between individual measurements, confirming poor reproducibility. Commercial graphite (KG) shows highly consistent responses with minimal

variation between curves. The comparison of peak-to-peak separation (ΔE) reveals increasing variability in the order KG < B ≈ A << SP. The highest relative standard deviation (RSD ≈ 72%) was observed for SP, indicating significant instability. In contrast, KG exhibits the lowest variability (~6.6%), confirming high reproducibility. Recycled samples A and B show moderate variability (~18–17%), suggesting partial preservation of electrochemical consistency. The anodic peak current analysis indicates that sample A provides the highest current response, suggesting the largest electroactive surface area; however, this is accompanied by relatively high variability (~12%). Sample B shows slightly lower current but significantly improved reproducibility (~7%). Sample SP again exhibits high variability (~18%), while KG demonstrates the lowest current but also the highest stability (~6%). The ratio of anodic to cathodic peak currents provides insight into electrochemical reversibility. Sample SP shows values closest to unity, indicating favorable electrochemical behavior, but this is accompanied by high variability (~19%). Conversely, KG exhibits the most stable ratio (~6%) but deviates more from ideal reversibility. Recycled samples A and B again show intermediate behavior, with sample B achieving the best compromise between reproducibility (~6.8%) and electrochemical performance.

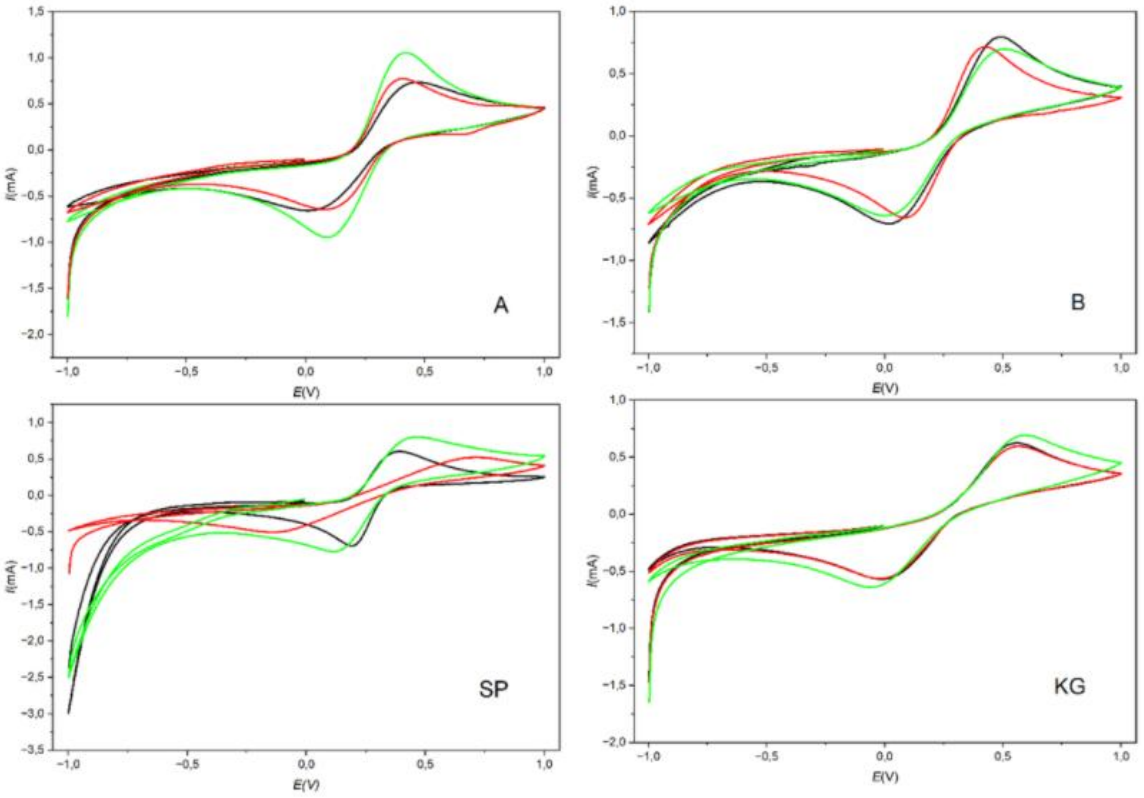

Figure 3 Cyclic voltammograms recorded in 5 mM $[Fe(CN)_6]^{4-}/[Fe(CN)_6]^{3-}$ and 1 M KCl solution at carbon paste electrodes (CPEs) prepared from samples A, B, SP, and KG. Each measurement was performed three times using independently prepared electrodes.

Overall, the results clearly demonstrate that reproducibility is strongly dependent on material structure and homogeneity. Commercial graphite provides the most stable and reproducible response across all evaluated parameters; however, among recycled materials, sample B shows comparable reproducibility while maintaining relatively high electrochemical activity. These findings confirm that recycled graphite materials can be successfully applied in carbon paste electrodes, with performance approaching that of commercial standards, and highlight their potential for sustainable electrochemical sensor development.

Acknowledgements

Funded by the EU NextGenerationEU through the Recovery and Resilience Plan for Slovakia under the project No. 09-I05-03-V02-00047.

References

[1] J. Wang, *Analytical Electrochemistry*, 3rd ed.; Wiley-VCH, 2006.
[2] K. Ragaert, L. Delva, K. Van Geem, „Mechanical and chemical recycling of solid plastic waste,“ *Waste Management*, vol. 69, pp. 24–58, Nov. 2017, doi: 10.1016/j.wasman.2017.07.044.

Optimization of Plasma-Induced Surface Activation of Polyaniline for Bioanalyte Sensing

K. Ozaltin[a]*, I. Sisolakova[b], J. Shepa[b], R. Orinakova[a,b], P. Saha[a]
[a] Centre of Polymer Systems, University Institute, Tomas Bata University in Zlín, Třída Tomáše Bati 5678, 76001 Zlín, Czech Republic
[b] Department of Physical Chemistry, Institute of Chemistry, Pavol Jozef Šafárik University in Košice, Moyzesova 11, 041 54 Kosice, Slovak Republic
*ozaltin@utb.cz

Conductive polymers (CPs), have emerged as highly promising materials for electrochemical biosensing due to their tunable electrical properties, structural versatility, and ability to undergo doping processes in response to analyte interactions [1]. These features make them attractive candidates for the development of sensitive, selective, and flexible sensor platforms, with growing interest in medical diagnostics and wearable technologies [2]. However, the sensing performance of CP-based interfaces is often limited by surface inertness, insufficient surface functionality, suboptimal wettability, and poorly controlled interfacial morphology, all of which hinder efficient biomolecule immobilization and electron transfer. Therefore, precise surface engineering is essential to improve interfacial properties and enhance overall sensing performance.

In this study, a comparative plasma-activation strategy for PANI films is being carried out using direct current (DC), alternating current (AC), and microwave (MW) plasma sources. The effects of plasma type, input power, and treatment duration are being systematically investigated in order to optimize surface properties relevant to bioanalyte sensing. Particular attention is being paid to the relationship between plasma conditions and the resulting physicochemical characteristics of the polymer surface.

Surface modification is being evaluated through contact angle measurements and surface energy analysis, while the evolution of morphology and surface topography is being examined using scanning electron microscopy (SEM) and atomic force microscopy (AFM). In parallel, Fourier-transform infrared spectroscopy (FTIR) is being used to monitor plasma-induced chemical changes, especially the formation of oxygen-containing functional groups such as hydroxyl (–OH) moieties. Preliminary observations indicate that plasma treatment can significantly alter the surface of PANI by increasing wettability, modifying roughness and effective surface area, and introducing reactive functionalities that are expected to improve interfacial biointeractions.

In addition to surface characterization, the influence of plasma activation on the electrochemical behavior of PANI-based interfaces is under investigation in order to establish process–structure–property relationships relevant to biosensing. The comparative evaluation of DC, AC, and MW plasma is expected to identify optimal activation conditions for constructing more efficient and tunable sensing surfaces for bioanalyte detection.

Acknowledgements

This research was sponsored by the NATO Science for Peace and Security Programme under grant id. G6106.

References

[1] I. Šišolaková, R. Gorejová, F. Chovancová, J. Shepa, F. A. Ngwabebhoh, A. S. Fedorková, P. Sáha and R. Oriňaková, " Polymer-based Electrochemical Sensor: Fast, Accurate, and Simple Insulin Diagnostics Tool," *Electrocatalysis,* vol. 14, pp. 697-707, Apr. 2023, doi.org/10.1007/s12678-023-00827-w.

[2] J. Hovancová, I. Šišoláková, R. Oriňaková, and A. Oriňak, "Nanomaterial-based electrochemical sensors for detection of glucose and insulin," *Journal of Solid State Electrochemistry*, vol. 21, no. 8, pp. 2147–2166, Aug. 2017, doi: 10.1007/s10008-017-3544-0.

MoNiFeP-Modified Carbon Fibres: Performance and Degradation under Hydrogen Evolution Reaction

M. Plevova[a]*, E. Mudra[a], M. Streckova[a]
[a] Institute of Materials Research, Slovak Academy of Sciences, Košice, Slovak Republic
*mplevova@saske.sk

Hydrogen is widely regarded as a promising alternative to fossil fuels due to its potential as a clean and sustainable energy carrier. It can be efficiently produced via water electrolysis powered by renewable energy sources, offering a pathway toward carbon-neutral energy systems. However, the practical implementation of water electrolysis is still hindered by several challenges, including the sluggish kinetics of the hydrogen evolution reaction (HER) in alkaline media and the dependence on expensive platinum-based catalysts under acidic conditions. Consequently, the development of cost-effective, highly active, and durable electrocatalysts remains a critical research objective.

In recent years, significant attention has been devoted to research of non-precious metal-based catalysts, particularly those containing transition metals such as Mn, Fe, Co, and Ni. These materials have been explored in various forms, including oxides, (oxy)hydroxides, phosphides, nitrides, and selenides. Among them, bi- and trimetallic transition-metal phosphides stand out due to their near-platinum-like HER activity and their ability to operate efficiently in both acidic and alkaline environments. Their enhanced performance is commonly attributed to the synergistic interactions between metal and phosphorus species. The incorporation of phosphorus leads to the formation of polarized metal-phosphorous bonds, where phosphorus sites facilitate hydrogen adsorption in acidic media, while in alkaline conditions they contribute to weakening the O–H bond and promoting water dissociation. Despite these advantages, phosphide catalysts are typically synthesized in powder form and require deposition onto conductive substrates, which can introduce additional interfacial resistance and negatively affect catalytic performance.

In this work, flexible, free-standing fibrous C/MoNiFeP electrodes were fabricated via electrospinning, providing a binder-free and conductive architecture. The electrochemical performance was evaluated in both 0.5 M H_2SO_4 and 1 M KOH using a standard three-electrode configuration. The prepared electrodes demonstrated good catalytic activity, achieving overpotentials of η_{10} = –344 mV in acidic and η_{10} = –223 mV in alkaline media. Stability investigations revealed significant dissolution of catalyst particles under acidic conditions. In alkaline media pronounced surface reconstruction was also observed. The particles, as well as the carbon matrix, dissolute, and transformation of highly active phosphide phase to phosphate happens.

Acknowledgements

This work was funded by the EU Next Generation EU through the Recovery and Resilience Plan for Slovakia under the project No 09I04-03-V02-00006.

From Atoms to Applications: Multiscale Modeling of Electrochemical Systems

N. Podrojkova[a]*, A. Guboova[b], M. Streckova[c], R. Orinakova[a], A. Fedorkova[a]
[a] Department of Physical Chemistry, Institute of Chemistry, Pavol Jozef Šafárik University in Košice, Moyzesova 11, 041 54 Kosice, Slovak Republic
[b] Department of Energy and Environmental Materials, SANKEN, Osaka University, Mihogaoka 8-1, Ibaraki, Osaka 567-0047, Japan
[c] Institute of Materials Research, Watsonova 47, 040 01 Košice, Slovakia
*natalia.podrojkova@upjs.sk

The global transition toward sustainable energy solutions has intensified the demand for high-performance electrochemical devices, including advanced water electrolyzers and large-scale energy storage systems. However, the efficiency of these technologies is fundamentally governed by complex, coupled phenomena that span multiple orders of spatial and temporal magnitude—from the quantum mechanical behavior of single atoms at the catalyst interface to the macroscopic fluid dynamics within device architectures. Bridging these distinct scales remains a critical challenge for the predictive design of next-generation materials. This contribution presents a comprehensive dual modeling approach that integrates high-level quantum mechanical calculations with continuum-level multiphysics simulations. By linking atomistic descriptors with macroscopic transport phenomena, this framework provides a robust methodology to characterize and optimize key electrochemical systems, such as transition-metal-based hydrogen evolution catalysts and redox flow batteries (RFBs), while offering significant potential for applications in electrochemical sensing and corrosion protection of biodegradable materials.

The first part of the work focuses on Density Functional Theory (DFT) calculations used to evaluate adsorption energetics and catalytic activity. Case studies include transition metal phosphides (MoP, CoP, FeP) for the hydrogen evolution reaction (HER) [1-3] and metal-doped graphene surfaces (Bi, Sn, Pb, Ti) for RFB applications using Quantum ESPRESSO distribution [4, 5]. Additionally, we examine the fundamental interactions between graphene and organic electrolyte molecules. These examples illustrate how atomistic modeling can rationalize material behavior, with analogous workflows being applicable to the study of electrochemical sensors or corrosion processes.

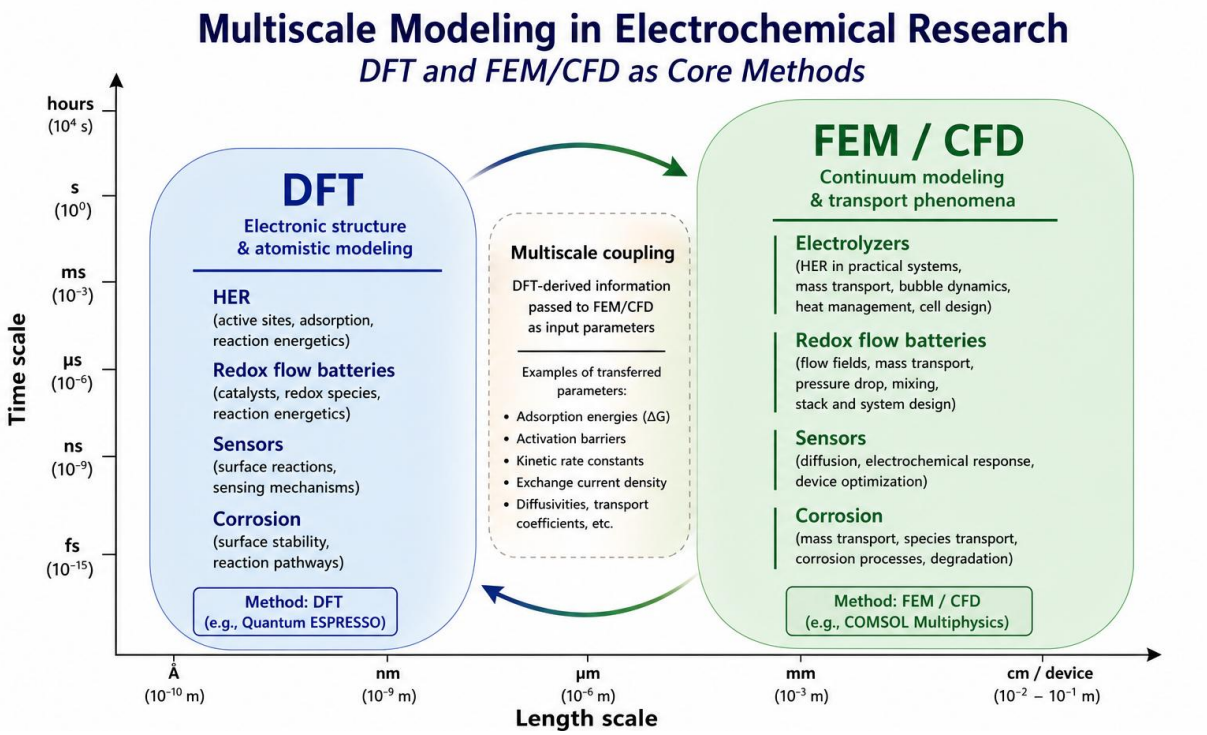

Figure 1 Multiscale modeling framework for electrochemical systems, linking density functional theory (DFT) with continuum approaches (FEM/CFD).

The second part transitions to continuum-level modeling using the Finite Element Method (FEM). Utilizing COMSOL Multiphysics [6], we analyze fluid dynamics and mass transport within RFB geometries to determine hydraulic resistance parameters essential for stack-level scaling. Beyond redox flow batteries, the versatility of the FEM approach is demonstrated through its application in modeling water electrolyzers, where gas-liquid transport is critical, and in electrochemical sensor design, where geometry optimization directly impacts sensitivity. Furthermore, the framework enables the simulation of local corrosion environments, accounting for ion concentration gradients and potential distributions.

By presenting these two modeling pillars, the work highlights a comprehensive toolkit for characterizing electrochemical systems. The integration of DFT-derived insights with engineering-scale simulations provides a robust, predictive pathway applicable across various domains—from optimizing catalyst surfaces to the structural design of sensors and energy conversion devices.

Acknowledgements

This work was supported by the HERAQUAS project (No. 09I03-03-V04-00086), focused on research and development in the field of hydrogen using quantum-chemical atomistic simulations, funded by the Recovery and Resilience Plan for Slovakia.

References

[1] N. Podrojková et al., "Experimental and computational analysis of Ni–P and Fe–P metal foams for enhanced hydrogen evolution reaction in alkaline media," *Sustain. Energy Fuels*, vol. 9, no. 18, pp. 5044-5056, Aug. 2025, doi: 10.1039/D5SE00527B.

[2] N. Podrojková et al., "A study of the mechanism of the hydrogen evolution reaction catalysed by molybdenum phosphide in different media," *Mater. Today Sustain.*, vol. 31, pp. 101141, Sep. 2025, doi: 10.1016/j.mtsust.2025.101141.

[3] A. Gubóová et al., "Bimetallic MoFe phosphide catalysts for the hydrogen evolution reaction," *Electrochim. Acta*, vol. 506, 145008, Dec. 2024, doi: 10.1016/j.electacta.2024.145008.

[4] P. Giannozzi et al., "Advanced capabilities for materials modelling with Quantum ESPRESSO," *J. Phys.: Condens. Matter,* vol. 29, pp. 465901, 2017, doi: 10.1088/1361-648X/aa8f79.

[5] P. Giannozzi et al., "QUANTUM ESPRESSO: a modular and open-source software project for quantum simulations of materials," *J. Phys.: Condens. Matter*, vol. 21, pp. 395502, 2009, doi: 10.1088/0953-8984/21/39/395502.

[6] COMSOL Multiphysics® v. 6.4. www.comsol.com. COMSOL AB, Stockholm, Sweden.

Assessment of Long-Term Stability of Recycled Graphite for Electrochemical Applications

I. Sisolakova[a]*, S. Vanchak[a], R. Filip[a], J. Shepa[a]
[a] Department of Physical Chemistry, Institute of Chemistry, Pavol Jozef Šafárik University in Košice, Moyzesova 11, 041 54 Kosice, Slovak Republic
*ivana.sisolakova@upjs.sk

Carbon paste electrodes (CPEs) represent a low-cost and versatile platform for electrochemical sensing, with growing interest in the use of sustainable materials [1]. In this study, recycled graphite obtained from waste sources was evaluated as an alternative to commercial carbon materials for electrode fabrication. The paste composition was optimized using coconut oil as a binder, with the optimal ratio determined as 1 mL per 5 g of graphite powder. Significant differences among recycled graphite samples (A–F) were evident both visually and electrochemically (Figure 1). Samples A, C, D, and F exhibited black coloration, while samples B and E were grey with a metallic luster; impurities were observed in sample F. The prepared pastes showed varying consistencies, with sample A being the most homogeneous and samples D–F the most granular.

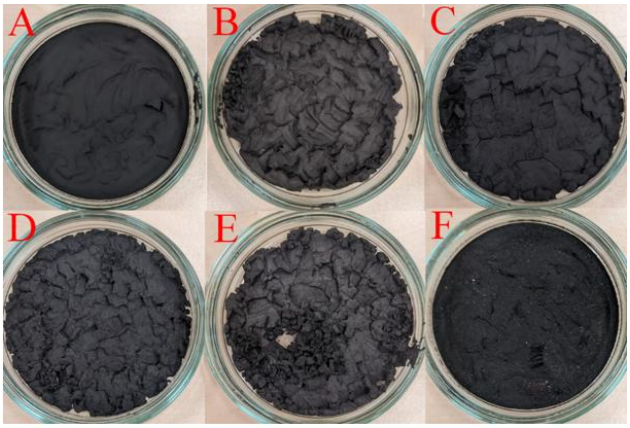

Figure 9 Carbon pastes prepared from samples of recycled graphite (A–F).

Electrochemical characterization using cyclic voltammetry in the $[Fe(CN)_6]^{4-}/[Fe(CN)_6]^{3-}$ redox system revealed that only samples A and B exhibited well-defined and characteristic voltammetric responses. Other samples showed additional peaks, increased capacitive currents, or absence of distinct redox peaks, indicating inferior electrochemical behavior.
Long-term stability tests demonstrated a general decrease in current response and an increase in peak separation after two months (Figure 2). Sample B showed more stable peak potentials over time, while sample A exhibited initially better kinetics. After three months, white crystalline deposits appeared on the paste surface, likely due to coconut oil migration, leading to reduced homogeneity; however, partial regeneration was possible by re-homogenization.

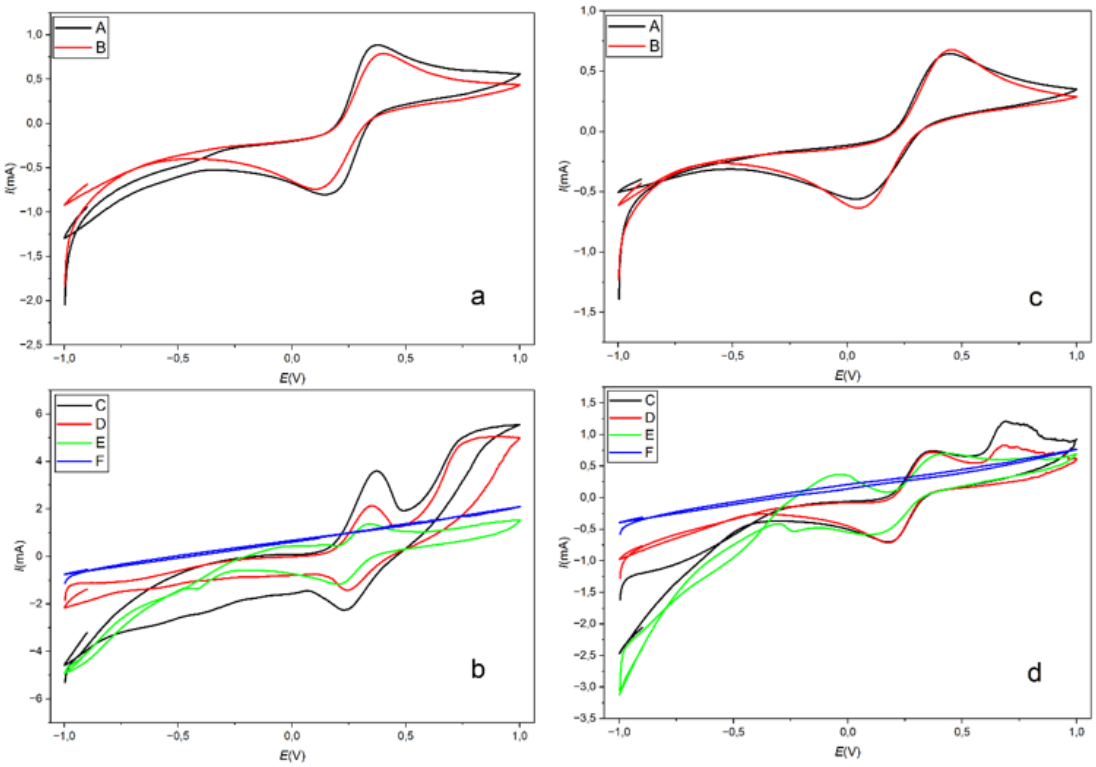

Figure 10 Cyclic voltammograms recorded in a 5 mM $[Fe(CN)_6]^{4-}/[Fe(CN)_6]^{3-}$ and 1 M KCl solution at CPEs made from samples of recycled graphite (A–F), measured immediately after preparation (a, b) and two months after preparation (c, d).

Based on the overall comparison, recycled graphite samples A and B demonstrated the most promising performance. These results confirm that recycled graphite can serve as a viable and sustainable alternative to commercial materials in carbon paste electrodes, with sample B representing the best compromise between electrochemical performance and stability.

Acknowledgements

Funded by the EU NextGenerationEU through the Recovery and Resilience Plan for Slovakia under the project No. 09I03-03-V04-00180.

References

[1] M. Zhang, C. Mullens, W. Gorski, *Anal. Chem.,* vol. 77, no. 19, pp. 6396–6401, Aug. 2005, doi: 10.1021/ac0508752.

Effect of pH on the Electrochemical Response of Commercial and Recycled Graphite-Based Electrodes

I. Sisolakova[a]*, S. Vanchak[a], R. Filip[a], J. Shepa[a]
[a] Department of Physical Chemistry, Institute of Chemistry, Pavol Jozef Šafárik University in Košice, Moyzesova 11, 041 54 Kosice, Slovak Republic
*ivana.sisolakova@upjs.sk

Electrochemical methods represent a powerful and versatile tool for the characterization of carbon-based materials, widely applied in sensing, energy storage, and environmental technologies. The electrochemical performance of these materials is strongly influenced by their surface chemistry, structural properties, and interactions with the electrolyte. Among the key factors, pH plays a crucial role, as it affects electrode kinetics, stability, and the onset of parasitic processes such as hydrogen evolution and the oxygen evolution reaction. Understanding pH-dependent behavior is therefore essential for evaluating the applicability of electrode materials under different operating conditions [1, 2]. Commercial carbon materials, such as Super P conductive carbon black and graphite powders, are widely used due to their good conductivity and relatively wide potential window [3]. However, increasing emphasis is being placed on sustainable alternatives, including recycled carbon materials. These materials present an environmentally friendly option, but their electrochemical stability and performance must be systematically compared with conventional commercial standards.

In this work, commercial materials (Super P and graphite powder) were compared with recycled graphite samples supplied by Fecupral, labeled A and B. The study focuses on evaluating the influence of pH over a wide range (≈1–13), with the aim of assessing electrochemical stability, identifying potential side reactions, and determining the suitability of recycled materials for practical applications.

The results show that samples A and commercial graphite exhibited no significant faradaic peaks within the potential window from −0.5 V to 1.0 V (Figure 1), indicating low background activity. At more positive potentials, the current increased, with a more pronounced rise at higher pH values and an onset around 1.25 V, corresponding to the oxygen evolution reaction. At negative potentials, the observed decrease in current was associated with hydrogen evolution.

Sample B displayed oxidation peaks at high pH, likely related to surface processes or trace impurities. The Super P electrode exhibited both oxidation and reduction peaks, particularly under extreme pH conditions. Interestingly, similar electrochemical features were observed at both highly acidic and highly alkaline environments, suggesting reduced stability of this material at extreme pH values. In contrast, oxidation features observed for samples A and commercial graphite were limited to the oxygen evolution region, confirming their higher stability.

All studied electrodes showed low background currents outside the regions of hydrogen and oxygen evolution, with only minor baseline shifts as a function of pH. An exception was Super P, which exhibited additional reduction features near +1 V under extreme pH conditions.

Overall, recycled graphite samples demonstrated comparable or improved stability relative to commercial materials, particularly in neutral and mildly acidic or alkaline environments. Sample A proved to be the most stable, with a usable potential window of approximately −1.0 V to 1.25 V. Sample B showed moderate instability, while Super P was the most susceptible to side reactions, especially at extreme pH.

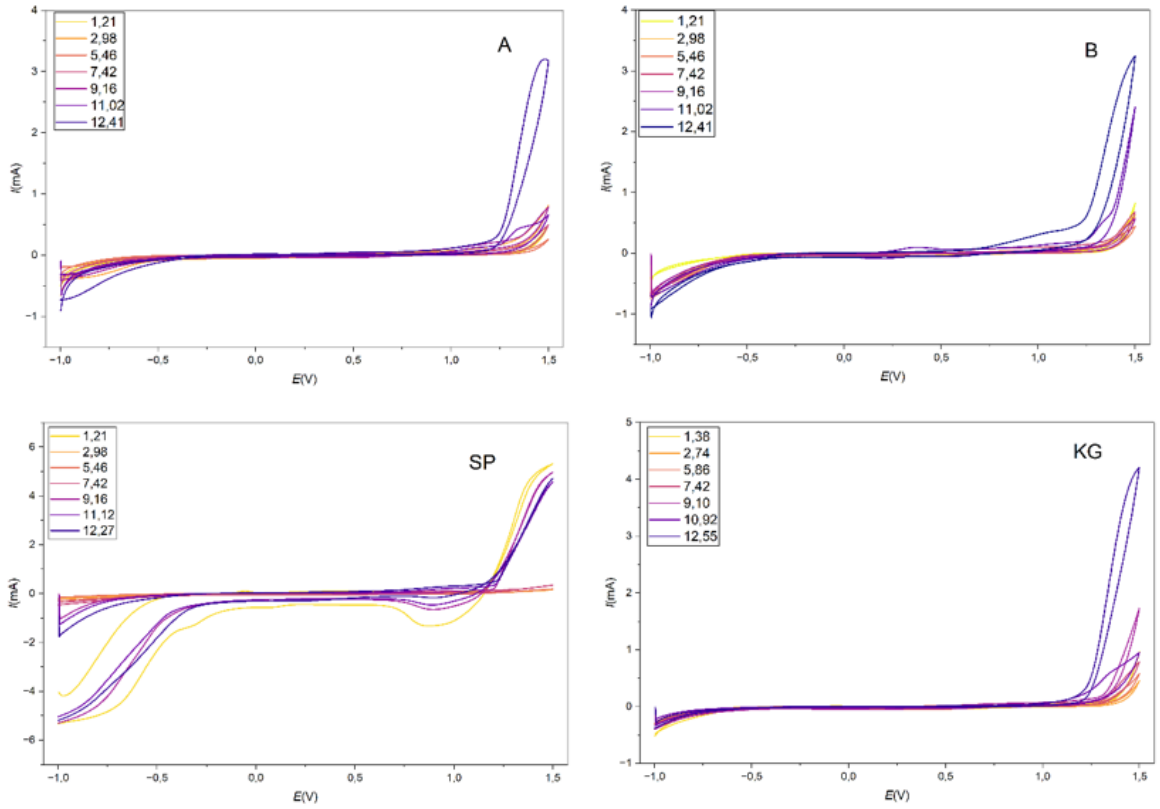

Figure 11 Cyclic voltammograms recorded in PBS solutions with varying pH values using carbon paste electrodes (CPEs) prepared from samples A, B, SP, and KG.

In conclusion, the results confirm that pH significantly affects the electrochemical response and stability of carbon-based electrodes, primarily through its influence on hydrogen and oxygen evolution processes. Recycled graphite materials from Fecupral, especially sample A, exhibit high stability and represent promising, sustainable alternatives to conventional materials. Their practical application is most suitable in neutral and moderately acidic or alkaline conditions, while extreme pH environments may lead to increased occurrence of parasitic reactions and reduced electrode stability.

Acknowledgements

Funded by the EU NextGenerationEU through the Recovery and Resilience Plan for Slovakia under the project No. 09I03-03-V04-00180.

References

[1] M. Zhang, C. Mullens, W. Gorski, *Anal. Chem.,* vol. 77, no. 19, pp. 6396–6401, Aug. 2005, doi: 10.1021/ac0508752.
[2] A. J. Bard, L. R. Faulkner, *Electrochemical Methods: Fundamentals and Applications*, 2nd ed., Wiley, New York, 2001.
[3] J. Wang, *Analytical Electrochemistry*, 3rd ed., Wiley-VCH, Hoboken, 2006.

Development of Non-Enzymatic Glucose Sensors Based on Titanium Dioxide Nanostructures: A Study on Ligand-To-Metal Charge Transfer and Amperometric Response

J. Shepa[a]*, R. Filip[a], M. Varga[b], I. Sisolakova[a], R. Orinakova[a]
[a] Department of Physical Chemistry, Institute of Chemistry, Pavol Jozef Šafárik University in Košice, Moyzesova 11, 041 54 Kosice, Slovak Republic
[b] Deutsche Telekom IT Solutions Slovakia, Moldavská cesta 8B, 040 11, Košice, Slovak Republic
*jana.shepa@upjs.sk

Introduction

The monitoring of blood glucose levels is a cornerstone of modern clinical diagnostics, particularly for the management of diabetes mellitus. Traditionally, enzymatic glucose sensors, utilizing glucose oxidase (GOx) or glucose dehydrogenase, have dominated the market due to their high selectivity. However, these biological sensors suffer from inherent limitations, including poor long-term stability, sensitivity to environmental conditions (temperature, pH, and humidity), and high production costs [1]. Consequently, there is a burgeoning research interest in non-enzymatic glucose sensors (NEGS), which rely on the direct electrocatalytic oxidation of glucose on the electrode surface, offering superior stability, reproducibility, and ease of fabrication [2].

Among the various materials explored for NEGS, titanium dioxide (TiO_2) has emerged as a promising candidate. While TiO_2 is a wide-bandgap semiconductor typically requiring UV excitation for activation, recent advancements have focused on its ability to form surface complexes with organic molecules. A critical breakthrough in this field is the utilization of the Ligand-to-Metal Charge Transfer (LMCT) complex. The formation of a specific chemical bond between the hydroxyl groups of glucose and the Ti(IV) sites on the TiO_2 surface enables the detection of glucose under visible light or specific electrochemical conditions. This LMCT interaction is significant because it shifts the optical response of TiO_2 into the visible region and facilitates electron transfer, which is essential for sensitive electrochemical sensing [3].

Furthermore, the trend in biosensing is shifting towards non-invasive detection in alternative fluids such as saliva and tears. Non-enzymatic sensors based on metal oxides like TiO_2 are particularly suited for these applications due to their robustness in complex biological matrices where enzymes might be inhibited by endogenous substances.

Experimental Section and Results

In this study, an Indium Tin Oxide (ITO) electrode was modified with TiO_2 nanoparticles (size 100 nm) to evaluate its performance as a non-enzymatic glucose sensing platform. The electrochemical behaviour was characterized using chronoamperometry, a technique where a constant potential is applied and the resulting current is monitored as a function of time upon the successive addition of glucose.

The experimental data illustrates the current-time (*I-t*) response of the TiO_2/ITO electrode (Figure 1). Upon each incremental addition of glucose into the electrolyte solution, a rapid and well-defined step-increase in the anodic current was observed. This current response is directly attributed to the catalytic oxidation of glucose facilitated by the TiO_2 nanostructures. The sharp rise to a steady-state current within seconds indicates a fast diffusion process and high catalytic activity of the modified electrode surface. A critical observation was made when the sample was irradiated with a halogen lamp after 30 seconds of measurement to monitor the signal change under illumination. A subsequent decrease in the reduction current was recorded, which serves as a strong indication of the formation of the LMCT complex. This phenomenon suggests that the current flows more efficiently following irradiation due to the significantly enhanced charge transfer at the TiO_2/glucose interface.

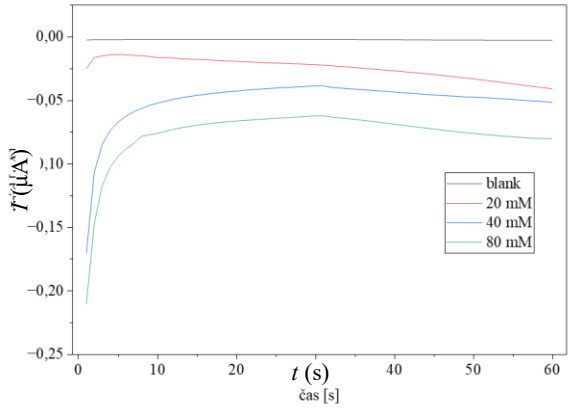

Figure 1 Chronoamperometric response for TiO_2/ITO electrode measured in glucose/PBS solution.

The magnitude of the current increase is proportional to the concentration of glucose added. The clear distinction between the current steps for different concentrations demonstrates the high sensitivity of the sensor. The stability of the baseline current between additions suggests that the TiO2 layer remains robustly attached to the ITO substrate and that the LMCT-driven process is reproducible. This linear relationship between current density and glucose concentration confirms the viability of TiO_2 nanoparticles on ITO for quantitative glucose analysis.

Conclusion

The integration of TiO_2 nanoparticles on ITO electrodes provides a highly effective platform for non-enzymatic glucose sensing. By leveraging the unique LMCT complex formation between TiO2 and glucose, the sensor overcomes the stability issues associated with enzymatic systems. Experimental chronoamperometric results confirm that the sensor exhibits a rapid response time and a clear dependence on glucose concentration. This study reinforces the potential of metal-oxide-based LMCT complexes in developing the next generation of stable, low-cost, and non-invasive electrochemical biosensors.

Acknowledgements

This work was funded by the EU NextGenerationEU through the Recovery and Resilience Plan of the Slovak Republic under project no. 09-I05-03-V02-00047.

References

[1] J. Liu, J. Shen, S. Ji, Q. Zhang, and W. Zhao, "Research progress of electrode materials for non-enzymatic glucose electrochemical sensors," *Sens. Diagn.*, vol. 2, pp. 36-45, 2023, doi: 10.1039/D2SD00165A.
[2] K. V. Jarnda, D. Wang, Qurrat-Ul-Ain, R. Anaman, V. E. Johnson, G. P. Roberts, P. S. Johnson, B. W. Jallawide, T. Kai and P. Ding,, "Recent advances in electrochemical non-enzymatic glucose sensor for the detection of glucose in tears and saliva: A Review," *Sensors & Actuators: A. Physical*, vol. 363, pp. 114778, Dec. 2023, doi: 10.1016/j.sna.2023.114778.
[3] J. Hovancová, I. Šišoláková, P. Vanýsek, R. Oriňaková, I. Shepa, M. Kaňuchová, N. Király, M. Vojtko, P. Čudek and A. Oriňak,, "Ligand-to-metal charge transfer (LMCT) complex: New approach to non-enzymatic glucose sensors based on TiO_2," *Journal of Electroanalytical Chemistry*, vol. 878, pp. 114589, Dec. 2020, doi: 10.1016/j.jelechem.2020.114589.

Electrochemical Detection of Gentamicin Using Metal-Organic Framework (GATCPP) Modified Screen-Printed Carbon Electrodes

J. Shepa[a]*, J. Demeterova[a], N. Kiraly[b], P. Obsatnik[b], I. Sisolakova[a], D. Volavka[c]
M. Almasi[b], P. Jarcuska[d], R. Orinakova[a], V. Zelenak[b]
[a] Department of Physical Chemistry, Institute of Chemistry, Pavol Jozef Šafárik University in Košice, Moyzesova 11, 041 54 Kosice, Slovak Republic
[b] Department of Inorganic Chemistry, Institute of Chemistry, Pavol Jozef Šafárik University in Košice, Moyzesova 11, 041 54 Kosice, Slovak Republic
[c] Department of Condensed Matter Physics, Pavol Jozef Šafárik University in Košice, Jesenná 9, 041 54 Kosice, Slovak Republic
[d] Department of Infectology and Travel Medicine, Pavol Jozef Šafárik University in Košice, Srobarova 2, 041 54 Kosice, Slovak Republic
*jana.shepa@upjs.sk

Introduction

The rising concern regarding antibiotic resistance have necessitated the development of advanced diagnostic tools. The monitoring of aminoglycoside antibiotics, such as gentamicin, is critical due to their potential nephrotoxic and ototoxic side effects when present in excessive concentrations. Traditional analytical techniques for gentamicin detection, such as liquid chromatography often face challenges including low efficiency of stationary phases and the requirement for complex mobile phases containing non-volatile salts [1]. Moreover, liquid chromatography represents robust, expensive technique required trained staff. To overcome these limitations, electrochemical sensing technology has emerged as a transformative domain. These sensors offer significant advantages, including simplicity, rapidity, high sensitivity, and cost-effectiveness [2]. Most importantly, electrochemical platforms are uniquely suited for point-of-care (POC) applications, enabling decentralized testing and real-time monitoring without the need for bulky instrumentation. The integration of functional nanomaterials, particularly metal-organic frameworks (MOFs), has further enhanced electrode performance by providing high surface areas and tuneable porosity. Recent studies have demonstrated that combining carbon-based materials like reduced graphene oxide (rGO) with metal oxides or MOFs can significantly improve electrocatalytic activity for gentamicin detection [3].

Experimental Results and Discussion

In this study, a Screen-Printed Carbon Electrode (SPCE) was modified with a GATCPP to evaluate its sensing capabilities toward gentamicin. The electrochemical behaviour was characterized using cyclic voltammetry in a suitable electrolyte medium 600 µM gentamicin in phosphate buffered saline (PBS) to simulate body fluids conditions (Figure 1). The modification of the SPCE with GATCPP facilitates enhanced electron transfer kinetics and provides specific active sites for the interaction with the analyte.

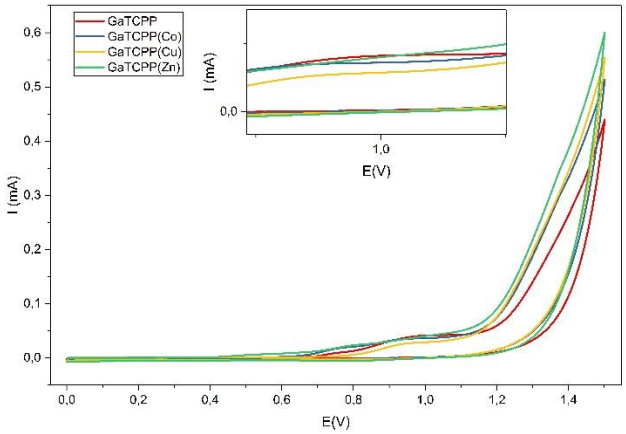

Figure 1 Cyclic voltammograms for 600 µM gentamicin/PBS solution on SPCE/GaTCPP (red curve), SPCE/GaTCPP(Co) (blue curve), SPCE/GaTCPP(Cu) (yellow curve), and SPCE/GaTCPP(Zn) (green curve).

Analysis of the cyclic voltammograms reveals distinct electrochemical signatures. Two prominent anodic peaks are observed during the potential scan. The first peak, appearing at a lower potential, corresponds to the intrinsic redox activity of the GATCPP framework itself, indicating successful immobilization and stability of the MOF on

the electrode surface. Upon the addition of gentamicin, a second, well-defined oxidation peak emerges at a higher potential. This peak is attributed to the electro-oxidation of gentamicin facilitated by the catalytic environment of the MOF. The separation between the MOF's intrinsic peak and the gentamicin oxidation peak allows for clear discrimination and quantification of the antibiotic. The shift toward higher potentials for gentamicin oxidation is consistent with the energy requirements for the transformation of its amino and hydroxyl functional groups on the modified surface.

Conclusion

The GATCPP-modified SPCE demonstrates robust performance for the electrochemical detection of gentamicin. By leveraging the high surface area of the MOF and the portability of screen-printed electrodes, this platform provides a promising pathway for POC diagnostics. The dual-peak response ensures high selectivity, distinguishing the framework's signal from the analyte's oxidation. Future work will focus on optimizing the MOF composition and scaling the sensor for complex biological matrices, aiming to mitigate the risks associated with antibiotic over-consumption and enhance patient safety in clinical settings.

Acknowledgements

This work was funded by the EU NextGenerationEU through the Recovery and Resilience Plan of the Slovak Republic under project no. 09-I05-03-V02-00047.

References

[1] V. Manyanga, K. Kreft, B. Divjak, J. Hoogmartens, and E. Adams, "Improved liquid chromatographic method with pulsed electrochemical detection for the analysis of gentamicin," *J of Chromatogr A.*, vol. 1189, no. 1-2, pp. 347-354, May 2008, doi: 10.1016/j.chroma.2007.12.041.

[2] M. M. Ahmed, J. Bai, L. Kong, J. Du, S. Azat and Q. Xu, "Recent advances in MOF-modified electrochemical sensor for point-of-care detecting cardiac biomarkers," *Trends in Analytical Chemistry*, vol. 189, pp. 118277, Aug. 2025, doi: 10.1016/j.trac.2025.118277.

[3] J. K. Himanshu, G. B. V. S. Lakshmi, A. K. Singh, and P. R. Solanki, "Reduced graphene oxide-gadolinium oxide-functionalized paper based immunosensor for electrochemical detection of gentamicin," *Biosensors and Bioelectronics: X*, vol. 17, pp. 100442, Apr. 2024, doi: 10.1016/j.biosx.2024.100442.

Electrochemical Detection of Gentamicin Using SPCE Modified with MIL-101(Cr)@CytC

L. Slabejova[a]*, I. Sisolakova[a], E. Sedlak[b], N. Kiraly[c], P. Obsatnik[c], J. Shepa[a]
[a] Department of Physical Chemistry, Institute of Chemistry, Pavol Jozef Šafárik University in Košice, Moyzesova 11, 041 54 Kosice, Slovak Republic
[b] Department of Biochemistry, Institute of Chemistry, Pavol Jozef Šafárik University in Košice, Moyzesova 11, 041 54 Kosice, Slovak Republic
[c] Department of Inorganic Chemistry, Institute of Chemistry, Pavol Jozef Šafárik University in Košice, Moyzesova 11, 041 54 Kosice, Slovak Republic
*laura.slabejova@upjs.sk

Introduction

Electrochemical sensors represent a promising tool for the rapid, sensitive, and selective detection of biologically active compounds, including antibiotics [1]. In recent years, increasing attention has been paid to the use of screen-printed carbon electrodes (SPCE), which enable miniaturization, low cost, and easy surface modification [2]. These properties make them suitable for applications in environmental analysis and pharmaceutical monitoring [1, 2]. Among the huge amount of pharmaceutical compounds, the determination of aminoglycoside antibiotics, such as gentamicin, is important for monitoring their concentrations in both biological and environmental samples, given their potential toxicity and the risk of antibiotic resistance [3]. To enhance the sensitivity and selectivity of electrochemical sensors, advanced nanomaterials are employed, including metal–organic frameworks (MOFs), which are characterized by high surface area and porous architectures suitable for immobilizing active molecules [4]. In this context, cytochrome c plays an important role as a redox-active biomolecule that mediates electron transfer, thereby enhancing the system's electrochemical response [5]. The combination of SPCE and MIL-101(Cr)@CytC thus represents an innovative approach to developing an efficient sensor for gentamicin determination.

Experiment and measurements

Electrochemical measurements were performed to evaluate the response of the prepared sensors: bare SPCE, SPCE modified with MOF MIL-101(Cr) (SPCE/CrMOF), and SPCE modified with MIL-101(Cr)@CytC (SPCE/Cr-MOF/Cyt C). Measurements were carried out in phosphate-buffered saline (PBS), as well as in PBS containing 600 μM gentamicin. To investigate the electrochemical behavior of the prepared sensor configurations, cyclic voltammetry (CV) was used at a scan rate of 100 $mV.s^{-1}$, within the potential window from 0 to 1.5 V.

Results and discussion

To study the electrochemical behavior of the prepared sensors, cyclic voltammetry measurements were performed in PBS (Figure 1A) and PBS containing gentamicin (Figure 1B). The results demonstrate clear differences between the individual electrode configurations. In PBS (Figure 1A), all electrodes exhibited similar voltammetric profiles without a noticeable oxidation peak. Differences in current response were observed between the prepared electrodes. The highest current was recorded for the SPCE/CrMOF/CytC electrode, followed by the bare SPCE, while the SPCE/CrMOF electrode showed the lowest response. Based on these results, several facts can be stated. First, MOF materials are generally relatively poorly conductive compared to standard electrode materials, so it is important to dope them to increase their conductivity. In this case, cytochrome C served as a suitable candidate, which clearly improved the current response of the studied material. Although the current response is at the level of a bare electrode, this material provides more active sites for the binding of the studied molecule due to the functional groups that act catalytically on the electrochemical oxidation of some molecules.
In the presence of gentamicin (Figure 1B), all electrodes showed an increase in current response and an oxidation peak at approximately 1.3 V, which is attributed to the oxidation of gentamicin. The highest current response was again observed for SPCE/CrMOF/CytC. The SPCE/CrMOF electrode showed a lower response, while the bare SPCE exhibited the lowest signal. Based on the measurements, the resulting determination is not only influenced by the conductivity of the given electrode material, but also by other properties such as the presence of suitable functional groups, which ultimately improve electrochemical oxidation and increase the current response, became apparent.

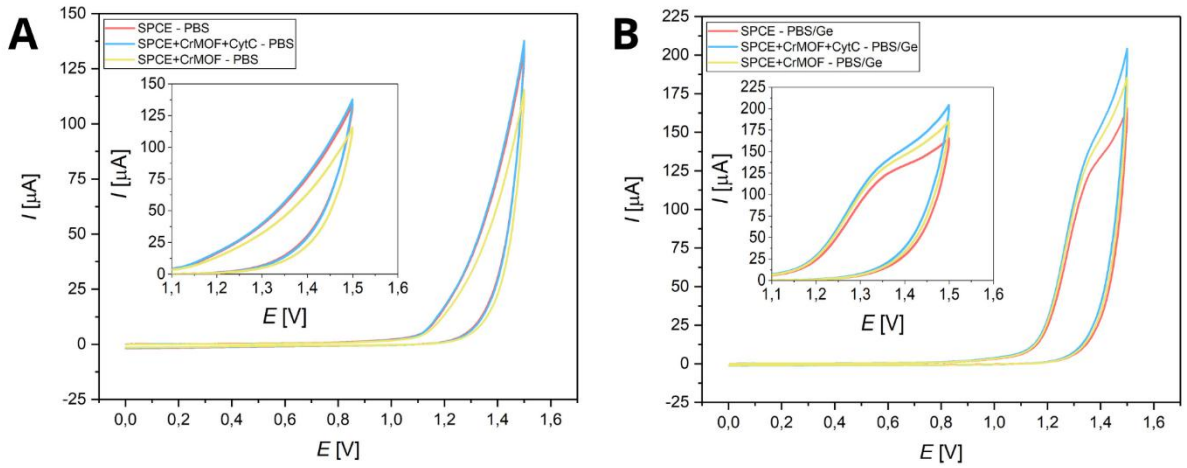

Figure 12 Cyclic voltammograms of SPCE, SPCE/CrMOF, and SPCE/CrMOF/CytC in PBS (A) and PBS containing 600 µM gentamicin (B).

Conclusions

The obtained results demonstrate that electrode surface modification significantly influences the electrochemical response toward gentamicin. Among the investigated configurations, the SPCE/CrMOF/CytC electrode exhibited the highest current response and the most pronounced oxidation peak at approximately 1.3 V, indicating superior analytical performance. The incorporation of MIL-101(Cr) contributed to an increased active surface area, while the presence of cytochrome c further enhanced electron transfer processes. Their combined effect resulted in improved sensitivity compared to the bare and MOF-modified electrodes. These findings confirm that the SPCE/CrMOF/CytC platform represents a promising approach for the electrochemical detection of gentamicin and highlight the potential of combining MOF materials with redox-active biomolecules in sensor development.

Acknowledgements

This work was funded by the EU NextGenerationEU through the Recovery and Resilience Plan of the Slovak Republic under project no. 09-I05-03-V02-00047.

References

[1] G. A. B. Mello, S. R. Benjamin, F. de Lima, and R. F. Dutra, "Recent Advances in Electrochemical Sensors for the Detection of Anti-Inflammatory and Antibiotic Drugs: A Comprehensive Review," *Biosensors (Basel),* vol. 15, no. 10, Oct. 2025, doi: 10.3390/bios15100676.
[2] N. Haroon and K. J. Stine, "Surface Modification of Screen-Printed Carbon Electrodes," *Coatings,* vol. 15, no. 10, 2025, doi: 10.3390/coatings15101182.
[3] M. Glinka, W. Wojnowski, and A. Wasik, "Determination of aminoglycoside antibiotics: Current status and future trends," *TrAC Trends in Analytical Chemistry,* vol. 131, 2020, doi: 10.1016/j.trac.2020.116034.
[4] M. Yin, L. Zhang, X. Wei, J. Sun, and D. Xu, "Detection of antibiotics by electrochemical sensors based on metal-organic frameworks and their derived materials," *Microchemical Journal,* vol. 183, 2022, doi: 10.1016/j.microc.2022.107946.
[5] M. Fedurco, J. Augustynski, C. Indiani, G. Smulevich, M. Antalík, M. Bánó, E. Sedlák, M. C. Glascock and J. H. Dawson., "Electrochemistry of unfolded cytochrome c in neutral and acidic urea solutions," *J Am Chem Soc,* vol. 127, no. 20, pp. 7638-46, May 2005, doi: 10.1021/ja050321g.

Design and functionalization of citric acid-based polyester networks for biomedical applications

T. Sopcak[a]*, L. Medvecky[a], T. Csanadi[a] , J. Brus[b], M. Urbanova[b], M. Giretova[a], R. Stulajterova, F. Kromka[a], M. Faberova[a]
[a] Institute of Materials Research of SAS, Watsonova 47, 04001 Kosice, Slovak Republic
[b] Institute of Macromolecular Chemistry of the Czech Academy of Sciences, Heyrovskeho nam. 2, 162 06, Prague 6, Czech Republic
*tsopcak@saske.sk

Biopolymers, alongside metals and ceramics, represent one of the fundamental classes of materials used in biomedical applications, including tissue engineering, regenerative medicine, gene therapy, and controlled drug delivery. Polymers containing ester bonds are particularly attractive in biomedical research, as they are biocompatible and also exhibit biodegradability and bioresorbability, enabling their use across a wide range of therapeutic and regenerative applications [1].

Typical representatives of aliphatic polyesters include polyhydroxybutyrates (PHBs), poly(lactic acid; PLA), poly(glycolic acid; PGA), poly(ε-caprolactone; PCL), and their copolymers. These materials are generally hydrophobic, thermally processable, and mechanically robust, making them suitable for fabricating 3D scaffolding systems while also allowing for chemical modification and tailoring of degradation rates. However, despite their widespread use, conventional aliphatic polyesters often face limitations such as relatively slow degradation rates, limited surface functionality, and the generation of acidic by-products during hydrolysis, which can affect local tissue responses and reduce bioactivity [2].

On the other hand, citrate-based polyesters represent another class of biodegradable polymers characterized by unique multifunctional properties, offering enhanced chemical versatility, tunable degradation rates, and the ability to incorporate various functional groups capable of modulating physicochemical and biological performance [3]. These polyesters are typically synthesized via polycondensation of multifunctional citric acid with diols (C2–C12) or polyols, either in the presence of a catalyst or through catalyst-free reactions, yielding cost effective polyesters with improved processability and tunable mechanical and degradation properties compared to their thermoplastic counterparts [3]. The first generation of citrate-based polyesters primarily comprises relatively simple formulations, among which poly(1,8-octanediol citrate; POC) represents a well-established example. POC exhibits elastomeric behavior with tensile strength and Young's modulus comparable to those of elastin from bovine ligaments, as well as elongation at break similar to that of native arteries and veins, while maintaining gradual biodegradation within approximately one year. Despite these favorable characteristics, conventional POC is water-insoluble and offers a relatively narrow range of mechanical properties and intrinsic bioactivity, which may limit its broader biomedical applicability. Consequently, various functionalization strategies have been explored to expand its structural versatility and enhance its biological and mechanical performance. Building on these initial citrate ester networks, various functionalization strategies have been developed to extend their performance, including urethane-doping to enhance mechanical strength, incorporation of unsaturated monomers for photocrosslinking, development of thermoresponsive hydrogels with controlled release, integration of bioactive inorganic components such as silica or hydroxyapatite for improved osteogenesis, and grafting of fluorescent moieties for imaging applications etc (Figure 1). Although POC-based polyesters have been widely utilized, they remain relatively hydrophobic, which can limit their interactions in aqueous biological environments. In contrast, glycerol-based polyesters represent another class of citrate-derived materials, featuring a more hydrophilic character due to the presence of three hydroxyl groups per monomer and generally shorter chain lengths, which provide additional sites for crosslinking and functionalization [4]. Despite the growing interest in glycerol-citrate systems, poly(glycerol citrate; GCA) has not yet been systematically studied or functionalized to the same extent as POC, leaving significant opportunities for tailoring its chemical and biological properties for advanced biomedical applications.

Based on this rationale, we investigated the functionalization of poly(glycerol citrate; GCA) with tannic acid (TA) and boric acid (B) to generate multifunctional, crosslinked polyester networks [5]. TA, a naturally derived polyphenolic biomolecule rich in hydroxyl groups, provides multiple reactive sites and intrinsic antioxidant and antibacterial properties, while boric acid represents a well-known inorganic crosslinking agent capable of forming reversible borate ester bonds and coordinated boron species within the polymer matrix. It was hypothesized that even low concentrations (1–2 wt%) of both additives would induce structural modifications within the GCA network, potentially modulating degradation behavior, mechanical performance, and bioactivity while maintaining antibacterial functionality [5] . A comprehensive characterization was performed using solid-state ^{13}C and ^{11}B NMR spectroscopy to confirm chemical incorporation and boron coordination environments, supported by thermal, mechanical, and physicochemical analyses to evaluate the structure–property relationships of the modified systems. The results demonstrate that tailored functionalization of glycerol-based citrate polyesters

represents a promising strategy for designing bioactive, degradable polymer networks for advanced biomedical applications.

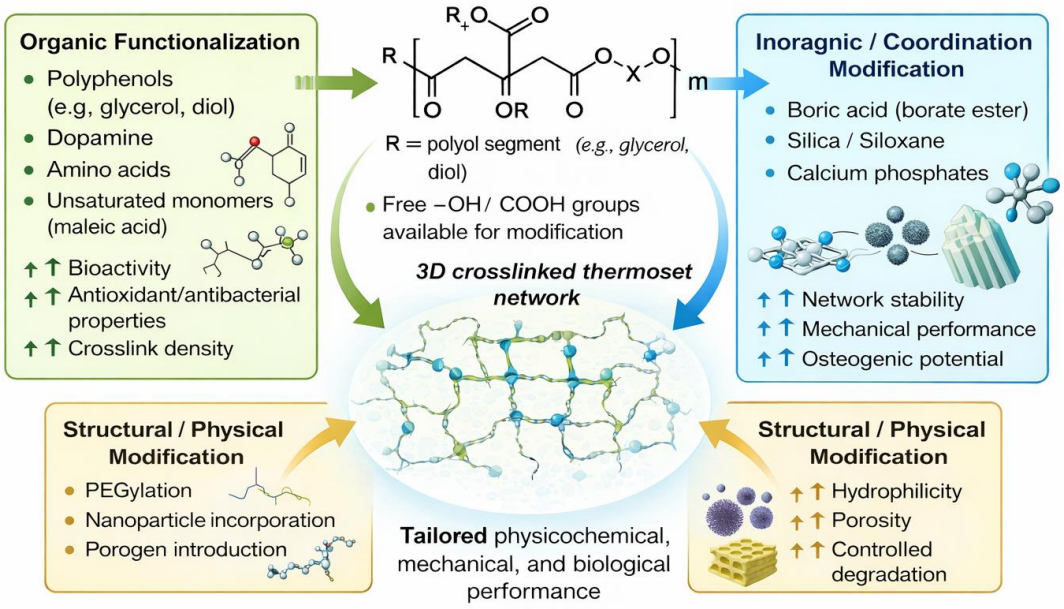

Figure 1 Overview of functionalization pathways in polyol–citrate thermoset networks.

Acknowledgements

This work was funded by the EU NextGenerationEU through the Recovery and Resilience Plan for Slovakia under the project No. 09I03-03-V04-00133.

References

[1] H. Tian, Z. Tang, X. Zhuang, X. Chen and X. Jing, "Biodegradable synthetic polymers: Preparation, functionalization and biomedical application," *Prog.Polym. Sci*., vol. 37, no. 2, pp 237-280, Feb. 2012, doi: 10.1016/j.progpolymsci.2011.06.004.

[2] K. Olonisakin, A. K. Mohanty , M. Thimmanagari and M. Misra, "Recent advances in biodegradable polymer blends and their biocomposites: a comprehensive review," *Green Chem.*, vol. 27, no. 38, pp. 11656-11704, Sep. 2025, doi: 10.1039/d5gc01294e.

[3] M. Wang, P. Xu and B. Lei, "Engineering multifunctional bioactive citrate-based biomaterials for tissue engineering," *Bioact. Mater.*, vol. 19, pp. 511-537, Jan. 2023, doi: 10.1016/j.bioactmat.2022.04.027.

[4] T. Sopcak, L. Medvecky, M. Giretova, R. Stulajterova, J. Brus, M. Urbanova, F. Kromka, M. Podobova and M. Faberova, "Fabrication of a glycerol-citrate polymer coated tricalcium phosphate bone cements: Structural investigation and material properties," *J. Polym. Res.*, vol. 28, no. 231, May 2021, doi: 10.1007/s10965-021-02596-w.

[5] T. Sopcak, L. Medvecky, T. Csanádi, J. Brus, E. Sidoryk, M. Urbanova, M. Dzupon, P. Jevinova, M. Giretova, O. Petrus, M. Podobova, R. Stulajterova, "Tannic and boric acid crosslinked glycerol–citrate polyesters: Structural, mechanical and biological performance," *Eur. Polym. J.*, vol. 241, Dec. 2025, doi: 10.1016/j.eurpolymj.2025.114367.

Development of a Software Application for the S2D Multisensor Diagnostic Platform

M. Varga[a], I. Sisolakova[b], J. Shepa[b], R. Orinakova[b,c]*, G. Urban[a,d]
[a] Deutsche Telekom IT Solutions Slovakia, Moldavská cesta 8B, 040 11, Košice, Slovak Republic
[b] Department of Physical Chemistry, Institute of Chemistry, Pavol Jozef Šafárik University in Košice, Moyzesova 11, 041 54 Kosice, Slovak Republic
[c] Tomas Bata University in Zlín, Tř. Tomáše Bati 5678, 760 01, Zlín, Czech Republic
[d] Technical University of Košice, Letná 1/9, 040 01, Košice, Slovak Republic
*ivana.sisolakova@t-systems.com

This paper presents the development of a specialized software application within the S2D (Bridging Sensors to Digits) project, serving as the essential interface for a novel, portable electrochemical diagnostic platform. The primary objective is to transform complex electrical responses from a multisensor array into comprehensible health data, facilitating the simultaneous measurement of bioanalytes such as insulin, glucose, cholesterol, and ascorbic acid, with the potential to include COVID-19 and other analytes in the near future.
The development process is governed by the Scrum agile framework, integrating rigorous Quality Assurance (QA) procedures to ensure a secure, robust, and intuitive user experience. This methodology enables the seamless translation of raw chemical signals into actionable results in under 15 seconds. By prioritizing high-quality software architecture, the project enables rapid on-site analysis that can be operated effectively without the need for extensive specialized training.
From an architectural standpoint, the system employs a component-based design that harmonizes high analytical precision with the strict requirements of mobility and data sovereignty. A key feature is the implementation of an edge computing model, which allows the platform to operate independently of internet connectivity, ensuring maximum privacy and GDPR compliance. The architecture further prioritizes a multi-tier security framework, utilizing offline role-based access control and localized data management, making it equally suitable for clinical environments and remote field settings.
This Proof of Concept demonstrates a synergistic bridge between low-cost sensing hardware and modern IT solutions. By managing the entire data lifecycle—from acquisition and validation to longitudinal visualization, the S2D platform simplifies complex medical procedures. By offering a scalable, secure, and modular framework that allows for seamless integration with artificial intelligence and cloud connectivity, the system democratizes access to professional diagnostics, empowering both patients and healthcare providers with autonomous diagnostic capabilities.

Acknowledgements

Funded by the EU NextGenerationEU through the Recovery and Resilience Plan for Slovakia under the project No. 09-I05-03-V02-00047.

References

[1] K. Schwaber and J. Sutherland, "The Scrum Guide: The Definitive Guide to Scrum: The Rules of the Game," Scrum.org, 2020. [Online]. Available: https://scrumguides.org.
[2] I. Sommerville, *Software Engineering*, 10th ed. Harlow, England: Pearson Education, 2015.
[3] R. Taylor, N. Medvidovic, and E. Dashofy, *Software Architecture: Foundations, Theory, and Practice*. Hoboken, NJ: John Wiley & Sons, 2009.
[4] Regulation (EU) 2016/679 of the European Parliament and of the Council of 27 April 2016 on the protection of natural persons with regard to the processing of personal data (General Data Protection Regulation), *Official Journal of the European Union*, L119, May 2016.
[5] S. K. Vashist and J. H. Luong, *Point-of-Care Diagnostics: Recent Advances and Future Trends*. Boca Raton, FL: CRC Press, 2018.
[6] D. Grieshaber, R. MacKenzie, J. Vörös, and E. Reimhult, "Electrochemical Biosensors - Sensor Principles and Architectures," *Sensors*, vol. 8, no. 3, pp. 1400-1458, Mar. 2008, 10.3390/s80314000.

Design and Implementation of a Software Solution for the S2D Multisensor Diagnostic Platform

M. Varga[a], I. Sisolakova[b], J. Shepa[b]*, R. Orinakova[b,c], G. Urban[a,d]
[a] Deutsche Telekom IT Solutions Slovakia, Moldavská cesta 8B, 040 11, Košice, Slovak Republic
[b] Department of Physical Chemistry, Institute of Chemistry, Pavol Jozef Šafárik University in Košice, Moyzesova 11, 041 54 Kosice, Slovak Republic
[c] Tomas Bata University in Zlín, Tř. Tomáše Bati 5678, 760 01, Zlín, Czech Republic
[d] Technical University of Košice, Letná 1/9, 040 01, Košice, Slovak Republic
*jana.shepa@upjs.sk

This paper presents a comprehensive framework that integrates technical hardware solutions, advanced nanomaterial research, and the development of a specialized software application into a unified diagnostic platform. The project aims to revolutionize diagnostics by transitioning from bulky, laboratory-bound equipment to a fully integrated, on-site detection system. By combining high-performance screen-printed electrodes (SPEs), advanced nanomaterial engineering, and a dedicated software interface, the platform provides a seamless, real-time diagnostic solution tailored for high-stakes environments.

Hardware Innovation and Field Stability

The foundation of this framework rests upon the implementation of SPEs, which offer a rapid, sensitive, and cost-effective alternative to conventional analytical methods. Ongoing research enhances sensor performance through high-stability non-enzymatic sensing, utilizing nickel and gold nanoparticles to replace traditional, temperature-sensitive enzymes. This innovation ensures that diagnostic kits remain operational in extreme field conditions where biological reagents would typically degrade. Furthermore, by utilizing electrochemical aptasensors, these devices can capture specific targets—such as viral spike proteins or health biomarkers—delivering a definitive electrical signal within minutes.

Software-Driven Analytics and Interface

To bridge the gap between complex electrochemical data and actionable field intelligence, the project incorporates a specialized software application. Serving as the essential interface for the portable platform, the software transforms complex electrical responses from a multisensor array into comprehensible health data in under 15 seconds.

- **Real-Time Interpretation**: The software utilizes standardized methodological protocols to interpret data instantly, eliminating the requirement for a trained laboratory analyst.
- **Data Protection**: The platform implements robust security measures to protect results, guaranteeing that data collected in the field remain secure and personalized.
- **User Interface**: Specifically engineered for military and emergency medical personnel, the software provides a simplified visual output to facilitate rapid, evidence-based medical decision-making on-site.

Miniaturization and Future Scalability

Through advanced nanomaterial engineering—specifically the synergy between conductive polymers and carbon nanotubes—sensors have been miniaturized to a level compatible with handheld measuring devices. The platform manages the entire data lifecycle, from initial acquisition to longitudinal visualization. By offering a scalable and modular framework that allows for the future integration of artificial intelligence and cloud connectivity, this system democratizes access to professional diagnostics, empowering both patients and healthcare providers with autonomous diagnostic capabilities.

Acknowledgements

This work was funded by the NATO Science for Peace and Security Programme under grant id G6106.

References

[1] Metrohm DropSens, "Virus detection: Fast, sensitive, and cost-effective with electrochemical testing," White Paper, WP-058EN-2020-05, May 2020.
[2] G. Martínez-Paredes, M. González-García, and A. Costa-García, "Genosensor for SARS Virus Detection Based on Gold Nanostructured Screen-Printed Carbon Electrodes," Electroanalysis, vol. 21, no. 3-5, pp. 379-385, 2009.

[3] S. Carinelli, M. Kühnemund, M. Nilsson, and M. I. Pividori, "Yoctomole electrochemical genosensing of Ebola virus cDNA by rolling circle and circle to circle amplification," Biosensors and Bioelectronics, vol. 93, pp. 65-71, 2017.
[4] D. Grieshaber, R. MacKenzie, J. Vörös, and E. Reimhult, "Electrochemical Biosensors - Sensor Design and Application," Sensors, vol. 8, no. 3, pp. 1400-1458, 2008.
[5] S. K. Vashist and J. H. Luong, Point-of-Care Diagnostics: Recent Advances and Future Trends. Boca Raton, FL: CRC Press, 2018.
[6] I. Šišoláková, et al., "Advanced Nanomaterial-Based Electrochemical Sensors for Non-Enzymatic Metabolic and Viral Diagnostics," Technical Report for NATO Science for Peace and Security (SPS) Project, 2024. (Táto referencia zastupuje jej príspevky v oblasti neenzymatického snímania a štandardizácie protokolov popísané v analýze).
[7] M. Veerapandian, R. Hunter, and S. Neethirajan, "Dual immunosensor based on methylene blue-electroadsorbed graphene oxide for rapid detection of the influenza A virus antigen," Talanta, vol. 155, pp. 250-257, 2016.
[8] U. Jarocka, et al., "An electrochemical immunosensor based on a 4,4'-thiobisbenzenethiol self-assembled monolayer for the detection of hemagglutinin from avian influenza virus H5N1," Sensors and Actuators B: Chemical, vol. 228, pp. 25-30, 2016.
[9] K. Schwaber and J. Sutherland, "The Scrum Guide: The Definitive Guide to Scrum: The Rules of the Game," Scrum.org, 2020. [Online]. Available: https://scrumguides.org
[10] Regulation (EU) 2016/679 of the European Parliament and of the Council of 27 April 2016 on the protection of natural persons with regard to the processing of personal data (General Data Protection Regulation), Official Journal of the European Union, L119, May 2016.
[11] I. Sommerville, Software Engineering, 10th ed. Harlow, England: Pearson Education, 2015.
[12] R. Taylor, N. Medvidovic, and E. Dashofy, Software Architecture: Foundations, Theory, and Practice. Hoboken, NJ: John Wiley & Sons, 2009.

Programmable Motility Regulation of Rigid-Flexible Micromotors

H. Yang[a], D. Zhang[a], H. Chen[a], L. Wang[a]*
[a] State Key Laboratory of Advanced Inorganic Fibers and Composites, School of Chemistry and Chemical Engineering, Harbin Institute of Technology, Harbin 150001, China
*leiwang_chem@hit.edu.cn

Catalytic micro/nanomotors (MNMs) are able to convert chemical energy into mechanical motion and possess autonomous motility capability, which hold great promise as intelligent devices across diverse fields, with their motion largely governed by the structure[1, 2]. Nevertheless, real-time regulation and programming of structure remained a critical challenge for motion control[3, 4]. To address this constraint, we incorporated polymer flexible materials sequestering cascade enzymes as a building block and constructed rigid-flexible micromotors (RFMMs), where their structure can be dynamically tuned in response to the solution environment. In addition, we employed the concept to quantitatively define the structural characteristics of RFMMs. Their structure was modulated through the ionic concentration, ionic type, and pH of the solution, which tuned the interfacial interaction between polymer flexible materials and rigid chassis, enabling a wide structure regulation, experimentally. We further established a structure–effect relationship linking structure to self-diffusiophoretic force, thereby achieving regulation of motility behavior (motion speed and mode) (Figure 1). This work overcomes the longstanding challenge of real-time structure control of MNMs and reveals how structure governs motility behavior via self-diffusiophoretic forces, offering a versatile strategy for motion regulation in precision micro/nano devices.

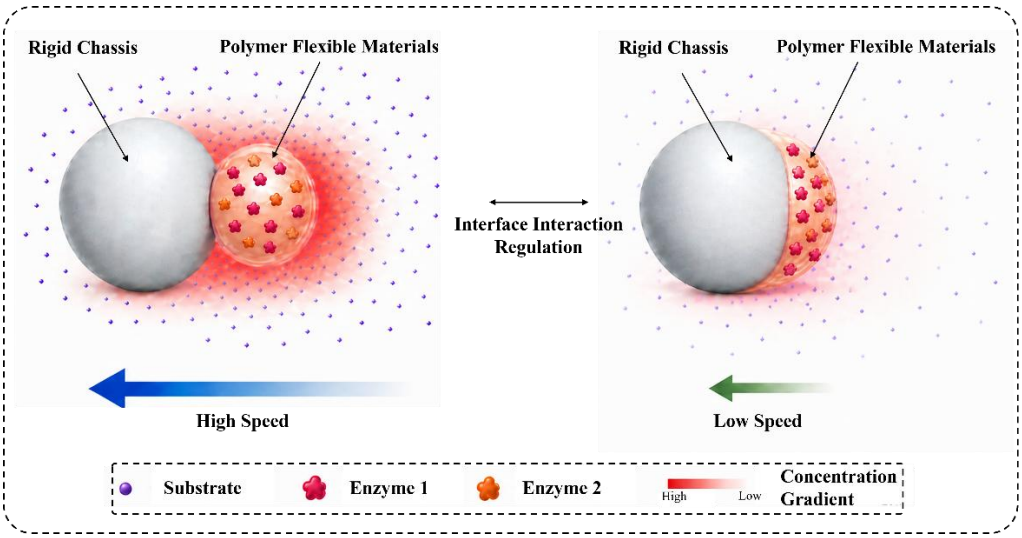

Figure 1 Schematic showing the motility behavior regulation process of rigid-flexible micromotors.

Acknowledgements

The authors appreciate the financial support from NSFC (52473109, 52530002, L.W.), the Natural Science Funding for Excellent Young Scholar of Heilongjiang Province (No. YQ2022E021, L.W.), the High-Level Longjiang Scholarship Talent Programme of Heilongjiang Province (L.W.) and Heilongjiang Provincial Natural Science Foundation of China (QC2025B006, H.C.). The authors also appreciate the international conference funding from Harbin Institute of Technology (H.Y.).

References

[1] H. Yang, L. Wang, et al., "MOF-based micro/nanomotors (MOFtors): Recent progress and challenges," *Coord. Chem. Rev.,* vol. 495, pp. 215372, Nov. 2023, doi: 10.1016/j.ccr.2023.215372.
[2] D. Zhang *et al.*, "Advanced Imaging Strategies based on Intelligent Micro/nanomotors," *Cyborg. Bionic. Syst.,* vol. 6, pp. 0384, Sep. 2025, doi: 10.34133/cbsystems.0384.
[3] D. Zhang, L. Wang, and X. Wu, "Rationally designed modular train-style nanorobots for multi-modal colorectal cancer therapy," *Matter,* vol. 9, no. 2, pp. 102662, Feb. 2026, doi: 10.1016/j.matt.2026.102662.
[4] L. Wang, *et al.*, "Continuous Microfluidic Self-Assembly of Hybrid Janus-Like Vesicular Motors: Autonomous Propulsion and Controlled Release," *Small,* vol. 11, no. 31, pp. 3762-3767, Apr. 2015, doi: 10.1002/smll.201500527.

Bioinspired-Micromotors with Reversible Buoyancy for Adaptive Motion

D. Zhang[a], H. Yang[a], W. Zhan[b], Y. Tian[b]*, L. Wang[a]*
[a] State Key Laboratory of Advanced Inorganic Fibers and Composites, School of Chemistry and Chemical Engineering, Harbin institute of Technology, Harbin 150001, China
[b] State Key Laboratory of Urban-rural Water Resources and Environment, School of environment, Harbin institute of Technology, Harbin 150090, China
*hit_tianyu@163.com
*leiwang_chem@hit.edu.cn

Artificial micro/nanomotors have attracted increasing attention due to their ability to convert external energy into autonomous motion, offering promising opportunities in precision medicine, environmental remediation, and microscale engineering [1, 2]. Considerable progress has been made in improving propulsion efficiency, directional control, and cargo transport [3, 4]. However, in fluidic environments, gravity, sedimentation, and buoyancy mismatch often constrain the vertical mobility and spatial distribution of micro/nanomotors, limiting their ability to actively explore three-dimensional space. Therefore, the development of micro/nanomotors capable of controllable vertical migration and adaptive spatial regulation is highly desirable for operation in complex aquatic environments.

Inspired by density regulation in plankton, we reported a bioinspired micromotor capable of adaptive vertical motion through reversible buoyancy regulation. The micromotor integrates a thermally responsive buoyancy-regulating wax matrix with a photothermal conversion component, enabling remote light-triggered actuation. Upon near-infrared irradiation, the micromotor undergoes reversible density modulation and consequent buoyancy switching, which drives cyclic vertical motion and adaptive redistribution within the fluidic environment (Figure 1). We systematically investigated the design principle, buoyancy-regulation mechanism, and photothermally responsive motion behaviour of the micromotors. Benefiting from this adaptive vertical motion, the micromotors can redistribute across different spatial regions, demonstrating their potential for programmable operation in complex fluidic environments. This study provides a bioinspired strategy for developing intelligent micromotors with adaptive motion behaviours, and may inspire future designs of fuel-free micromotor systems for three-dimensional navigation, adaptive environmental remediation, and programmable matter transport.

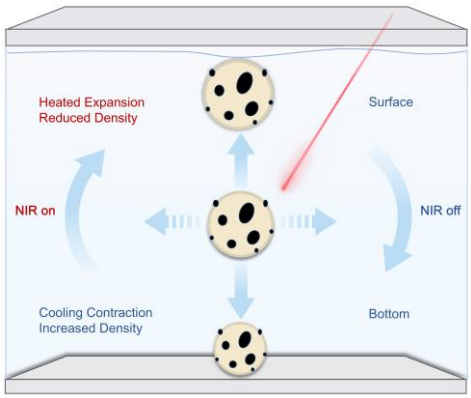

Figure 1 Schematic diagram of regulated buoyancy switching in bioinspired micromotors.

Acknowledgements

This work was supported by NSFC (52530002, 52473109, L.W.) and the International Conference Funding Program from Harbin Institute of Technology (D.Z.).

References

[1] D. Zhang, L. Wang and X. Wu, "Rationally designed modular train-style nanorobots for multi-modal colorectal cancer therapy, " *Matter,* vol. 9, no. 2, pp. 102662, Feb. 2026, doi: 10.1016/j.matt.2026.102662.
[2] D. Zhang, L. Lin, C. Deng, et al. "Advanced Imaging Strategies Based on Intelligent Micro/Nanomotors," *Cyborg Bionic Syst*., vol. 6, pp. 0384, Sep. 2025, doi:10.34133/cbsystems.0384.
[3] D. Zhang, X. Sun, H. Yang, et al, "Application of Nanozyme-based Micro/nanomotors in Smart Drug Delivery," *Chem. J. Chinese Universities,* vol. 46, no. 1, pp. 20240468, Nov. 2024. doi: 10.7503/cjcu20240468.
[4] H. Yang, L. Wang, et al., "MOF-based micro/nanomotors (MOFtors): Recent progress and challenges," *Coord. Chem. Rev.*, vol. 495, pp. 215372, Nov. 2023. doi: 10.1016/j.ccr.2023.215372.

The 10th International Conference on Novel Materials Fundamentals and Applications
Book of Abstracts

Edited by: Mgr. Soňa Király

Publisher: Pavol Jozef Šafárik University in Košice
ŠafárikPress Publishing

Year: 2026
Pages: 98
Author's sheets: 9,47
Edition: first

ISBN 978-80-574-0521-4 (e-publication)
DOI: https://doi.org/10.33542/TIC-0521-4